VOLUME 34 DECEMBER 1956 NUMBER 12B

Canadian Journal of Physics

Editor: H. E. DUCKWORTH

Associate Editors:

L. G. ELLIOTT, *Atomic Energy of Canada, Ltd., Chalk River*
J. S. FOSTER, *McGill University*
G. HERZBERG, *National Research Council of Canada*
L. LEPRINCE-RINGUET, *Ecole Polytechnique, Paris*
B. W. SARGENT, *Queen's University*
G. M. VOLKOFF, *University of British Columbia*
W. H. WATSON, *University of Toronto*
G. A. WOONTON, *McGill University*

Published by THE NATIONAL RESEARCH COUNCIL
OTTAWA CANADA

CANADIAN JOURNAL OF PHYSICS

(Formerly Section A, Canadian Journal of Research)

Under the authority of the Chairman of the Committee of the Privy Council on Scientific and Industrial Research, the National Research Council issues THE CANADIAN JOURNAL OF PHYSICS and six other journals devoted to the publication, in English or French, of the results of original scientific research. Matters of general policy concerning these journals are the responsibility of a joint Editorial Board consisting of: members representing the National Research Council of Canada; the Editors of the Journals; and members representing the Royal Society of Canada and four other scientific societies.

EDITORIAL BOARD

Representatives of the National Research Council

A. N. Campbell, *University of Manitoba*
G. E. Hall, *University of Western Ontario*
H. G. Thode, *McMaster University*
D. L. Thomson, *McGill University*
W. H. Watson (Chairman), *University of Toronto*

Editors of the Journals

D. L. Bailey, *University of Toronto*
T. W. M. Cameron, *Macdonald College*
K. A. C. Elliott, *Montreal Neurological Institute*
G. A. Ledingham, *National Research Council*
Léo Marion, *National Research Council*
R. G. E. Murray, *University of Western Ontario*
H. E. Duckworth, *McMaster University*

Representatives of Societies

D. L. Bailey, *University of Toronto*
Royal Society of Canada
T. W. M. Cameron, *Macdonald College*
Royal Society of Canada
K. A. C. Elliott, *Montreal Neurological Institute*
Canadian Physiological Society
R. G. E. Murray, *University of Western Ontario*
Canadian Society of Microbiologists
H. G. Thode, *McMaster University*
Chemical Institute of Canada
T. Thorvaldson, *University of Saskatchewan*
Royal Society of Canada
H. E. Duckworth, *McMaster University*
Royal Society of Canada; Canadian Association of Physicists

Ex officio

Léo Marion (Editor-in-Chief), *National Research Council*
F. T. Rosser, Director, Division of Administration, *National Research Council*

Manuscripts for publication should be submitted to Dr. Léo Marion, Editor-in-Chief, Canadian Journal of Physics, National Research Council, Ottawa 2, Canada.
(For instructions on preparation of copy, see **Notes to Contributors** (inside back cover).)

Proof, correspondence concerning proof, and orders for reprints should be sent to the Manager, Editorial Office (Research Journals), Division of Administration, National Research Council, Ottawa 2, Canada.

Subscriptions, renewals, requests for single or back numbers, and all remittances should be sent to Division of Administration, National Research Council, Ottawa 2, Canada. Remittances should be made payable to the Receiver General of Canada, credit National Research Council.

The journals published, frequency of publication, and prices are:

Canadian Journal of Biochemistry and Physiology	Bimonthly	$3.00 a year
Canadian Journal of Botany	Bimonthly	$4.00 a year
Canadian Journal of Chemistry	Monthly	$5.00 a year
Canadian Journal of Microbiology	Bimonthly	$3.00 a year
Canadian Journal of Physics	Monthly	$4.00 a year
Canadian Journal of Technology	Bimonthly	$3.00 a year
Canadian Journal of Zoology	Bimonthly	$3.00 a year

The price of single numbers of all journals is 75 cents.

Canadian Journal of Physics

Issued by THE NATIONAL RESEARCH COUNCIL OF CANADA

VOLUME 34 DECEMBER 1956 NUMBER 12B

THE RAMAN SPECTRUM OF ACETYLENE[1]

BY T. FELDMAN,[2] G. G. SHEPHERD,[3] AND H. L. WELSH

ABSTRACT

The rotational and rotation-vibrational Raman spectra of acetylene at one atmosphere pressure were investigated with high spectrographic dispersion. The rotational structures of the three Raman-active fundamentals, ν_1, ν_2, and $\nu_4{}^1$, were resolved and analyzed. The band origins, rotational constants, and certain anharmonicity coefficients were derived.

INTRODUCTION

The acetylene molecule is linear and symmetrical, and has five distinct fundamental modes of vibration. The two totally symmetric (Σ_g^+) modes, ν_1 and ν_2, and the doubly degenerate (Π_g) mode, ν_4, are active only in the Raman effect; the remaining two modes, $\nu_3(\Sigma_u^+)$ and $\nu_5(\Pi_u)$, are active only in infrared absorption.* The extensive earlier work on the Raman and infrared spectra has been summarized and discussed by Herzberg (1945). Recent studies of the infrared spectrum at high dispersion have been made by Bell and Nielsen (1950), Talley and Nielsen (1950), and Wiggins, Shearer, Shull, and Rank (1954).

Several investigations of the Raman spectrum of the gas have been made at comparatively low dispersion. Lewis and Houston (1933) observed the resolved rotational spectrum and identified a weak line at 1967.4 cm.$^{-1}$ as the Q branch of the ν_2 band. Glockler and Morrell (1936) measured the ν_1 line at 3373.7 cm.$^{-1}$. Bhagavantam and Rao (1936) observed two broad weak lines at 589 and 646 cm.$^{-1}$, which undoubtedly represent the maxima in the unresolved O, P and R, S branches of the $\nu_4{}^1$ band, the Q branch being very weak.

In the present investigation the Raman spectrum of the gas was observed with a reciprocal linear dispersion of 10.5 cm.$^{-1}$ per mm. at 4358 Å. The Raman source and spectrograph have been described by Welsh, Stansbury, Romanko, and Feldman (1955). The reduction of the spectrograms was carried out as outlined by Romanko, Feldman, and Welsh (1955). Commercial acetylene gas was used at a pressure of one atmosphere.

[1]Manuscript received August 2, 1956.

Contribution from the McLennan Laboratory, University of Toronto, Toronto, Ontario. This research was supported by Grant No. 1001-01, Project D46-10-01-01 of the Defence Research Board of Canada.

[2]Holder of the E. F. Burton Fellowship in Physics, School of Graduate Studies, University of Toronto, 1954–55. Present address: Bell Telephone Laboratories, Inc., Whippany, N.J., U.S.A.

[3]Holder of a Scholarship of the National Research Council of Canada, 1954–56.

*The nomenclature used follows that of Herzberg (1945).

RESULTS AND DISCUSSION

The Rotational Spectrum

The rotational Raman spectrum excited by Hg 4358 was recorded in 36 hr. with a spectral slit width of 0.35 cm.$^{-1}$ and without the cylindrical lens in front of the photographic plate. The spectrum consists only of S lines ($\Delta J = +2$) with the characteristic 1:3 intensity alternation. The corresponding Stokes and anti-Stokes frequency shifts were averaged, and a least-squares analysis of the 19 observed $S(J)$ frequencies gave the rotational constants $B_0 = 1.1767 \pm 0.0007$ and $D_0 = 5.3 \times 10^{-7}$ cm.$^{-1}$. This value of B_0 is the same as that obtained in the early work of Lewis and Houston (1933). When, as in the present case, the observed frequencies show some scatter, a better value of B_0 can be obtained by assuming a theoretical centrifugal stretching constant D_0. When the value, $D_0 = 1.64 \times 10^{-6}$ cm.$^{-1}$, calculated from the formula of Shaffer and Nielsen (1941) was used, the analysis gave $B_0 = 1.1769 \pm 0.0004$ cm.$^{-1}$. This shows a satisfactory agreement with the infrared values, 1.17692 ± 0.0001 by Herzberg and Spinks (1934), 1.1769 by Bell and Nielsen (1950), and 1.17658 ± 0.0003 by Wiggins, Shearer, Shull, and Rank (1954).

The ν_1 Band

The Q branch of the ν_1 band, excited by Hg 4047, was photographed in 4 hr., and the extensive rotational structure shown in Fig. 1(*a*) in 97 hr. The band has O, Q, and S branches, corresponding to $\Delta J = 0, \pm 2$, with a 1:3 intensity

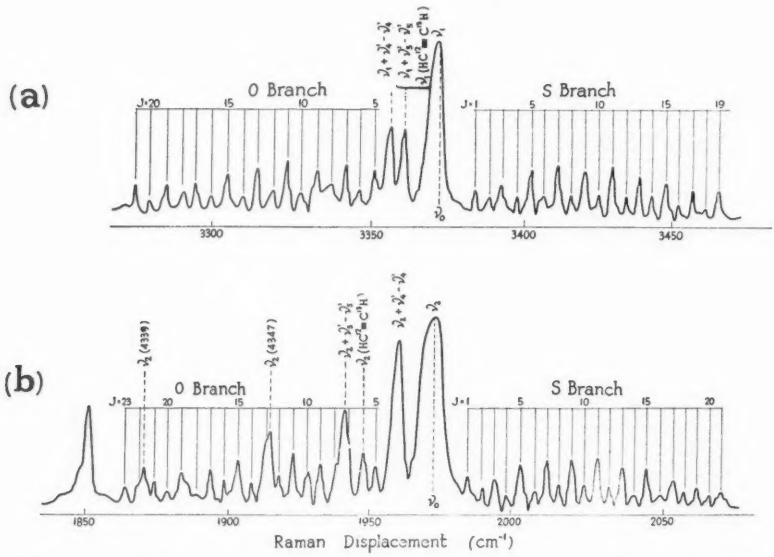

FIG. 1. Microphotometer traces of the totally symmetric Raman bands of gaseous acetylene: (*a*) ν_1, (*b*) ν_2.

alternation in the O and S branches as in the rotational spectrum. The assignments, given in Table I, are unambiguous except for two extraneous lines, at

TABLE I

OBSERVED FREQUENCIES IN THE ν_1 RAMAN BAND OF C_2H_2

$\Delta\nu$ (cm.$^{-1}$)	Assignment	$\Delta\nu$ (cm.$^{-1}$)	Assignment	$\Delta\nu$ (cm.$^{-1}$)	Assignment
3273.5	$O(21)$	3346.1	$O(6)$	3425.3	$S(10)$
3278.0	$O(20)$	3351.1	$O(5)$	3430.0	$S(11)$
3283.4	$O(19)$	3356.3	$\nu_1+\nu_4{}^1-\nu_4{}^1$	3434.5	$S(12)$
3288.7	$O(18)$	3360.7	$\nu_1+\nu_5{}^1-\nu_5{}^1$, ν_1 (HC^{12}≡C^{13}H)	3439.1	$S(13)$
3292.8	$O(17)$			3443.1	$S(14)$
3299.8	$O(16)$	3371.9	$\nu_1(Q_{max})$	3448.0	$S(15)$
3303.0	$O(15)$	3384.6	$S(1)$	3452.3	$S(16)$
3308.0	$O(14)$	3388.8	$S(2)$	3457.0	$S(17)$
3313.0	$O(13)$	3393.1	$S(3)$	3461.4	$S(18)$
3317.7	$O(12)$	3398.1	$S(4)$	3465.5	$S(19)$
3322.4	$O(11)$	3402.7	$S(5)$	3356.7*	$\nu_1+\nu_4{}^1-\nu_4{}^1$
3327.1	$O(10)$	3407.1	$S(6)$	3360.6*	$\nu_1+\nu_5{}^1-\nu_5{}^1$, ν_1 (HC^{12}≡C^{13}H)
3332.3	$O(9)$	3411.8	$S(7)$		
3337.2	$O(8)$	3416.1	$S(8)$	3371.7*	$\nu_1(Q_{max})$
3341.7	$O(7)$	3421.1	$S(9)$		

*Excited by Hg 4078.

3360.7 and 3356.0 cm.$^{-1}$, superimposed upon the regular O series. If allowance is made for the intensities of the underlying O lines, the relative intensities of the lines at 3360.7, 3356.0 cm.$^{-1}$, and the Q branch at 3371.9 cm.$^{-1}$ are roughly 0.07: 0.09: 1.00. A simple calculation shows that the "hot" bands, $\nu_1+\nu_4{}^1-\nu_4{}^1$ and $\nu_1+\nu_5{}^1-\nu_5{}^1$, which have as initial states the low lying doubly degenerate levels $\nu_4{}^1 = 613$ and $\nu_5{}^1 = 731$ cm.$^{-1}$, respectively, should have the relative intensities 0.10 and 0.06 as compared with the ν_1 band. The Q branch at 3356.0 cm.$^{-1}$ will therefore be interpreted as $\nu_1+\nu_4{}^1-\nu_4{}^1$ and that at 3360.7 as $\nu_1+\nu_5{}^1-\nu_5{}^1$. This region of the spectrum should also show the ν_1 band of the isotopic molecule HC^{12}≡C^{13}H with an intensity about 1/100 of that of the main band. With band stretching constants calculated from the observed totally symmetric frequencies, the value 3360.6 cm.$^{-1}$ was obtained for ν_1 of HC^{12}≡C^{13}H; it can therefore be assumed that the isotopic band is superimposed on $\nu_1+\nu_5{}^1-\nu_5{}^1$. With the value of B_0 taken as 1.1769 cm.$^{-1}$, a regression solution performed on the 28 observed O and S lines gave $\nu_0 = 3372.5$ and $B_1 = 1.1699$ cm.$^{-1}$.

The ν_2 Band

The ν_2 band, excited by Hg 4358, was photographed in an exposure time of 97 hr.; a microphotometer trace is shown in Fig. 1(*b*) and the frequencies are listed in Table II. In addition to the rotational structure, several Q branches are present on the low frequency side of the band. Two of these are readily identified as ν_2 excited by Hg 4347 and Hg 4339. By arguments similar to those used for the ν_1 band, the two lines at 1960.3 and 1941.4 cm.$^{-1}$ can be attributed to $\nu_2+\nu_4{}^1-\nu_4{}^1$ and $\nu_2+\nu_5{}^1-\nu_5{}^1$, respectively. The ν_2 band of HC^{12}≡C^{13}H has a calculated frequency of 1947.0 cm.$^{-1}$, and can therefore be assumed to be superimposed on the $O(6)$ line at 1948.0, which shows an anomalously large intensity.

TABLE II

OBSERVED FREQUENCIES IN THE ν_2 RAMAN BAND OF C_2H_2

$\Delta\nu$ (cm.$^{-1}$)	Assignment	$\Delta\nu$ (cm.$^{-1}$)	Assignment	$\Delta\nu$ (cm.$^{-1}$)	Assignment
1852.0	$3\nu_4^1$ (?) ν_2 (C_2HD) (?)	1928.3	$O(10)$	2017.5	$S(8)$
		1932.8	$O(9)$	2022.2	$S(9)$
1865.1	$O(23)$	1938.4	$O(8)$	2026.8	$S(10)$
1972.8*	$\nu_2(Q_{max})$	1941.1	$\nu_2+\nu_5^1-\nu_5^1$	2031.4	$S(11)$
1874.6	$O(21)$	1948.0	ν_2 ($HC^{12}{\equiv}C^{13}H$)	2035.7	$S(12)$
1879.7	$O(20)$	1952.0	$O(5)$	2040.5	$S(13)$
1884.9	$O(19)$	1960.3	$\nu_2+\nu_4^1-\nu_4^1$	2045.1	$S(14)$
1894.4	$O(17)$	1973.2	$\nu_2(Q_{max})$	2049.2	$S(15)$
1899.1	$O(16)$	1984.9	$S(1)$	2054.1	$S(16)$
1903.9	$O(15)$	1990.1	$S(2)$	2058.5	$S(17)$
1908.9	$O(14)$	1994.4	$S(3)$	2062.6	$S(18)$
1913.9	$O(13)$	1998.9	$S(4)$	2066.9	$S(19)$
1973.3†	$\nu_2(Q_{max})$	2003.8	$S(5)$	2075.9	$S(21)$
1918.2	$O(12)$	2008.8	$S(6)$	2084.1	$S(23)$
1923.3	$O(11)$	2013.2	$S(7)$		

*Excited by Hg 4339.
†Excited by Hg 4347.

The rather prominent line at 1852.0 cm.$^{-1}$ is difficult to classify. The most obvious assignment is $3\nu_4^1$, the second overtone of the doubly degenerate frequency at 613 cm.$^{-1}$, assuming a positive anharmonic term. The upper state has the symmetry species $\Pi_g+\Phi_g$ but only the transition $\Pi_g-\Sigma_g^+$ should be active in the Raman effect. Since the band shows a strong Q branch, unlike the ν_4^1 band shown in Fig. 2, it is necessary to postulate that it owes its intensity to a Coriolis interaction with ν_2. This interaction would be in accordance with Jahn's rule.

The observed frequency is very close to that of the Q branch of the ν_2 band of the isotopic molecule C_2HD at 1852.6 cm.$^{-1}$; however, since the intensity of the line is relatively high, this identification would be tenable only under the improbable assumption that the Raman tube had been contaminated in some previous experiment involving deuterated compounds.

The remaining lines in this region form the O and S branches of ν_2. A least squares analysis gave the values $\nu_0 = 1973.4$ and $B_1 = 1.1711$ cm.$^{-1}$.

The ν_4^1 Band

The rotational energy of acetylene in the vth state of a doubly degenerate vibration is

$$F_v(J) = B_v\{J(J+1)-l^2\}-D_v\{J(J+1)-l^2\}^2, \qquad J = l, l+1, \ldots,$$

where l, the vibrational angular momentum about the internuclear line, assumes the integral values $v, v-2, \ldots, 1$ or 0. The value of l is usually indicated by a following superscript on the designation of the vibration. Placzek and Teller (1933) have shown that, although the O, P, R, and S branches have their usual intensities, the Q branch in this type of band is extraordinarily weak, with an intensity comparable with the first lines of the other branches. The microphotometer trace of the ν_4^1 band (Fig. 2) obtained in a 115 hr. exposure shows this predicted structure. A least squares analysis of 23 unblended O and S lines, with assignments as in Table III, gave $B_1 = 1.1745$ and

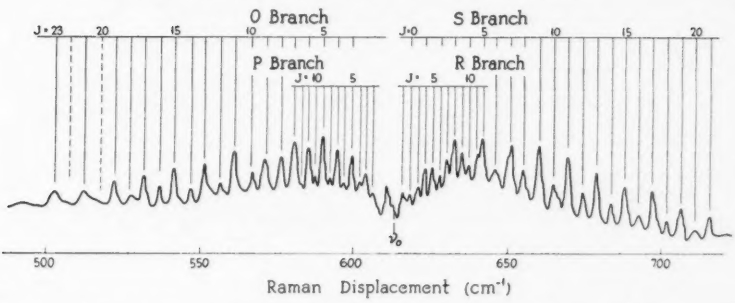

FIG. 2. Microphotometer trace of the doubly degenerate ν_4^1 Raman band of gaseous acetylene.

TABLE III

OBSERVED FREQUENCIES IN THE ν_4^1 RAMAN BAND OF C_2H_2

$\Delta\nu$ (cm.$^{-1}$)	Assignment	$\Delta\nu$ (cm.$^{-1}$)	Assignment	$\Delta\nu$ (cm.$^{-1}$)	Assignment
515.3	$O(21)$	595.8	$O(4)$; $P(7)$	642.7	$S(5)$
524.8	$O(19)$	597.9	$P(6)$	647.5	$S(6)$
534.2	$O(17)$	600.1	$O(3)$; $P(5)$	651.8	$S(7)$
539.3	$O(16)$	604.7	$P(3)$	656.1	$S(8)$
543.5	$O(15)$	607.2	$P(2)$	660.8	$S(9)$
549.1	$O(14)$	611.7	$\nu_4^1(Q_{max})$	665.7	$S(10)$
553.2	$O(13)$	616.6	$R(1)$	670.5	$S(11)$
558.6	$O(12)$	619.0	$R(2)$	675.5	$S(12)$
562.5	$O(11)$	621.7	$R(3)$	679.9	$S(13)$
568.3	$O(10)$	623.9	$S(1)$: $R(4)$	684.4	$S(14)$
572.6	$O(9)$	626.2	$R(5)$	689.1	$S(15)$
577.4	$O(8)$	628.7	$S(2)$; $R(6)$	693.8	$S(16)$
581.4	$O(7)$	631.0	$R(7)$	698.4	$S(17)$
584.6	$P(12)$	633.5	$S(3)$; $R(8)$	703.1	$S(18)$
586.6	$O(6)$; $P(11)$	635.7	$R(9)$	707.9	$S(19)$
588.8	$P(10)$	638.1	$S(4)$; $R(10)$	712.8	$S(20)$
591.2	$O(5)$; $P(9)$	640.9	$R(11)$	717.2	$S(21)$
593.5	$P(8)$				

†Excited by Hg 4347.

$\nu_0 = 613.5$ cm.$^{-1}$. The measured frequency of the Q branch, 611.7 cm.$^{-1}$, shows a shift of roughly B_1 from the band origin, in accordance with the rotational energy formula.

The twofold degeneracy of a vibrational state with a given l can be removed with increasing rotation. This so-called l-type doubling has the consequence that the upper rotational levels of the O, Q, and S branches are not the same as those of the P and R branches. However, an analysis of the unblended P and R lines gave, within the experimental error, the same value of B_1 as was obtained from the O and S lines. The l-type doubling therefore appears to be too small to be observed under the present experimental conditions.

SUMMARY

The molecular constants derived from the analysis of the Raman-active bands of acetylene are summarized in Table IV, and are compared with those derived from infrared combination bands by Herzberg and Spinks (1934) and

TABLE IV

MOLECULAR CONSTANTS (CM.$^{-1}$) FOR THE RAMAN-ACTIVE VIBRATIONS OF C_2H_2

	This investigation	Infrared absorption	
		Herzberg and Spinks (1934)	Bell and Nielsen (1950)
Band origins			
ν_1	3372.5	—	3373.2
ν_2	1973.5	—	1974.0
ν_4^1	613.5	—	613.3
Rotation–vibration constants			
α_1	0.0070	0.00617	—
α_2	0.0058	0.00647	—
α_4	0.0025	0.0006	—
Anharmonicity constants			
x_{15}	−11.8	—	−10.02
x_{25}	−31.8	—	− 1.1
x_{14}	−16.2	—	+ 1.64 −18.16
x_{24}	−12.9	—	− 5.96

Bell and Nielsen (1950). The analysis of the rotational structure of the bands yields the band origins, ν_0, and the rotation–vibration interaction constants, $\alpha = B_0 - B_1$. The agreement between the Raman and infrared values of these constants is satisfactory, except perhaps for α_4 where the Raman value is significantly greater than the infrared value. The observation of difference bands of the type $\nu_1+\nu_4^1-\nu_4^1$ leads to the determination of certain anharmonicity constants, x_{ij}, from relations of the type $(\nu_1+\nu_4^1-\nu_4^1)-\nu_1 = x_{14}$. For these constants the agreement with the infrared values is in most cases very poor. If the infrared value, $x_{25} = -1.1$ cm.$^{-1}$, is correct, the band $\nu_2+\nu_5^1-\nu_5^1$ would be almost superimposed on the Q branch of ν_2 and might not be detected; however, there seems to be no alternative assignment for the line at 1941.4 cm.$^{-1}$, which has moreover the correct intensity for $\nu_2+\nu_5^1-\nu_5^1$. Bell and Nielsen (1950) give two different assignments of infrared combination bands leading to the alternative values, +1.64 and −18.16 cm.$^{-1}$, for x_{14}; the Raman results indicate that the assignment leading to the latter value is probably correct.

REFERENCES

BELL, E. E. and NIELSEN, H. H. 1950. J. Chem. Phys. **18**: 1382.

BHAGAVANTAM, S. and RAO, A. V. 1936. J. Chem. Phys. **4**: 293; Proc. Indian Acad. Sci. A, **3**: 135.

GLOCKLER, G. and MORRELL, C. E. 1936. J. Chem. Phys. **4**: 15.

HERZBERG, G. 1945. Molecular spectra and molecular structure. Vol. II. Infrared and Raman spectra of polyatomic molecules. D. Van Nostrand Company, Inc., New York.

HERZBERG, G. and SPINKS, J. W. T. 1934. Z. Physik, **91**: 386.

LEWIS, C. M. and HOUSTON, W. V. 1933. Phys. Rev. **44**: 903.

PLACZEK, G. and TELLER, E. 1933. Z. Physik, **81**: 209.

ROMANKO, J., FELDMAN, T., and WELSH, H. L. 1955. Can. J. Phys. **33**: 588.

SHAFFER, W. H. and NIELSEN, A. H. 1941. J. Chem. Phys. **9**: 847.

TALLEY, R. M. and NIELSEN, A. H. 1950. J. Chem. Phys. **18**: 1680.

WELSH, H. L., STANSBURY, E. J., ROMANKO, J., and FELDMAN, T. 1955. J. Opt. Soc. Amer. **45**: 338.

WIGGINS, T. A., SHEARER, J. N., SHULL, E. R., and RANK, D. H. 1954. J. Chem. Phys. **22**: 547.

THE RAMAN SPECTRUM OF DIDEUTEROACETYLENE[1]

By L. Krause[2] and H. L. Welsh

ABSTRACT

The rotational and rotation-vibrational Raman spectra of dideuteroacetylene were photographed at one atmosphere pressure with high spectrographic dispersion. The rotational structure of the ν_4^1 band was resolved and analyzed, but only the Q branches of the ν_1 and ν_2 bands were observed.

INTRODUCTION

The dideuteroacetylene molecule, like ordinary acetylene, is linear and symmetrical, and has five fundamental modes of vibration. The two totally symmetric (Σ_g^+) modes, ν_1 and ν_2, and one doubly degenerate (Π_g) mode, ν_4, are active only in the Raman effect; the remaining two modes, ν_3 (Σ_u^+) and ν_5 (Π_u), are active only in infrared absorption.* The Raman spectrum of gaseous C_2D_2 was investigated at low dispersion by Glockler and Morrell (1936), who observed the Q branches of the ν_1 and ν_2 bands. The infrared spectrum has been studied by Randall and Barker (1934), Stitt (1940), Plyler and Gailar (1951), Saksena (1952), Talley and Nielsen (1954), and Overend and Thompson (1955). The more recent of these infrared investigations have used high spectral resolution and have yielded accurate values of many rotational and vibrational constants.

The present investigation of the Raman spectrum of gaseous C_2D_2 parallels that of C_2H_2 by Feldman, Shepherd, and Welsh (1956). The spectrograms were obtained with the Raman source and spectrograph described by Welsh, Stansbury, Romanko, and Feldman (1955). Because of the low intensity of the vibrational bands of C_2D_2 the camera lens ($f/20$) with shorter focal length was used; this gave a reciprocal linear dispersion of 15.6 cm.$^{-1}$ per mm. at 4358 Å.

Dideuteroacetylene was prepared by passing heavy water vapor over calcium carbide. Although the pyrex apparatus and the CaC_2 powder were flamed under vacuum to remove traces of ordinary water, the spectrum of the gas showed some bands of the isotopic compounds C_2HD and C_2H_2. In addition, a trace of ND_3 was also present, possibly arising from calcium nitride as an impurity in the carbide.

RESULTS AND DISCUSSION

The Rotational Spectrum

The rotational Raman spectrum excited by Hg 4358 was photographed with a spectral slit-width of 0.6 cm.$^{-1}$ in a 24 hr. exposure without the cylindrical lens in front of the photographic plate. Since the rotational selection rule for a

[1]Manuscript received August 2, 1956.
Contribution from the McLennan Laboratory, University of Toronto, Toronto, Ontario. This research was supported by Grant No. 1001-01, Project D46-10-01-01 of the Defence Research Board of Canada.

[2]Holder of the California Standard Company Graduate Fellowship, School of Graduate Studies, University of Toronto, 1953–54. Present address: Department of Physics, Memorial University of Newfoundland, St. John's, Nfld.

*The nomenclature used follows that of Herzberg (1945).

linear molecule is $\Delta J = +2$, only an S branch is present. Corresponding Stokes and anti-Stokes frequency shifts were averaged, and a least squares analysis of the 26 observed $S(J)$ frequencies gave the rotational constants, $B_0 = 0.8484$ and $D_0 = 9.8 \times 10^{-7}$ cm.$^{-1}$. This value of B_0 is somewhat larger than the values, 0.84787 obtained by Saksena (1952) and Talley and Nielsen (1954), and 0.8479 cm.$^{-1}$ by Overend and Thompson (1955). It is probable that the Raman result is in error because the rotational spectrum of the ground vibrational state is overlaid by the rotational spectra of molecules in the first vibrational state of the ν_4 and ν_5 normal modes; about 30% of the molecules are in these excited vibrational states at room temperature.

The Totally Symmetric Bands

A large number of Q branches were observed in the region 4300 to 4770 Å; the frequencies and the frequency shifts from the appropriate exciting line are listed in Table I. In addition to the totally symmetric bands of C_2D_2, ν_1 and ν_2 of C_2HD and ν_2 of C_2H_2 were observed.

TABLE I

VIBRATIONAL LINES IN THE RAMAN SPECTRUM OF C_2D_2

ν (cm.$^{-1}$)	$\Delta\nu$ (cm.$^{-1}$) from Hg 4358	$\Delta\nu$ (cm.$^{-1}$) from Hg 4047	$\Delta\nu$ (cm.$^{-1}$) from Hg 4078	Assignment
22756.1			1759.8	$\begin{cases}\nu_2+\nu_4^1-\nu_4^1\ (C_2D_2)\\ \nu_2+\nu_5^1-\nu_5^1\ (C_2D_2)\end{cases}$
22752.1			1763.8	ν_2 (C_2D_2)
22732.4		1972.2		ν_2 (C_2H_2)
22666.4			1849.4	$\begin{cases}\nu_2+\nu_4^1-\nu_4^1\ (C_2HD)\\ \nu_2+\nu_5^1-\nu_5^1\ (C_2HD)\end{cases}$
22663.2			1852.7	ν_2 (C_2HD)
22285.5		2419.8		ν_1 (ND_3)
22001.5		2703.8		ν_1 (C_2D_2)
21913.2	1024.8			$2\nu_4^o$ (C_2D_2)
21371.3		3334.0		ν_1 (C_2HD)
21231.8				ν_2 (C_2D_2)*
21191.6	1746.5			ν_2 ($DC^{12}{\equiv}C^{13}D$)
21177.7	1760.3			$\begin{cases}\nu_2+\nu_4^1-\nu_4^1\ (C_2D_2)\\ \nu_2+\nu_5^1-\nu_5^1\ (C_2D_2)\end{cases}$
21173.9	1764.1			ν_2 (C_2D_2)
21088.6	1849.5			$\begin{cases}\nu_2+\nu_4^1-\nu_4^1\ (C_2HD)\\ \nu_2+\nu_5^1-\nu_5^1\ (C_2HD)\end{cases}$
21085.5	1852.6			ν_2 (C_2HD)
20965.8	1972.2			ν_2 (C_2H_2)

*$\Delta\nu$ = 1763.5 cm.$^{-1}$ from Hg 4347.

The ν_1 band of C_2D_2 is extraordinarily weak and only the Q branch could be photographed in exposure times up to 120 hr. The measured frequency shift, 2703.8 cm.$^{-1}$, is somewhat greater than the value, 2700.5 cm.$^{-1}$, obtained by Glockler and Morrell (1936), but is in good agreement with the band origin, 2703.56 cm.$^{-1}$, determined by Talley and Nielsen (1954) from the sum of the frequencies of the $\nu_1-\nu_5^1$ and ν_5^1 infrared bands.

The Q branch of the ν_2 band was photographed with Hg 4358, Hg 4347, and Hg 4078 as exciting lines; the band excited by Hg 4047 was obscured by Hg 4358. The most accurate value of the frequency shift is probably 1764.2

cm.$^{-1}$, which may be compared with the value, 1762.4 cm.$^{-1}$, measured by Glockler and Morrell (1936), and the band origin, 1764.7 cm.$^{-1}$, determined by Talley and Nielsen (1954) from the $\nu_2-\nu_5^1$ and ν_5^1 infrared bands. Two additional lines, at 1746.5 and 1760.4 cm.$^{-1}$, appear in the vicinity of ν_2. The first of these is assigned to the ν_2 band of the isotopic molecule $DC^{12}{\equiv}C^{13}D$, since its frequency agrees with the value, 1746.2 cm.$^{-1}$, calculated with the bond stretching constants obtained from the observed symmetric frequencies; the low intensity of the line confirms the assignment. The line at 1760.3 cm.$^{-1}$ is clearly one of the "hot" bands $\nu_2+\nu_4^1-\nu_4^1$ or $\nu_2+\nu_5^1-\nu_5^1$, or a superposition of both. Since its intensity relative to ν_2 was estimated as 0.3, the line must be assigned to a superposition of the two bands. The anharmonicity constant, x_{2i}, calculated from the relation $(\nu_2+\nu_i^1-\nu_i^1)-\nu_2 = x_{2i}$ (i = 4 or 5), is -3.8 cm.$^{-1}$. The infrared analysis of Talley and Nielsen (1954) gave $x_{24} = -3.89$ and $x_{25} = -5.06$ cm.$^{-1}$.

A weak line at 1024.80 cm.$^{-1}$ from Hg 4358 can be ascribed only to the totally symmetric overtone, $2\nu_4^o$; its large separation from the other totally symmetric bands indicates that it is a pure overtone and does not arise from a Fermi degeneracy. The anharmonicity constant, x_{44}, calculated from the relation $(2\nu_4^o)-2\nu_4^1 = 4x_{44}$, with $\nu_4^1 = 511.18$ cm.$^{-1}$ as obtained in this investigation, is 0.61 cm.$^{-1}$; this coincides with the value quoted by Talley and Nielsen (1954).

The frequency shifts of the Raman lines assigned to the impurity molecules, C_2H_2 and C_2HD, are summarized in Table II, and compared with values ob-

TABLE II

VIBRATIONAL RAMAN LINES OF C_2HD AND C_2H_2

$\Delta\nu$ (cm.$^{-1}$)	Assignment	Values of $\Delta\nu$ obtained by other authors
1972.2	ν_2 (C_2H_2)	1972.8 (Feldman, Shepherd, and Welsh 1956)
1849.4	$\nu_2+\nu_4^1-\nu_4^1$ (C_2HD) $\nu_2+\nu_5^1-\nu_5^1$ (C_2HD)	———
1852.6	ν_2 (C_2HD)	1851.2 (Glockler and Morrell 1936)
3334.0	ν_1 (C_2HD)	3334.8 (Glockler and Morrell 1936)

tained by other authors. The estimated intensity of the line at 1849.4 cm.$^{-1}$ relative to ν_2 of C_2HD is 0.3; it is therefore probable that it is a superposition of the two "hot" bands, $\nu_2+\nu_4^1-\nu_4^1$ and $\nu_2+\nu_5^1-\nu_5^1$.

The ν_4^1 Band

The doubly degenerate ν_4^1 band, excited by Hg 4358, was photographed in 120 hr. with a spectral slit-width of 0.8 cm.$^{-1}$; a microphotometer trace of the spectrogram is shown in Fig. 1. Like the corresponding band in C_2H_2 (Feldman, Shepherd, and Welsh 1956) the band shows *O*, *P*, *R*, and *S* branches and a very weak *Q* branch. The rotational lines show the 2:1 intensity alternation arising from the nuclear spin of the deuterium atom. The weaker *P* lines coincide with *O* lines, and the stronger *R* lines coincide with *S* lines; for this reason the *P* branch appears to persist to higher *J* values than the *R* lines. However, in

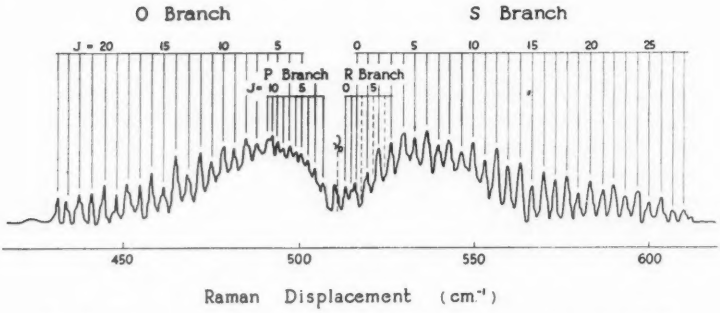

FIG. 1. Microphotometer trace of the doubly degenerate ν_4^1 band of C_2D_2.

neither of these two branches were the lines sufficiently well resolved to permit accurate frequency measurements.

The frequencies and assignments of the *O* and *S* lines are given in Table III. The regression formula

$$\Delta\nu = \nu_0 - B_1 + \tfrac{3}{4}(B_1 - B_0) + 2(B_1 + B_0)m + (B_1 - B_0)m^2,$$

where $m = -J + \frac{1}{2}$ for the *O* lines and $m = J + 3/2$ for the *S* lines, was used to determine the molecular constants. The frequencies were first corrected for

TABLE III

OBSERVED FREQUENCIES IN THE ν_4^1 RAMAN BAND OF C_2D_2

$\Delta\nu$ (cm.$^{-1}$)	Assignment	$\Delta\nu$ (cm.$^{-1}$)	Assignment	$\Delta\nu$ (cm.$^{-1}$)	Assignment
431.4	*O*(24)	487.8	*O*(7)	552.8	*S*(11)
434.1	*O*(23)	491.3	*O*(6)	555.9	*S*(12)
437.5	*O*(22)	493.3	*O*(5)	559.3	*S*(13)
441.0	*O*(21)	497.5	*O*(4)	562.9	*S*(14)
444.3	*O*(20)	500.2	*O*(3)	566.2	*S*(15)
448.0	*O*(19)	510.3	Q_{max}	569.8	*S*(16)
451.2	*O*(18)	514.8	*S*(0)	573.3	*S*(17)
454.3	*O*(17)	518.6	*S*(1)	576.4	*S*(18)
457.9	*O*(16)	522.3	*S*(2)	579.8	*S*(19)
461.3	*O*(15)	525.8	*S*(3)	583.3	*S*(20)
464.9	*O*(14)	529.1	*S*(4)	586.9	*S*(21)
468.0	*O*(13)	532.7	*S*(5)	590.0	*S*(22)
471.4	*O*(12)	536.0	*S*(6)	593.4	*S*(23)
474.6	*O*(11)	539.1	*S*(7)	597.0	*S*(24)
478.0	*O*(10)	542.4	*S*(8)	600.3	*S*(25)
481.2	*O*(9)	545.8	*S*(9)	603.7	*S*(26)
484.8	*O*(8)	549.3	*S*(10)	607.8	*S*(27)
				610.6	*S*(28)

centrifugal stretching using $D_1 = D_0 = 8\times10^{-7}$ cm.$^{-1}$, obtained from the theoretical formula of Shaffer and Nielsen (1941). A least squares analysis of the unblended lines gave $\nu_0 = 511.12$, $B_0 = 0.8478$, and $B_1 = 0.8482$ cm.$^{-1}$. The *Q* branch at 510.3 cm.$^{-1}$ is thus shifted from the band origin, ν_0, by the amount $B_1 \sim 0.8$ cm.$^{-1}$, as predicted from the theory. The frequency of the

band origin as calculated by Talley and Nielsen (1954) from infrared combination bands is 511.38 cm.$^{-1}$, in good agreement with the Raman value. The rotation–vibration interaction constant, $\alpha^{OS} = B_0 - B_1$, is -0.0004 cm.$^{-1}$ from the Raman data; this agrees with the infrared value of α^{PR} given by Overend and Thompson (1955), but is opposite in sign to the value given by Talley and Nielsen (1954).

The results of the present Raman investigation of C_2D_2 show in general very satisfactory agreement with the most recent infrared work at high dispersion.

REFERENCES

FELDMAN, T., SHEPHERD, G. G., and WELSH, H. L. 1956. Can. J. Phys. **34**: 1425.

GLOCKLER, G. and MORRELL, C. E. 1936. J. Chem. Phys. **4**: 15.

HERZBERG, G. 1945. Molecular spectra and molecular structure. Vol. II. Infrared and Raman spectra of polyatomic molecules. D. Van Nostrand Company, Inc., New York, N.Y.

OVEREND, T. and THOMPSON, H. W. 1955. Proc. Roy. Soc. A, **232**: 291.

PLYLER, E. K. and GAILAR, N. 1951. J. Research Natl. Bur. Standards, **47**: 248.

RANDALL, H. M. and BARKER, E. F. 1934. Phys. Rev. **45**: 124.

SAKSENA, B. D. 1952. J. Chem. Phys. **20**: 95.

SHAFFER, W. H. and NIELSEN, A. H. 1941. J. Chem. Phys. **9**: 847.

STITT, F. 1940. J. Chem. Phys. **8**: 56.

TALLEY, R. M. and NIELSEN, A. H. 1954. J. Chem. Phys. **22**: 2030.

WELSH, H. L., STANSBURY, E. J., ROMANKO, J., and FELDMAN, T. 1955. J. Opt. Soc. Amer. **45**: 338.

CROSS SECTIONS OF DISSOCIATIVE RECOMBINATION[1]

By Ernest Bauer[2] and Ta-You Wu[3]

ABSTRACT

We consider the following process. A hydrogen molecular ion H_2^+ in its ground state, $1s\sigma\ ^2\Sigma_g^+$, captures a free electron of low energy and splits up into two hydrogen atoms in the states $H(1s) + H(2s)$ or $H(1s) + H(2p)$. The cross sections for transitions into these two states are calculated in a "Born approximation" as functions of electron energy for energies less than 1 ev., and are found to be of gas kinetic order of magnitude (10^{-15} cm.^{2}).

I. INTRODUCTION

By "dissociative recombination" is meant the process

$$XY^+ + e \rightarrow X' + Y'' \tag{1}$$

in which a molecular ion XY^+ recombines with an electron e and then dissociates into two neutral atoms X, Y, either or both of which may be in an excited state. It was suggested by Bates and Massey (1946) that the observed high value of the recombination coefficient ($\alpha \cong 10^{-8}$ cm.^{3}/sec.) in the E-layer of the ionosphere may be due to the recombination between O_2^+ and e according to (1). In laboratory experiments, Biondi and Holstein (1951) have found strong evidence for the process (1) in helium, namely

$$He_2^+ + e \rightarrow He' + He'',$$

and for a value $\sim 10^{-8}$ cm.^{3}/sec. for the recombination coefficient α. No theoretical calculations of the cross section of a process of type (1) seem to have been made. The object of the present work is to attempt to estimate, by a model calculation, the cross section of the simplest process of the type (1), namely X = Y = hydrogen atom.

II. FORMULATION OF THE THEORY

We wish to estimate the cross section of the process

$$H_2^+ + e \rightarrow H' + H'' \tag{2}$$

in which the collision between an electron of energy $\hbar^2k^2/2m$ and a hydrogen molecular ion in its ground electronic state leads to two hydrogen atoms in their ground or excited states. It is convenient to regard (2) as a two-stage process consisting of the capture of the electron by the ion H_2^+ to give a hydrogen molecule in an excited electronic state which is unstable,

$$H_2^+ + e \rightarrow H_2^*, \tag{3}$$

[1]Manuscript received June 26, 1956.

Contribution from the Institute of Mathematical Sciences, New York University, New York, New York, and the Division of Pure Physics, National Research Council, Ottawa, Canada. Issued as N.R.C. No. 4126.

This work was supported in part by Contract No. AF-19(122)-463 with the U.S. Air Force through sponsorship of the Geophysical Research Directorate of the Air Force Cambridge Research Center, Air Research and Development Command.

[2]Institute of Mathematical Sciences, New York University, New York, New York.

[3]Division of Pure Physics, National Research Council, Ottawa, Canada.

and the subsequent dissociation of this molecule into two neutral atoms,

$$H_2^* \rightarrow H' + H''. \tag{4}$$

Because the electron mass is small compared with the nuclear mass, the capture process (3) may be regarded as a "vertical" (Franck–Condon) transition in the sense that the nuclear separation R remains unchanged during the capture process. If we denote the electronic energy of the systems H_2^+, H_2^* at the nuclear separation R by $E(H_2^+; R)$, $E(H_2^*; R)$, then the energy relation for the process (3) imposes a relation between the kinetic energy of the incident electron, $\hbar^2k^2/2m$, and the nuclear separation R:

$$E(H_2^+; R_k)+\hbar^2k^2/2m = E(H_2^*; R_k)\,. \tag{5}$$

For incident electrons having a range of energies, there would be a corresponding range of values R_k at which the "vertical" transitions (3) can take place.

From the state H_2^*, the system may either proceed backward,

$$H_2^* \rightarrow H_2^+ + e, \tag{6}$$

or dissociate according to (4). Let the probabilities of (4) and (6) be p_d and p_a respectively. Let the cross section of the capture process (3) for the formation of H_2^* be σ_c. Then the cross section of the dissociative recombination (2) is given by

$$\sigma_{DR} = \sigma_c\, p_d/(p_d+p_a)\,. \tag{7}$$

Now the process (6) is similar to the Auger transition in atoms, and so the probabilities p_a may be expected to be similar in order of magnitude to those for atoms. The probability per second, p_d, that two repulsive atoms separate is of order

$$p_d = \lim_{t\to 0} v/R\,,$$

where v is the velocity at nuclear separation R, and this probability is large compared with p_a. Thus our problem is reduced to calculating the capture cross section σ_c of (3).

To obtain σ_c, consider the reverse process (6). Let the wave function of the two electrons in the bound state H_2^* be denoted by ψ_β, and that in the continuum $H_2^+ + e$ by ψ_k. The probability per second of a transition of the system from the state ψ_β to the state ψ_k under the perturbation V' is

$$P_{\beta k} = \left(\frac{2\pi}{\hbar}\right)\left|\int \psi_k^* V' \psi_\beta\, d\tau\right|^2 \rho_E,$$

$$\rho_E = \frac{m\hbar k}{(2\pi\hbar)^3}\,\Omega\, d\omega, \tag{8}$$

where the ejected electron has momentum $\hbar k$ in directions lying within the solid angle $d\omega$; ρ_E is the number of states ψ_k per unit energy range about the energy E, and Ω is the normalization volume available for the free electron. The probability per second of the capture of an electron of momentum $\hbar k$ is

then obtained by dividing $P_{\beta k}$ by the total number of states, $4\pi k^3\Omega/3$, over which the result (8) has been obtained by integration, namely

$$P_{k\beta} = 3(m/2\pi\hbar^2)^2 \frac{1}{k^3} \left| \int \psi_k^* V' \psi_\beta \, d\tau \right|^2 v \frac{d\omega}{4\pi}, \tag{9}$$

$$mv = \hbar k.$$

The total cross section of the capture process (3) is obtained by integrating $P_{k\beta}/(v/\Omega)$ over all directions ω. If we ignore any dependence of the matrix element $(\psi_k, V'\psi_\beta)$ on the direction of k, we obtain

$$\sigma_c(R) = 3(m/2\pi\hbar^2)^2 \frac{1}{k^3} |(\psi_k, V'\psi_\beta)|^2\Omega. \tag{10}$$

(The factor Ω will eventually drop out when the wave function ψ_k for the state $H_2^+ + e$ is properly normalized. See below.)

The above expressions for $P_{k\beta}$ and σ_c refer to the capture probability and cross section, respectively, at a fixed nuclear separation R, as is indicated by the notation $P_{k\beta}(R)$, $\sigma_c(R)$. To include the effect of the nuclear vibration, it is obvious that one should multiply $P_{k\beta}(R)$, $\sigma_c(R)$ by the probability of finding the system H_2^+ at the nuclear separation R, and should then integrate over R. This probability is

$$|\psi_v(R)|^2 \, dR = (\gamma/\pi)^{\frac{1}{2}} \exp\{-\gamma(R-R_e)^2\} dR, \qquad \gamma = M\omega_1/\hbar, \tag{11}$$

for a molecular ion H_2^+ in its vibrational ground state. $2M$ here is the mass of the hydrogen atom, ω_1 the angular frequency of vibration, and R_e the equilibrium nuclear separation of the system H_2^+.

It remains to specify the perturbation V' in the formulas above for our problem. The process (3) is a rearrangement collision, and it is necessary to define the zeroth-order Hamiltonian H^0 and the perturbation V' in such a way that the perturbation theory formula (8) is valid. One way is to choose the states ψ_β, ψ_k to be states of the same Hamiltonian so that the wave functions ψ_β, ψ_k are orthogonal. We shall accordingly treat the following system as the unperturbed Hamiltonian:

$$H^0 = -\frac{\hbar^2}{2m}(\nabla_1^2+\nabla_2^2) - e^2\left(\frac{1}{r_{1A}}+\frac{1}{r_{1B}}+\frac{1}{r_{2A}}+\frac{1}{r_{2B}}\right)+\frac{e^2}{R}, \tag{12}$$

where r_{1A} is the distance between electron 1 and nucleus A, R the internuclear distance, etc. The electron–electron interaction is regarded as the perturbation:

$$V' = e^2/r_{12}. \tag{13}$$

In this formulation, the state ψ_β of H_2^* is one representing two electrons, each in an eigenstate of H_2^+, while ψ_k of $H_2^+ + e$ is a state representing one electron in the normal state of H_2^+ and the other electron in the continuum in the field of the two nuclei. At first sight this separation of the Hamiltonian of the system into $H^0 + V'$ seems strange, but it has the advantage of satisfying the orthogonality requirement mentioned above, and is accordingly free from such difficulty as the prior–post ambiguity which is associated with the use of non-orthogonal states in the usual treatment of rearrangement collisions (Schiff 1949).

III. DETAILED FORMULATION FOR THE PROBLEM $H_2^+ + e \rightarrow H_2^*$

To make a calculation of the capture cross section of (3), we need to know the electronic energies of the zeroth-order Hamiltonian (12) in the form of potential energy curves as a function of nuclear separation R. Since H^0 in (12) does not include the electron–electron interaction (13), the eigenstates of (12) are not the actual states of the molecule H_2. For consistency in the perturbation theory, and for the formula (8) to be valid, we must use the wave functions and electronic energies of H^0 in (12) rather than those of the actual molecule. However, we can use the same spectroscopic notation for both the orbitals and the molecular states as for the actual system.

In Fig. 1 are drawn the potential curves for a few states of H^0. The energies of the H_2^+ ion are simply taken from the well-known work of Teller (1930). For the states of H_2, the energies shown are obtained from those of the two appropriate H_2^+ states, i.e., by adding the energies of the two H_2^+ states and subtracting e^2/R, since the nucleus–nucleus repulsion has been counted twice in adding the energies of the two H_2^+ states. As has been mentioned in the

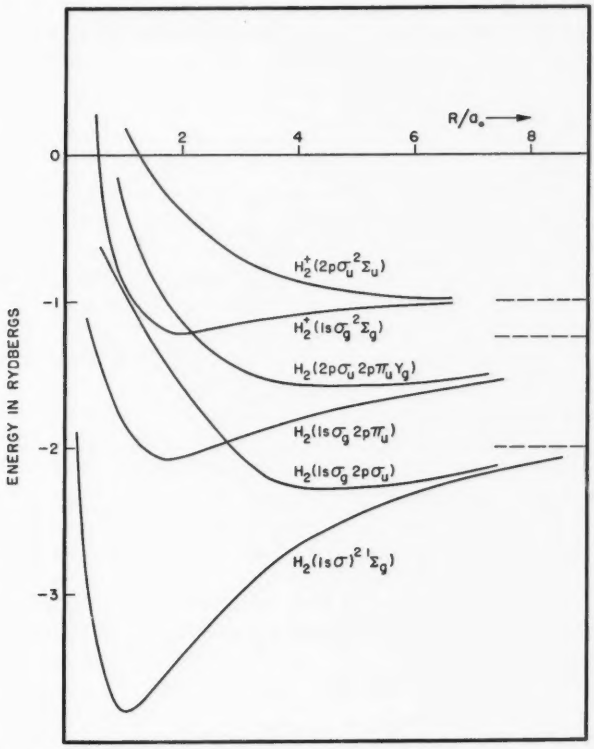

FIG. 1. Electronic energies of some states of "H_2^+" and "H_2". See §III in text.

preceding paragraph, the energy curves of the H_2 states so obtained are not meant to be those of the actual states of the H_2 molecule, but have been constructed for a consistent application of the perturbation theory.

The energies of H_2^+ states have the following asymptotic form as $R \to \infty$ (Eyring *et al.* 1944):

$$\begin{aligned} &H_2^+(2p\pi_u\ ^2\Pi_u) \to H(2p) + H^+, \\ &H_2^+(2s\sigma_g\ ^2\Sigma_g) \to H(2s) + H^+, \\ &H_2^+(2p\sigma_u\ ^2\Sigma_u) \to H(1s) + H^+, \\ &H_2^+(1s\sigma_g\ ^2\Sigma_g) \to H(1s) + H^+, \end{aligned} \tag{14}$$

and those of the H_2 states

$$\begin{aligned} &H_2(2p\sigma_u\ 2s\sigma_g\ Z_u) \text{ repulsive} \to H(1s) + H(2s), \\ &H_2(2p\sigma_u\ 2p\pi_u\ Y_g) \text{ repulsive} \to H(1s) + H(2p), \\ &H_2(1s\sigma_g\ 2p\pi_u\ ^{1,3}\Pi_u) \to H(1s) + H(2p), \\ &H_2(1s\sigma_g\ 2p\sigma_u\ ^3\Sigma_u) \to H(1s) + H(1s), \\ &H_2(1s\sigma_g\ 1s\sigma_g\ ^1\Sigma_g) \to H(1s) + H(1s). \end{aligned} \tag{15}$$

We see from Fig. 1 that the potential energy curve of the repulsion state $H_2(2p\sigma_u\ 2p\pi_u\ Y_g)$ crosses that of $H_2^+(1s\sigma_g\ ^2\Sigma_g)$, the ground state of H_2^+. As the $H_2^+(2p\pi_u)$ and $H_2^+(2s\sigma_g)$ states have much the same energies, the energy curves of $H_2(2p\sigma_u\ 2s\sigma_g\ ^{1,3}\Sigma_u)$ (not shown in Fig. 1) will be very similar to those of $H_2(2p\sigma_u\ 2p\pi_u\ ^{1,3}\Pi_g)$, and hence will cross that of $H_2^+(1s\sigma_g\ ^2\Sigma_g)$. According to the discussion at the beginning of §II, we see that "vertical" transitions from $H_2^+(1s\sigma_g\ ^2\Sigma_g)$ to the repulsive states $H_2(2p\sigma_u\ 2p\pi_u\ ^{1,3}\Pi_g)$ and $H_2(2p\sigma_u\ 2s\sigma_g\ ^{1,3}\Sigma_u)$ (i.e., the capture of an electron by H_2^+ in the state $1s\sigma_g\ ^2\Sigma_g$ at a fixed nuclear separation R to form H_2 in these repulsive states) are possible. (Note that the potential energy curves of states $H_2(1s\sigma_g\ nl\lambda)$ in this approximation H^0 do not cross that of $H_2^+(1s\sigma_g\ ^2\Sigma_g)$ for any bound state $nl\lambda$, and that hence these states need not be considered here.)

There are of course other states of H_2 which asymptotically for large R go over to $H(1s) + H(3s)$, $H(1s) + H(3p)$, $H(1s) + H(3d)$, etc., and whose energy curves are repulsive and intersect that of $H_2^+(1s\sigma_g\ ^2\Sigma_g)$. The energy curves of these states will in general intersect that of $H_2^+(1s\sigma_g\ ^2\Sigma_g)$ at larger distances R, and the "vertical" captures near the equilibrium separation R_e of $H_2^+(1s\sigma_g\ ^2\Sigma_g)$ would correspond to greater energies of the captured electron. Both because of this higher electron energy and the general behavior of the matrix element in (10), one may expect the capture cross sections leading to dissociation of H_2 into $H(1s) + H(nl)$ to become smaller as n and l become higher. Also, the Y and Z states in (15) may be singlet or triplet states. In the present work, we shall for definiteness consider the capture into the triplet states, namely,

$$\begin{aligned} &H_2^+(1s\sigma_g\ ^2\Sigma_g) + e \to H_2(2p\sigma_u\ 2p\pi_u\ ^3Y_g), \\ &H_2^+(1s\sigma_g\ ^2\Sigma_g) + e \to H_2(2p\sigma_u\ 2s\sigma_g\ ^3Z_u). \end{aligned} \tag{16}$$

From the energy curves of the states $H_2^+(1s\sigma_g\ ^2\Sigma_g)$, $H_2(^3Y_g)$ in Fig. 1, and a

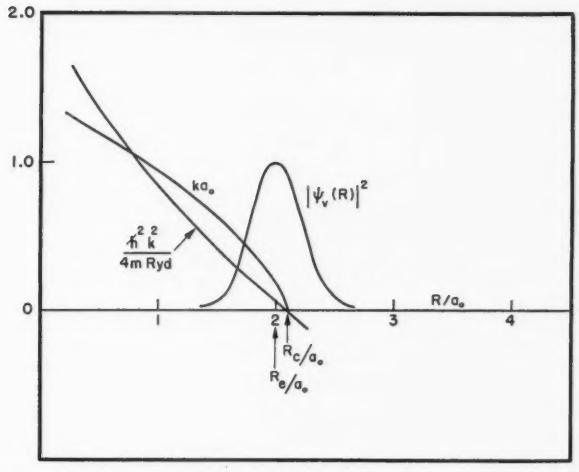

FIG. 2. Relation between electronic energy and nuclear separation in "vertical" capture transitions. See §III in text.

similar one for $H_2(^3Z_u)$, and from the relation (5) between the electron energy $\hbar^2k^2/2m$ and the nuclear separation R_k for a vertical transition in (15), we obtain the curves of $E_k = \hbar^2k^2/2m$ vs. R_k, and ka_0 vs. R_k in Fig. 2. The square of the vibrational ground state wave function of $H_2^+(1s\sigma_g\ ^2\Sigma_g)$, $|\psi_{v0}(R)|^2$ of (11), is also shown there. $|\psi_{v0}(R)|^2$ falls off very rapidly for values of R different from the equilibrium distance R_e, and thus only a small range of $R = R_k$ (and hence of k^2) contributes appreciably to the capture cross section when $\sigma_c(R)$ of Eq. (10) is averaged over all values of R.

We see from Fig. 2 that over this relevant range of R, the relation between R_k and k^2 is approximately linear, i.e.,

$$R_k = R_c - wE_k, \qquad w = -\partial R_k/\partial E_k, \qquad E_k = \hbar^2k^2/2m, \tag{17}$$

R_c being the distance at which the two potential curves cross each other. From (10) and (11), one thus obtains the cross section for the capture of an electron of energy lying between E_k and $E_k + dE_k$,

$$\sigma_c(E_k)dE_k = \sigma_c(R_k)(\gamma/\pi)^{\frac{1}{2}} \exp\{-\gamma(-wE_k + R_c - R_e)^2\} w\, dE_k, \tag{18}$$

where $\sigma_c(R)$ is given by Eq. (10).

From Eq. (18), one obtains for the number of captures in a given state per second when a beam of electrons having $N(E_k)dE_k$ electrons per unit volume in an energy range E_k to $E_k + dE_k$ is incident on molecular ions of concentration N_I the expression

$$N_c = wN_I\left(\frac{\gamma}{\pi}\right)^{\frac{1}{2}} \frac{\hbar k}{m} \int \exp\{-\gamma(R_c - R_e - wE_k)^2\}\, \sigma_c(R_k)\, N(E_k)\, dE_k. \tag{18a}$$

For captures by H_2^+ in the ground state $^2\Sigma_g$ into the Y, Z states in (16) of H_2, the numerical values of the constants for the $H_2^+(^2\Sigma_g)$ state are as follows:

$$\gamma = 9.62/a_0^2,$$
$$R_c - R_e \cong 0.05\ a_0,$$
$$w = 1.25\ a_0^2/e^2.$$

To calculate the capture cross section, one needs the wave functions ψ_β, ψ_k in (10), which are of course eigenfunctions of H^0 of (12). Instead of constructing ψ_β, ψ_k from bound and continuum state eigenfunctions of H_2^+, we shall construct them from atomic orbitals as an approximation. Thus we shall take for the atomic orbitals of electron 1 around the nucleus A,

$$\begin{aligned}
&1s: \quad a_0(1) \equiv a_{1s}(\mathbf{r}_1) &&= (\alpha^3/\pi)^{\frac{1}{2}} \exp(-\alpha r_{1A}),\\
&2s: \quad a_t(1) \equiv a_{2s}(\mathbf{r}_1) &&= \tfrac{1}{2}(\alpha^3/2\pi)^{\frac{1}{2}}\,(1-\tfrac{1}{2}\alpha r_{1A}) \exp(-\tfrac{1}{2}\alpha r_{1A}),\\
&2p_x: a_s(1) \equiv a_{2p_x}(\mathbf{r}_1) &&= \tfrac{1}{4}(\alpha^5/2\pi)^{\frac{1}{2}} r_{1A} \exp(-\tfrac{1}{2}\alpha r_{1A}) \sin\theta_{1A} \cos\phi_{1A},
\end{aligned} \tag{19}$$

where $\alpha = 1/a_0$, and similarly for the orbitals $b_0(1)$, etc., around nucleus B. The continuum orbitals are approximated by plane waves, normalized within the volume Ω:

$$\begin{aligned}
a_f(1) &= (1/\sqrt{\Omega}) \exp(i\mathbf{k} \cdot \mathbf{r}_{1A}),\\
b_f(1) &= (1/\sqrt{\Omega}) \exp(i\mathbf{k} \cdot \mathbf{r}_{1A}), \text{ etc.}
\end{aligned} \tag{20}$$

It is clearly not very satisfactory to approximate the continuum hydrogenic wave functions by plane waves at the very low energies considered here (below 1 ev.). This approximation has been made as it is quite impossible to consider an evaluation of the matrix elements with any more complicated wave function.

The molecular orbitals are constructed of these atomic orbitals to have the even or odd property; thus, for example, from (14), (16), (19),

$$\begin{aligned}
1s\sigma_g &= a_0(1)+b_0(1),\\
2p\sigma_u &= a_0(1)-b_0(1), \text{ etc.}
\end{aligned}$$

For the repulsive states of H_2, we take the following properly symmetrized wave functions (triplet states):

$$\begin{aligned}
\Psi(Y_g) &= N_{Y_g}[\{a_0(1)-b_0(1)\}\{a_s(2)-b_s(2)\}-\{a_s(1)-b_s(1)\}\{a_0(2)-b_0(2)\}],\\
\Psi(Z_u) &= N_{Z_u}[\{a_0(1)-b_0(1)\}\{a_t(2)+b_t(2)\}-\{a_t(1)+b_t(1)\}\{a_0(2)-b_0(2)\}].
\end{aligned} \tag{21}$$

For the states $H_2^+ + e$, we also construct molecular wave functions (triplet states)

$$\begin{aligned}
\Psi(I_g) &= N_{I_g}[\{a_f(1)+b_f(1)\}\{a_0(2)+b_0(2)\}-\{a_0(1)+b_0(1)\}\{a_f(2)+b_f(2)\}],\\
\Psi(I_u) &= N_{I_u}[\{a_f(1)-b_f(1)\}\{a_0(2)+b_0(2)\}-\{a_0(1)+b_0(1)\}\{a_f(2)-b_f(2)\}].
\end{aligned} \tag{22}$$

The normalization constants are

$$\begin{aligned}
N_{Y_g}^2 &= \tfrac{1}{8}[(1-I_{00})(1-I_{ss})-\tfrac{1}{4}(I_{0s}+I_{s0})^2]^{-1},\\
N_{Z_u}^2 &= \tfrac{1}{8}[(1-I_{00})(1+I_{tt})-\tfrac{1}{4}(I_{0t}-I_{t0})^2]^{-1},\\
N_{I_g}^2 &= \tfrac{1}{8}[(1+I_{00})(1+\cos\mathbf{k} \cdot \mathbf{R})]^{-1},\\
N_{I_u}^2 &= \tfrac{1}{8}[(1+I_{00})(1-\cos\mathbf{k} \cdot \mathbf{R})]^{-1},
\end{aligned} \tag{23}$$

where

$$I_{\lambda\mu} = \int a_\lambda^*(r)\, b_\mu(r)\, d^3\mathbf{r} \tag{24}$$

and λ, $\mu = 0, t, s$ for $1s$, $2s$, $2p_x$ respectively as indicated in Eq. (19). In the expressions for $N_{I_g}{}^2$, $N_{I_u}{}^2$, integrals involving a bound state and a continuum orbital like (a_λ, b_f) have been neglected.

Since $V' = e^2/r_{12}$ is symmetric with respect to inversion about the center of symmetry of the system, only the following transitions give non-vanishing cross sections:

$$G\colon\ I_g \leftrightarrow Y_g; \qquad U\colon\ I_u \leftrightarrow Z_u. \tag{25}$$

The evaluation of the matrix elements of V', and of the cross section, for these two transitions is outlined below.

IV. THE CROSS SECTION FOR THE *U*-TRANSITION

First we wish to evaluate the transition matrix element

$$(\Psi(Z_u),\ V'\Psi(I_u)) = \int \Psi^*(Z_u)\ V'\Psi(I_u)\, d\tau \tag{26}$$

where $V' = e^2/r_{12}$, and the wave functions are given in Eqs. (21), (22). The calculation is simplified by the following considerations:

(i) Because V' and the wave functions $\Psi(Z_u)$, $\Psi(I_u)$ are symmetric in the variables $\mathbf{r}_1$, $\mathbf{r}_2$, the number of independent terms in (26) is precisely half that indicated by the direct expansion of (26).

(ii) Each of the individual terms of (26) is of the form

$$(a_\lambda b_\mu,\ V' a_\nu b_f)$$

and contains three bound state atomic orbitals about nuclei A and B in some combination, and also the plane wave function a_f or b_f of Eq. (20). It depends on the states λ, μ, ν, and on the two vectors $\mathbf{k}$ and $\mathbf{R} = AB$. Changing the sign of R is achieved by interchanging all a- and b-orbitals in the term, while to change the sign of $\mathbf{k}$ we take the complex conjugate of the term (recall that all the bound state orbitals of Eq. (19) are real). Thus, if in any term of (26) we interchange a and b, and simultaneously take the complex conjugate of the expression, we leave the term unchanged. For example

$$(a_\lambda b_\mu,\ V' a_\nu b_f) = (a_\mu b_\lambda,\ V' a_f b_\nu)^*.$$

Now all the terms simplified in this way add up so that there remain only contributions like

$$\iint a_\lambda(1)\, b_\mu(1)\, \frac{e^2}{r_{12}}\, a_\nu(2)\{b_f(2) + b_f^*(2)\}\, d^3\mathbf{r}_1\, d^3\mathbf{r}_2$$

and none containing $\{b_f(2) - b_f^*(2)\}$. Hence the matrix element $(\Psi(Z_u)\, V',\ \Psi(I_u))$ depends on the wave vector $\mathbf{k}$ through functions $\cos(\mathbf{k}\cdot\mathbf{r})$ rather than $\sin(\mathbf{k}\cdot\mathbf{r})$, and it is convenient to introduce new free particle wave functions:

$$\begin{aligned} a_k(1) &= (1/\sqrt{\Omega})\cos\,\mathbf{k}\cdot\mathbf{r}_{1A}, \\ b_k(1) &= (1/\sqrt{\Omega})\cos\,\mathbf{k}\cdot\mathbf{r}_{1B}, \text{ etc.} \end{aligned} \tag{27}$$

This consideration again reduces the number of terms to half the previous number, and we are left with the expression

$$(28)\quad (\Psi(Z_u), V'\Psi(I_u))/4N_{I_u}N_{Z_u} =$$

$$\iint a_0(1)\{a_t(1)+b_t(1)\}\frac{e^2}{r_{12}}\{a_0(2)-b_0(2)\}\{a_k(2)-b_k(2)\}d^3\mathbf{r}_1\, d^3\mathbf{r}_2$$

$$+\iint \{b_0(1)\}^2\frac{e^2}{r_{12}}\{a_t(2)+b_t(2)\}\{a_k(2)-b_k(2)\}d^3\mathbf{r}_1\, d^3\mathbf{r}_2.$$

We shall now make the approximation

$$(29)\quad \iint a_0(1)\{a_t(1)+b_t(1)\}\frac{e^2}{r_{12}}\{a_0(2)-b_0(2)\}\{a_k(2)-b_k(2)\}d^3\mathbf{r}_1\, d^3\mathbf{r}_2$$

$$\cong (1+I_{tt})\iint a_0(1)\, a_t(1)\frac{e^2}{r_{12}}\{a_0(2)-b_0(2)\}\{a_k(2)-b_k(2)\}d^3\mathbf{r}_1\, d^3\mathbf{r}_2,$$

$$I_{tt} = \int a_t(\mathbf{r})\, b_t(\mathbf{r})\, d^3\mathbf{r}.$$

The approximation (29) should not introduce a very large error; without it the evaluation of the matrix elements would be exceedingly difficult.

In evaluating the various integrals it is convenient to use elliptic coordinates ξ, η, ϕ referred to the nuclei A, B as foci:

$$r_{1A} = \tfrac{1}{2}R(\xi_1+\eta_1), \qquad r_{1B} = \tfrac{1}{2}R(\xi_1-\eta_1), \text{ etc.},$$

$$(30)\qquad d^3\mathbf{r}_1 = \tfrac{1}{8}R^3(\xi^2-\eta^2)d\xi\, d\eta\, d\phi,$$

$$(\mathbf{k}\,.\,\mathbf{r}) = (k_x\cos\phi+k_y\sin\phi)\tfrac{1}{2}R[(\xi^2-1)(1-\eta^2)]^{\frac{1}{2}}+\tfrac{1}{2}k_zR\xi\eta,$$

where k_z is the component of $\mathbf{k}$ along the AB or z-axis, and k_x, k_y are its components along two mutually perpendicular axes that are perpendicular to AB. The origin of the rectangular coordinates is the mid-point of the line AB.

It is very difficult to evaluate the matrix element $(\Psi(Z_u), V'\Psi(I_u))$ as it stands, even with the simplification (29). Thus we expand $(\Psi(Z_u), V'\Psi(I_u))$ in powers of k and consider only the first few terms. The physical justification for this comes essentially from the following consideration. From Fig. 2, we see that for the two transitions in question here, large values of k correspond to nuclear separations R_k very different from the equilibrium nuclear separation R_e. As pointed out before (following Eq. (16)), the rapid decrease of the probability of finding R at R with the increase in the distance $R - R_e$ will make the contribution to the capture cross section $\sigma_c(E_k)$ in (18) of fast electrons by $H_2^+(^2\Sigma_g)$ ion very small.

We see that the k-dependence of $(\Psi(Z_u), V'\Psi(I_u))/4N_{I_u}N_{Z_u}$ in Eq. (28) is that of

$$\sqrt{\Omega}.\{a_k(2) - b_k(2)\} = \cos\mathbf{k}\,.\,\mathbf{r}_{2A} - \cos\mathbf{k}\,.\,\mathbf{r}_{2B}$$

$$= 2\sin(\tfrac{1}{2}\mathbf{k}\,.\,\mathbf{R})\sin(\mathbf{k}\,.\,\mathbf{r}_2)$$

$$= k_zR(\mathbf{k}\,.\,\mathbf{r}_2) - \tfrac{1}{6}k_zR(\mathbf{k}\,.\,\mathbf{r}_2)^3 - \tfrac{1}{2^4}(\mathbf{k}\,.\,\mathbf{r}_2)(k_zR)^3 + \ldots .$$

We can see that in the lowest order only the k_z term does not vanish because none of the bound atomic orbitals in the U-process has any orbital angular

momentum, so that a_0, b_0, a_t, b_t are independent of ϕ. To show this, consider the simple case where $\mathbf{k} = (k_x, 0, 0)$, $(\mathbf{k} \cdot \mathbf{r}_2) = k_x \cos\phi$. (function of ξ_2, η_2), and the lowest order contribution to the matrix element becomes a volume integral of the form

$$\iiint d\xi\, d\eta\, d\phi\, k_x \cos\phi \text{ . (function of } \xi, \eta) = 0. \tag{31}$$

The corresponding term in k_y also vanishes in the lowest order, as can be seen by the same argument. However, the k_x and k_y terms do not automatically vanish in higher orders. In our investigation of the next term, which is of order k^4 in $a_k - b_k$, we restrict ourselves to the special case in which

$$\mathbf{k} \text{ is parallel to } AB, \text{ i.e. } \mathbf{k} = (0, 0, k_z). \tag{32}$$

The assumption (32) is not necessary for the lowest order term. The second (correction) term, however, is very lengthy to evaluate even with (32).

We can see from Eq. (23) that if we expand N_{I_u} in powers of k, we get

$$N_{I_u} \cong (1/k_z) + k_z + \ldots,$$

so that the normalized transition matrix element is given by an expression of the form

$$(\Psi(Z_u),\ V'\Psi(I_u)) \cong k_z + k_z^3 + \ldots,$$

where the coefficients are the sums and differences of a number of terms of the type

$$\int_1^\infty \xi^m e^{-\alpha\xi}\, d\xi \int_{-1}^{+1} \eta^n e^{-\beta\eta}\, d\eta$$

for various values of m, n, α, β. If we substitute the numerical value of this matrix element, evaluated at $R = R_e \cong 2a_0$, in Eq. (10), then we find the following expression for the capture cross section of the U-transition:

$$\begin{aligned} \sigma_U(R_e) &= u_0(k_z^2/k^3) - u_1(k_z^4/k^3) + O(k^3), \\ u_0 &= 5.38 \times 10^{-17} \text{ cm.}^2, \\ u_1 &= 6.30 \times 10^{-16} \text{ cm.}^2 \end{aligned} \tag{33}$$

where k is measured in units of a_0^{-1}, a_0 being the Bohr radius. The result for a few electron energies is given in Table I.

TABLE I

THE CROSS SECTION FOR THE G- AND U-TRANSITIONS ((25) IN THE TEXT) IN H_2 AS A FUNCTION OF ENERGY (σ_G HAS BEEN CALCULATED FOR THE CASE (38), AND σ_U FOR THE CASE (32))

Energy of incident electron, ev.		0	0.0258	0.10	1.16
Electron wave number, k, in a_0^{-1}		0	0.04355	0.08575	0.292
σ_G	in 10^{-16} cm.^{2}	0	7.9	15.5	53
σ_U	in 10^{-16} cm.^{2}	∞	12.3	6.28	1.84
Ratio $u_1 k_z^2/u_0$ for U-process*		0	0.022	0.086	1.0

*Both σ_G and σ_U are calculated from the first term in Eqs. (37) and (33) respectively. The next term in σ_U is taken into account by multiplying the value given above by $(1 - u_1 k_z^2/u_0)$. It is thus clear that the last column, corresponding to an energy of 1.16 ev., is entirely unreliable.

While neither the expansions in powers of k following (30) nor that in (33) are valid for large k, the result of using (33) in (18) is valid since the contribution to the capture cross section $\sigma_c(E_k)$ from fast electrons is rendered small by the weighting of the vibrational wave function and any inaccuracy in $\sigma_c(R_k)$ for large k is made unimportant.

That the cross section σ_U diverges as $1/k$ at low energies is simply the general behavior of a capture cross section; the physically relevant quantity is not the cross section but the transition probability per unit time, which is

$$v\sigma = \sigma\hbar k/m \to (\hbar/m)u_0 \text{ as } k \to 0, \tag{34}$$

i.e., it has a finite value for zero energy.

V. THE CROSS SECTION FOR THE G-TRANSITION

In evaluating the transition matrix element

$$(\Psi(Y_g), V'\Psi(I_g)) = \int \Psi^*(Y_g)\,\frac{e^2}{r_{12}}\,\Psi(I_g)\,d\tau, \tag{35}$$

we again use the properties (i), (ii) of the previous section, and an approximation similar to (29), to get the result

$$(\Psi(Y_g),\ V'\Psi(I_g))/4N_{Y_g}N_{I_g} = \tag{36}$$

$$\iint \{b_0(1)\}^2\,\frac{e^2}{r_{12}}\,\{a_s(2)-b_s(2)\}\{a_k(2)+b_k(2)\}d^3\mathbf{r}_1\,d^3\mathbf{r}_2$$

$$+(1+I_{00})\iint a_s(1)\,a_0(1)\,\frac{e^2}{r_{12}}\,\{a_0(2)-b_0(2)\}\{a_k(2)+b_k(2)\}d^3\mathbf{r}_1\,d^3\mathbf{r}_2.$$

If we again expand the matrix element in powers of k, we find that the lowest order term vanishes in the ϕ-integration, because now the only function containing ϕ is a_s or b_s; the argument is analogous to that of the previous section. In detail, the k-dependence of $(\Psi(Y_g),\ V'\Psi(I_g))/4N_{Y_g}N_{I_g}$ is that of

$$\begin{aligned}\sqrt{\Omega}\,.\,\{a_k(2)+b_k(2)\} &= 2\cos(\tfrac{1}{2}\mathbf{k}\,.\,\mathbf{R})\cos(\mathbf{k}\,.\,\mathbf{r}_2)\\ &= 2\{1-\tfrac{1}{8}(k_zR)^2-\tfrac{1}{2}(\mathbf{k}\,.\,\mathbf{r}_2)^2+\ \ldots\ \}\end{aligned}$$

and the lowest term that does not vanish upon integrating over ϕ is one of the type

$$k_xk_z\iint d\xi\,d\eta\ \times(\text{function of } \xi,\ \eta).$$

It is clear on physical grounds why only the k_xk_z term survives; the $\cos\phi$ term in a_s or b_s indicates that orbital angular momentum about the x-axis has to be excited (recall that a_s, b_s are $2p_x$ orbitals), and this is clearly impossible if the momentum of the incident electron is wholly along the z-axis AB.

No attempt has been made to calculate the next higher order term; thus to the lowest order in k we find that the capture cross section σ_G evaluated at $R = R_e \cong 2a_0$ is

$$\sigma_G(R_e) = g_0(k_x^2k_z^2/k^3)+O(k^3), \tag{37}$$

$$g_0 = 7.26\times10^{-14}\ \text{cm.}^2,$$

where k is again measured in units of a_0^{-1}. (Recall that the molecular axis AB defines the z-direction, while the orbital angular momentum of the $2p$ electron defines the x-direction.) The reason why σ_G vanishes for zero energy, unlike σ_U, is evidently that orbital angular momentum has to be excited in the G-transition but not in the U-transition.

VI. DISCUSSION

The capture cross section for both G- and U-transitions, evaluated at $R = R_e$, is listed in Table I for a few electron energies. The numerical values of the cross section clearly depend on the direction of the incident electron; thus σ_U has been calculated for the case (32) in which the initial direction of the electron momentum $\mathbf{k}$ is parallel to the nuclear axis AB, while σ_G has been calculated for the case

$$\mathbf{k} = (k/\sqrt{2}, 0, k/\sqrt{2}), \tag{38}$$

i.e., the electron is incident at an angle $\pi/4$ to the axis AB, and at an angle $\pi/4$ to the direction about which orbital angular momentum is excited during the G-transition. These particular directions are used simply because they give the maximum value for the corresponding cross section at any energy.

To recapitulate, it is to be emphasized that the present work must be regarded only as an estimation of the general order of magnitude of the cross sections of dissociative recombinations by carrying out a calculation for a hypothetical system. The model adopted is described by (12), (13) and in §III, which is not exactly the process (2) but is self-consistent from the point of view of the application of the perturbation theory. The most serious approximation is that of using plane waves in (20) for the electron in the continuum. As already mentioned below (20), this approximation has been made only because without it any calculations seem impracticable. It is difficult from purely theoretical considerations to say with definiteness by what factor the result is uncertain because of this approximation; but the general order of the cross sections (i.e., gas kinetic) obtained seems to be compatible with the empirical evidence in the case of helium (Biondi and Holstein 1951).

REFERENCES

BATES, D. R. and MASSEY, H. S. W. 1946. Proc. Roy. Soc. (London), A, **187**: 261.
BIONDI, M. A. 1951. Phys. Rev. **83**: 1078.
BIONDI, M. A. and HOLSTEIN, T. 1951. Phys. Rev. **82**: 962.
EYRING, H., WALTER, J., and KIMBALL, G. E. 1944. Quantum chemistry. John Wiley & Sons, Inc., New York. p. 203 ff.
SCHIFF, L. I. 1949. Quantum mechanics. McGraw-Hill Book Company, Inc., New York. p. 233.
TELLER, E. 1930. Z. Physik, **61**: 458.

THE RAMAN SPECTRUM OF CYCLOPROPANE[1]

By P. M. Mathai,[2] G. G. Shepherd,[3] and H. L. Welsh

ABSTRACT

The Raman spectra of gaseous and liquid cyclopropane were examined with high spectrographic dispersion. The resolved rotational spectrum of the gas gave $B_0 = 0.6697 \pm 0.0005$ cm.$^{-1}$. Although no rotational structure in the vibrational bands was resolved, the spectrum of the gas clarifies the frequency assignments. Nine of the ten Raman active frequencies were recorded; of particular interest are $\nu_1 = 3038.0$, $\nu_8 = 3019.9$, and $\nu_{13} = 1188.0$ cm.$^{-1}$. The inactive frequency ν_4 was assigned to a faint line at 1132.5 cm.$^{-1}$. The ζ constants of some of the degenerate vibrations were determined from the intensity contours of the bands. Comparison of the spectrum of the liquid with that of the gas shows how the former has led to incomplete vibrational assignments.

INTRODUCTION

Cyclopropane, C_3H_6, is the simplest of the cyclic hydrocarbons. Infrared and Raman data support the $\mathbf{D}_{3h}$ structure generally accepted by chemists; this structure has also been confirmed by the electron diffraction studies of Bastiansen and Hassel (1946) and Dunitz and Schomaker (1952). Of the fourteen fundamental vibrations (Table III) of the molecule ten (A_1', E', E'' species) are active in the Raman effect, six (A_2'', E') are active in infrared absorption, and two (A_1'', A_2') are inactive. The earlier investigations on the Raman and infrared spectra have been summarized by Herzberg (1945). More recently the infrared spectrum has been investigated, in some cases at high dispersion, by Sinha (1950), Neill (1953), Baker and Lord (1955), and Guenthard, Lord, and McCubbin (1956).

The Raman spectrum of liquid cyclopropane has been studied by a number of workers including Ananthakrishnan (1936), Harris, Ashdown, and Armstrong (1936), Linnett (1938), and Baker and Lord (1955). The Raman spectrum of the vapor has received less attention; Ananthakrishnan photographed four maxima, and Harris, Ashdown, and Armstrong one maximum.

In the present investigation the Raman spectra of the vapor and the liquid were photographed at high dispersion. Although rotational structure was resolved only in the pure rotational spectrum, the data obtained on the vibrational bands of the vapor have made significant additions to the vibrational assignments.

EXPERIMENTAL

The Raman source and the spectrograph have been described in detail (Welsh, Stansbury, Romanko, and Feldman 1955). With a cylindrical lens in front of the photographic plate the rotation-vibrational spectra of gases can be photographed with a reciprocal linear dispersion of 10.5 cm.$^{-1}$ per mm.

[1]Manuscript received July 30, 1956.
Contribution from the McLennan Laboratory, University of Toronto, Toronto, Ontario. This research was supported by Grant No. 1001-01, Project D46-10-01-01, of the Defence Research Board of Canada.
[2]Present address: Union Christian College, Alwaye, South India.
[3]Holder of a National Research Council Scholarship, 1954–56.

and a practical resolving power, at least in the case of non-polar molecules, of 1 cm.$^{-1}$. Commercial cyclopropane with a purity of 99.5% was used at a pressure of 3 atm. The spectrum of the liquid was photographed with the same high dispersion spectrograph and a Wood-type Raman tube, 10 mm. in diameter, with an illuminated section 10 cm. long. The tube was mounted vertically and gas from the storage cylinder was admitted through a copper capillary tube sealed in a constriction at the end of the tube with DeKhotinsky cement. At the temperature of the cold tap water which was circulated through the cooling jacket the vapor condensed at a pressure of 6.5 atm. The tube was irradiated by a vertical spiral mercury lamp with water-cooled electrodes.

An iron arc comparison was used to measure the frequency shifts of the maxima in the vibrational spectrum. A more accurate comparison for measuring the rotational Raman shifts was obtained by photographing the spectrum in juxtaposition with the rotational spectrum of oxygen.

RESULTS AND DISCUSSION

The Rotational Spectrum

The rotational spectrum was photographed without the cylindrical lens in front of the photographic plate in an exposure of 60 hr. on Kodak 103a-O spectroscopic plates with Hg 4358 as the exciting line. The frequency shifts were measured with a Hilger comparator by two observers and the results averaged. Table I gives the average of the corresponding Stokes and anti-

TABLE I

THE ROTATIONAL RAMAN SHIFTS OF C_3H_6

$\lvert\Delta\nu\rvert$, cm.$^{-1}$	Assignment	$\lvert\Delta\nu\rvert$, cm.$^{-1}$	Assignment
38.79	$S(13)$	68.21	$S(24)$
41.58	$S(14)$	70.93	$S(25)$
44.25	$S(15)$	73.63	$S(26)$
46.83	$S(16)$	76.27	$S(27)$
49.52	$S(17)$	78.77	$S(28)$
52.10	$S(18)$	81.45	$S(29)$
54.81	$S(19)$	84.12	$S(30)$
57.51	$S(20)$	86.92	$S(31)$
60.18	$S(21)$	89.57	$S(32)$
62.88	$S(22)$	92.28	$S(33)$
65.46	$S(23)$	94.65	$S(34)$

Stokes lines and the rotational assignments, $S(J)$. The S lines with lower J values and all of the R lines were obscured by halation of the plate in the neighborhood of the exciting line.

The Raman shifts of the S lines ($\Delta J = +2$) for the symmetric top model are

$$|\Delta\nu| = B_0(4J+6) - D_J(4J+6)(2J^2+6J+6) - D_{JK}(4J+6)K^2,$$

$J = 0, 1, 2, \ldots, K = 0, 1, 2, \ldots, J$, where $B_0 = h/8\pi^2 cI_B^\circ$ and the D's are small centrifugal stretching constants.* The term in D_{JK} will be neglected

*The nomenclature used corresponds in the main to that of Herzberg (1945).

since the small splitting to which it gives rise was not observable. The values of the rotational constants obtained from a least squares analysis of the data are $B_0 = 0.6697 \pm 0.0005$ cm.$^{-1}$ and $D_J = 0.83 \times 10^{-6}$ cm.$^{-1}$. The constant B_0 has been determined previously by several authors from the rotational structure of parallel infrared bands. The values obtained are 0.668 by Smith (1941), 0.664 by Sinha (1950), and 0.6696 ± 0.0028 cm.$^{-1}$ by Guenthard, Lord, and McCubbin (1956). The Raman value shows a very satisfactory agreement with the most recent and probably the most accurate of the infrared values.

The Vibrational Spectrum

Eight spectrograms of the vibrational Raman spectrum of the gas were obtained, but in none of these was any rotational structure apparent. The maxima observed for the vapor and the liquid are listed in Table II with

TABLE II

OBSERVED MAXIMA IN THE VIBRATIONAL RAMAN SPECTRA OF GASEOUS AND LIQUID C_3H_6

Frequency, cm.$^{-1}$		Assignment
Liquid	Gas	
	736.6	$\nu_{14}(e'')$ $^{P}Q_K$(max)
	741.4	$\nu_{14}(e'')$ $^{R}Q_K$(max)
867	866.0	$\nu_{11}(e')$
1131	1132.5	$\nu_4(a_1'')$
	1146.0	$\nu_{13}(e'')$ $^{P}O_K + {}^{P}P_K$(max)
1178	1177.7	$\nu_{13}(e'')$ $^{R}Q_K$(max)
	1198.5	$\nu_{13}(e'')$ $^{P}Q_K$(max)
1188	1188.2	$\nu_3(a_1')$
	1442.5	$\nu_9(e')$
	1454.0	$\nu_2(a_1')$, $2\nu_{14}(A_1')$
1502	1504.6	
2851	2866.7	$2\nu_9(A_1')$
2950	2959.5	$2\nu_2(A_1')$, $4\nu_{14}(A_1')$
	3014.8	
3009	3018.5	$\nu_8(e')$ $^{S}Q_K$(max)
	3021.4	$\nu_8(e')$ $^{O}Q_K$(max)
	3036.0	
3027	3038.0	$\nu_1(a_1')$
	3075.0	
3073	3089.8	$\nu_{12}(e'')$ $^{R}Q_K$(max)
	3109.0	$\nu_{12}(e'')$ $^{P}Q_K$(max) $^{P}S_K + {}^{P}R_K$(max)

assignments based on the discussion given below. The frequencies were measured from the microphotometer traces of several spectrograms taken with different exposure times, which for the vapor varied from 3 to 100 hr. and for the liquid from 1 to 12 hr. In Figs. 1 and 2 microphotometer traces of the vapor and liquid spectra are reproduced.

The Totally Symmetric Bands

The three totally symmetrical Raman frequencies ν_1, ν_2, and ν_3 have been fairly well identified in the spectrum of the liquid from depolarization measurements. However, the high dispersion spectrum of the gas permits a greater precision in the assignments.

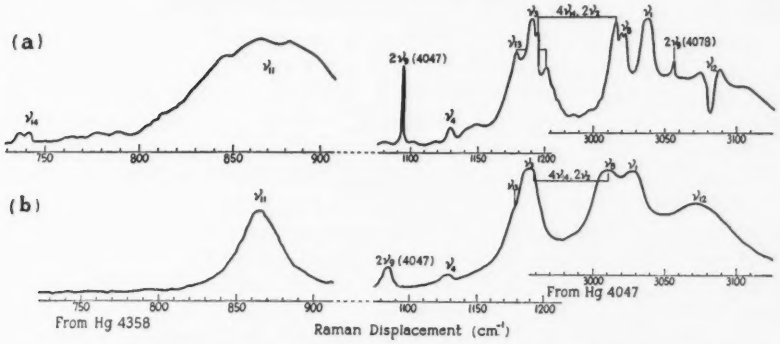

FIG. 1. Microphotometer traces of the vibrational Raman spectra of gaseous (*a*), liquid (*b*), cyclopropane in the 700–1200 cm.$^{-1}$ region from Hg 4358 and the 2950–3100 cm.$^{-1}$ region from Hg 4047. Unless otherwise indicated, the frequency scales refer to bands directly above them.

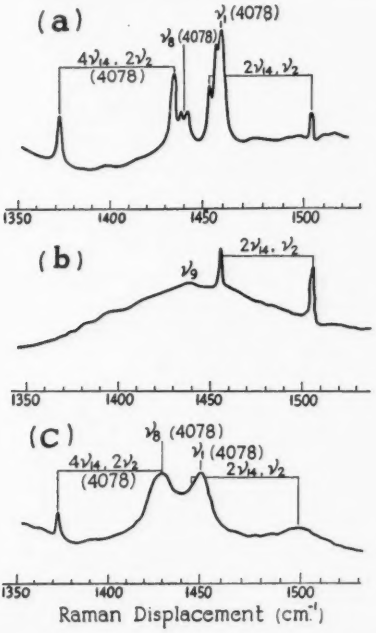

FIG. 2. Microphotometer traces of the vibrational Raman spectra of gaseous (*a*, *b*) and liquid (*c*) cyclopropane. In (*b*) a filter solution ($NaNO_3$) was used to remove Hg 4047 and Hg 4078 from the exciting radiation.

The single band at 1188 cm.$^{-1}$ in the liquid has been identified as the C_3 ring breathing frequency, ν_3. In the gas the maximum occurs at the same frequency but is accompanied by two satellite bands at 1177.7 and 1198.5

cm.$^{-1}$. At first sight these appear to be the maxima in the rotational wings of ν_3, but an intensity calculation shows that the separation of the maxima is too small. They are therefore assigned to the maxima in the ${}^RQ_K$ and ${}^PQ_K$ branches of the degenerate band ν_{13} (e''). This band should occur in this region but has not been identified previously. In the liquid the two maxima merge because of the hindered rotation, so that the single strong band observed in the liquid is in fact a superposition of ν_3 and ν_{13}. A barely detectable shoulder at 1178 cm.$^{-1}$ in the liquid spectrum may be the single maximum of ν_{13}. The fact that the 1177.7 cm.$^{-1}$ maximum is slightly more intense than that at 1198.5 cm.$^{-1}$ in the vapor spectrum is probably caused by the fact that the ν_3 band of $C_2{}^{12}C^{13}H_6$ is superimposed on it; a simple calculation shows that the frequency of the isotopic molecule is near 1175 cm.$^{-1}$.

The symmetrical CH_2 deformation frequency ν_2 is assigned to the two sharp lines in the gas at 1454.0 and 1504.6 cm.$^{-1}$. The splitting of the frequency is due to a Fermi degeneracy with $2\nu_{14}(A_1')$, the fundamental of which is at 738.8 cm.$^{-1}$. In Fig. 2(*b*) it is seen that the intensities of the two lines are almost equal, so that the Fermi degeneracy is practically exact. The unperturbed frequency of ν_2 is therefore 1479 cm.$^{-1}$, and the components of the doublet cannot be given even approximately the separate assignments, ν_2 and $2\nu_{14}$.

The symmetrical stretching frequency ν_1 has been identified by previous investigators with the strong doublet at 3027 and 3009 cm.$^{-1}$ in the liquid; however, the assignment is complicated by the occurrence in this region of ν_8 which is both infrared and Raman active. The spectrum of the gas in Fig. 1 clarifies the situation. As shown below, the two maxima at 3018.5 and 3021.4 cm.$^{-1}$ are almost certainly the maxima of the Q_K branches of ν_8. The ν_1 frequency therefore corresponds to the strong band at 3038.0 cm.$^{-1}$ in the gas. In Fermi degeneracy with ν_1 are ($2\nu_2$, $4\nu_{14}$) at 3014.8 and 2959.5 cm.$^{-1}$. The components of ($2\nu_2$, $4\nu_{14}$) have comparable intensities as in the (ν_2, $2\nu_{14}$) doublet. The occurrence here of a third overtone, unusual in the Raman effect, is a consequence of the close resonance of ν_2 and $2\nu_{14}$. The high dispersion spectrograms explain the observation of Ananthakrishnan (1936) that the 3009 and 3027 cm.$^{-1}$ lines of the liquid show a remarkable change in relative intensity in passing to the vapor; the major part of the intensity of the 3009.5 cm.$^{-1}$ line of the liquid is due to the ν_8 band, and this part of the intensity spreads out over a large frequency region when the molecule is freely rotating in the vapor.

In light exposures the Q branch of ν_1 was found to be accompanied by a weaker satellite shifted by 2 cm.$^{-1}$ towards lower frequency values; this is seen most clearly in the ν_1 band excited by Hg 4078 in Fig. 2. The "satellite" may be caused by a perturbation of some of the intermediate J levels of the upper state of ν_1, leading to a break in the degraded intensity of the Q branch.

The Doubly Degenerate Bands

If cyclopropane has $\mathbf{D}_{3h}$ symmetry, as has been assumed, there should be four Raman active vibrations of the species E' and three of the species E'';

the E' vibrations are also infrared active. As shown by Placzek and Teller (1933) and Herzberg (1945), the selection rules are $\Delta J = 0, \pm 1, \pm 2$ for both species, $\Delta K = \pm 2$ for the E' species, and $\Delta K = \pm 1$ for the E'' species. The E' bands therefore consist of a series of subbands with ${}^{O}Q_K$ and ${}^{S}Q_K$ branches, where the superscripts O and S refer to the transitions $\Delta K = -2$ and $\Delta K = +2$, respectively, each of these Q_K branches being accompanied by O, P, R, and S branches corresponding to the transitions $\Delta J = \pm 1, \pm 2$. The structure of the E'' bands is similar except that the Q_K branches must be labelled ${}^{P}Q_K$ and ${}^{R}Q_K$. The structure of the degenerate bands is thus very complicated, and individual transitions, $(J', K'-J'', K'')$, can be resolved only in light molecules. However, it might be expected that the Q_K branches would appear as resolved lines superimposed on a practically continuous background formed by the O, P, R, and S branches of subbands. The frequencies of the Q_K branches are given by the formulae:

$$E' \text{ species: } \nu_0^{\text{sub}} = \nu_0 + 4[A(1+\zeta) - B] \pm 4[A(1+\zeta/2) - B]K,$$

$$E'' \text{ species: } \nu_0^{\text{sub}} = \nu_0 + [A(1-2\zeta) - B] \pm 2[A(1-\zeta) - B]K.$$

In these expressions ν_0 is the band origin, and ζ the vibrational angular momentum of the particular degenerate vibration considered; it is assumed that $A' = A'' = A$ and $B' = B'' = B$. The plus sign in the third term on the right-hand side of the equations holds for $\Delta K = 1, 2$, and the minus sign for $\Delta K = -1, -2$. It should be noted, however, that each of the Q_K branches is composite since it contains all transitions, $\Delta J = 0$, for a series of J values; if $B' \neq B''$, the components are displaced by the amounts $(B'-B'')J(J+1)$.

In the spectrograms obtained no resolution of the individual Q_K branches was apparent for any of the degenerate bands. In some cases this may be caused by the spacing $4[A(1+\zeta/2) - B]$ or $2[A(1-\zeta) - B]$ being too small, or by the fact that $(B'-B'')$ is sufficiently different from zero. However, some of the bands show two maxima which must be identified with the maxima in the two series of Q_K branches present in each case. In principle, if the A and B values are known for the molecule, the distance between these maxima can be used to determine the value of ζ for the corresponding vibrational form. Since the lines in the Q_K series are to a first approximation equidistant, the intensity profile of the unresolved band corresponds to the envelope of the intensities of the individual lines. A calculation of the theoretical intensities can thus be used to calculate approximate values of ζ and ν_0 for the band.

The intensity of a Q_K branch is given by the expression

$$I(Q_K) = C\nu^4 \sum_{J=K^*}^{\infty} I(J, K) = C\nu^4 \sum_{J=K^*}^{\infty} g_{JK} B_{JK} \exp(-F(J, K)hc/kT),$$

where C is a constant which determines the absolute intensity, ν the frequency which may be assumed constant over the band, g_{JK} the statistical weight, and B_{JK} the transition probability derived by Placzek and Teller (1933) in terms of J and K. The rotational energy, of the ground vibrational state, $F(J, K)$, is given by:

$$F(J, K) = B_0 J(J+1) + (A_0 - B_0)K^2,$$

where $K = 0, 1, 2, \ldots$, and $J = K, K+1, K+2, \ldots$. The summation over the J value from $J = K^*$ to $J = \infty$ in the intensity formula is slightly different for the various Q_K branches: for ${}^{O}Q_K$ and ${}^{P}Q_K$, $K^* = K$; for ${}^{R}Q_K$, $K^* = K+1$; for ${}^{S}Q_K$, $K^* = K+2$. The statistical weights g_{JK} for cyclopropane have been determined by Wilson (1935). In addition to the usual factor, $(2J+1)$, g_{JK} has a second factor which gives an intensity alternation in K of 20:20:24 for $K = 3n-2, 3n-1, 3n$, where n is an integer. For the $K = 0$ line there is an additional intensity alternation in J of 8:16.

The intensity calculations were carried out on FERUT, the electronic digital computer of the Computation Centre, University of Toronto. Since it was not known how rapidly the summation in J would converge, it was arranged for the computer to terminate the series automatically when the ratio $I(J, K):I(Q_K)$ became less than 1:100. For the ${}^{O}Q_K$ and ${}^{S}Q_K$ lines, about thirty J values were required; for the ${}^{R}Q_K$ and ${}^{P}Q_K$ lines, about twenty. The values used for the rotational constants were $B_0 = 0.6697$ cm.$^{-1}$, as determined in this investigation, and $A_0 = 0.423$ cm.$^{-1}$, calculated from the C—C distance 1.52 Å, the C—H distance, 1.08 Å, and the H—C—H angle 118°, determined from electron diffraction data (Bastiansen and Hassel 1946).

The results of the intensity calculations are shown in Fig. 3 as plots of $I(Q_K)$ against K, for the E' and E'' series. The K value for the maximum for each series can be read off from the graphs, and the relations between the separation of the maxima in the series of Q_K branches, $\Delta\nu_{PR}$ or $\Delta\nu_{OS}$, and the ζ constant can then be calculated. The relations are $\Delta\nu_{OS} = -4.95+4.24\zeta$ for the E' species, and $\Delta\nu_{PR} = -9.88-16.92\zeta$ for the E'' species. These

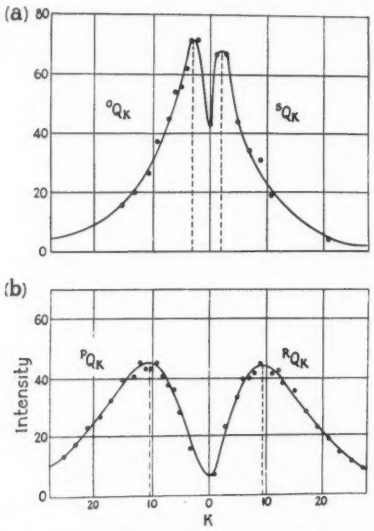

FIG. 3. Calculated relative intensities of the Q_K branches of C_3H_6 as a function of K for (*a*) the E' vibrational species, (*b*) the E'' species.

equations are given in graphical form in Fig. 4. It will be noted that for the E' species the separation can vary from -0.7 to -9.2 cm.$^{-1}$, and for the E'' species, from -26.8 to $+7.0$ cm.$^{-1}$. A negative value of $\Delta\nu$ means that the ${}^{O}Q$ (or ${}^{P}Q$) branch is on the high frequency side of ν_0 and the ${}^{S}Q$ (or ${}^{R}Q$) branch

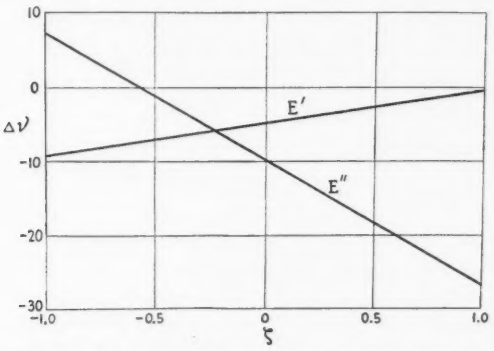

FIG. 4. The separation of the maxima in the Q_K branches, $\Delta\nu$, of C_3H_6 as a function of ζ for the E' and E'' species.

on the low frequency side; this reversal of the usual situation can occur because $A-B$ is negative for cyclopropane. The observed magnitude of $\Delta\nu$ can be used in some cases to identify the species. Thus, the spacings of the 1177.7 and 1198.5 cm.$^{-1}$ maxima and of the 3075.0 and 3089.8 cm.$^{-1}$ maxima show that these must be E'' bands.

The band origin, ν_0, of a degenerate band is approximately, but not exactly, halfway between the maxima in the Q subbranches. From the formulae for $\nu_0{}^{\text{sub}}$ and the K values for the maxima determined from Fig. 3, it can easily be shown that the band origins are given by:

$$E' \text{ species: } \nu_0 = \tfrac{1}{2}({}^{O}Q_K{}^{\max} + {}^{S}Q_K{}^{\max}) - 2A - 3A\zeta + 2B,$$

$$E'' \text{ species: } \nu_0 = \tfrac{1}{2}({}^{P}Q_K{}^{\max} + {}^{R}Q_K{}^{\max}) + A - B.$$

Of the four E' bands, which are both infrared and Raman active, only ν_8, ν_9, and ν_{11} were observed. The ν_8 band, with maxima at 3018.5 and 3021.4 cm.$^{-1}$, shows the unresolved Q branch pattern of Fig. 3, and the analysis gives $\zeta = 0.49$ and $\nu_0 = 3019.9$ cm.$^{-1}$. The band which has been associated with ν_8 in infrared absorption shows a single Q branch maximum with accompanying P and R maxima. According to the high dispersion infrared work of Smith (1941) the Q branch maximum is at 3024 cm.$^{-1}$, thus showing a discrepancy of some 4 cm.$^{-1}$ with the Raman observations. Since it is fairly certain that neither the Raman nor the infrared frequency can have an experimental error of this magnitude, it is suggested that the infrared band might be assigned to the combination tone $2\nu_{10}+\nu_5(E')$, which has the approximate frequency $2\times1028.4+963 = 3020$ cm.$^{-1}$. It is realized that this interpretation involves the assumption that the combination tone $2\nu_{10}+\nu_5$ has a greater infrared intensity than the fundamental ν_8 band; however, this seems more reasonable

than ascribing the Raman band to a high order combination tone. The Coriolis constant, $\zeta_8 = 0.49$, obtained from the Raman analysis, appears too high for a C—H stretching vibration and shows poor agreement with the value, $0 < \zeta_8 < +0.05$, calculated by Guenthard, Lord, and McCubbin (1956) from a normal coordinate treatment of the molecule. The calculated value of ζ_8 would require the separation of the Q_K maxima to be 4.5 cm.$^{-1}$, whereas the measured value is 2.9 cm.$^{-1}$. The discrepancy may well be caused by a slight displacement of the maxima by a difference in the rotational constants of the upper and lower vibrational states.

The ν_9 band is very weak and could be observed only when the 3000 cm.$^{-1}$ lines excited by Hg 4078 were removed by a filter; it consists of a single broad maximum at 1442.5 cm.$^{-1}$. The ν_{11} band shows in the vapor a single broad maximum at 866 cm.$^{-1}$, flanked by two weaker maxima about 37 cm.$^{-1}$ apart. The latter obviously correspond to the maxima in the rotational wings. In neither of these bands were two Q_K maxima observed, although the calculated values of $\Delta\nu_{OS}$ are -4.4 and -9.0 cm.$^{-1}$, using the ζ constants of Guenthard, Lord, and McCubbin (1956). It must therefore be concluded that the proposed method for obtaining values from the band contours is unsatisfactory when the spacing of the Q_K maxima is small, as in the E' bands of cyclopropane.

All three E'' bands were observed. The ν_{12} band (Fig. 1) shows the expected contour, and the separation of the Q_K maxima at 3075.0 and 3089.8 cm.$^{-1}$ gives $\zeta = 0.29$ and $\nu_0 = 3082.2$ cm.$^{-1}$. The subsidiary maximum at 3109.0 cm.$^{-1}$ corresponds to the maximum in the high frequency rotational wing.

The CH_2 rocking frequency ν_{13} has not been previously observed, although estimates of its frequency have been made by various authors. Linnett (1938) suggested the value 1250 cm.$^{-1}$, to account for the 382 cm.$^{-1}$ line observed by Harris, Ashdown, and Armstrong (1936) as the difference tone $\nu_{13}-\nu_{11}$. Saksena (1939) predicted the value 1252 cm.$^{-1}$ from a normal coordinate calculation. Kistiakowsky and Rice (1940) interpreted the 382 cm.$^{-1}$ line* as $\nu_{13}-\nu_{14}$ which gives 1125 cm.$^{-1}$ for ν_{13}; this value was considered to be more in line with the specific heat data. In the present study ν_{13} is identified with the two maxima, 1177.7 and 1198.5 cm.$^{-1}$, which occur on either side of the ν_3 line in the vapor spectrum; the analysis gives $\zeta_{13} = 0.63$ and $\nu_0 = 1188.0$ cm.$^{-1}$. The band origin thus coincides with the maximum of the ν_3 band. The broad weak maximum at 1146 cm.$^{-1}$, which is not present in the liquid spectrum, can be assigned to the maximum in the overlapping ${}^RO_K$ and ${}^RP_K$ branches.

The ν_{14} band appears as a weak doublet at 736.6 and 741.4 cm.$^{-1}$ in the spectrum of the vapor. The separation of the maxima, 4.8 cm.$^{-1}$, allows two values of ζ_{14}, -0.86 or -0.29, according as $\Delta\nu_{PR}$ is taken as a positive or negative quantity. From the discussion of the ζ sum rule which follows, the value -0.86 appears more satisfactory and gives $\nu_0 = 738.8$ cm.$^{-1}$.

*This line was not observed in the present investigation. However, it may well be real and can be assigned to $\nu_1-\nu_{11}$, which would have the frequency $1132-738 = 394$ cm.$^{-1}$ in the vapor. This difference band should also be active in infrared absorption.

According to Lord and Merrifield (1952) and Boyd and Longuet-Higgins (1952), the ζ sum rule for the E'' vibrations of C_3H_6 is

$$\zeta_{12}+\zeta_{13}+\zeta_{14} = -1+B/2A = -0.21.$$

The observed sum is $\zeta_{12}+\zeta_{13}+\zeta_{14} = 0.06$ or 0.63 according as ζ_{14} is taken as -0.86 or -0.29; it thus appears that $\zeta_{14} = -0.86$ is more probable. The discrepancy between the theoretical and experimental ζ sums is a measure of the accuracy of the procedure used for obtaining ζ constants from unresolved E'' Raman bands. The error in the individual ζ constants is probably not greater than ± 0.10. The method seems therefore to be a useful contribution to the problem of obtaining molecular constants from unresolved Raman and infrared bands, a problem which will be of particular importance for heavier molecules.

The Inactive Frequencies

A very weak but unmistakable maximum occurs at 1132.5 cm.$^{-1}$ in the gas; it is less well-defined in the liquid (Fig. 1). Since all infrared and Raman active fundamentals can be accounted for otherwise, and since no overtone or combination band occurs in this region, the line must be ascribed to one of the inactive fundamentals, $\nu_4(a_1'')$ and $\nu_5(a_2')$. Baker and Lord (1955) have found that the values 1125 and 975 cm.$^{-1}$ for ν_4 and ν_5, respectively, give the best assignment of the infrared combination tones; the 1132.5 cm.$^{-1}$ line will therefore be assigned to $\nu_4(a_1'')$. Its activity in the Raman effect can be ascribed to either a Coriolis interaction with nearby frequencies or to an "upper-stage" transition, presumably, $(\nu_{14}+\nu_4)-\nu_{14}$.

The identification of ν_4 leads to the frequency of ν_5. A parallel infrared band at 2095.7 cm.$^{-1}$ is assigned by Baker and Lord (1955) to either $\nu_4+\nu_5$ or $2\nu_{13}$. On the basis of the present investigation, $2\nu_{13}$ is excluded as a possibility; the combination band thus gives 963 cm.$^{-1}$ for ν_5.

CONCLUSIONS

Table III contains a summary of the fundamental frequencies of C_3H_6 in the vapor state. All of the frequencies have now been determined directly from Raman and infrared spectra, except the inactive ν_5 whose frequency is estimated from an infrared overtone band. There is perhaps some doubt about the description of the bands; for example, ν_{13} and ν_{14} may eventually be interchanged. However, those questions can probably be settled by a normal coordinate calculation now that a complete set of fundamental frequencies is available.

The investigation of cyclopropane has illustrated some potentialities of high dispersion Raman spectra of gases, even when the rotational structures of the vibrational bands are not resolved. Because of the hindering of molecular rotation in liquids there is usually no marked difference between the shapes of degenerate and non-degenerate bands of symmetric top molecules. It is therefore necessary to depend on depolarization measurements, and these do not always lead to reliable vibrational assignments. Thus, in liquid cyclopropane the 1188 cm.$^{-1}$ band is really a superposition of ν_3 and ν_{13}, and the

TABLE III

FUNDAMENTAL FREQUENCIES OF CYCLOPROPANE IN THE VAPOR STATE

Designation	Species	Description	Activity	Frequency	
				Raman	Infrared*
ν_1	A_1'	CH stretching	R	3038.0(Q)	
ν_2	A_1'	CH_2 deformation	R	1504.6(Q) 1454.0(Q)	
ν_3	A_1'	C_3 ring breathing	R	1188.0(Q)	
ν_4	A_1''	CH_2 twisting	Inactive	1132.5(Q)	
ν_5	A_2'	CH_2 bending	Inactive		(963)†
ν_6	A_2''	CH stretching	I		3102.0(Q)
ν_7	A_2''	CH_2 rocking	I		854.0(Q)
ν_8	E'	CH stretching	I, R ($\Delta K = \pm 2$)	3019.9(ν_0)	3028.1(Q)
ν_9	E'	CH_2 deformation	I, R ($\Delta K = \pm 2$)	1442.0(max)	1441.8(Q)
ν_{10}	E'	CH_2 bending	I, R ($\Delta K = \pm 2$)	-----	1028.6(Q)
ν_{11}	E'	C_3 ring deformation	I, R ($\Delta K = \pm 2$)	866.0(max)	868.5(Q)
ν_{12}	E''	CH stretching	R ($\Delta K = \pm 1$)	3082.2(ν_0)	
ν_{13}	E''	CH_2 rocking	R ($\Delta K = \pm 1$)	1188.0(ν_0)	
ν_{14}	E''	CH_2 twisting	R ($\Delta K = \pm 1$)	738.8(ν_0)	

*The infrared frequencies are taken from Baker and Lord (1955).
†Derived from the infrared combination band $\nu_4+\nu_5 = 2095.5$ cm.$^{-1}$

3009.5 cm.$^{-1}$ band is mainly ν_8 with $2\nu_2$ superimposed; these facts could not be established from depolarization measurements, however accurate. One therefore suspects that many vibrational assignments made from the Raman spectra of liquids are spurious, or at least incomplete, especially in more complex molecules. In the spectra of gases the difference in appearance of degenerate and non-degenerate bands is so marked that mistakes in identification must be much less frequent. In addition, the intensity contours of unresolved degenerate bands can be turned to good account in distinguishing degenerate species and in the calculation of approximate ζ constants, provided the spectrographic dispersion is high enough to separate the Q_K maxima. In this respect, Raman spectra have an advantage over infrared spectra since, in the latter, the Q_K branches have only a single intensity maximum.

ACKNOWLEDGMENTS

The authors are indebted to Professor W. H. Watson, Director of the Computation Centre, University of Toronto, for the use of computing facilities. They wish to thank Professor R. C. Lord for the opportunity of examining the paper by Guenthard, Lord, and McCubbin (1956) in advance of publication, and Professor G. B. B. M. Sutherland for the loan of the 1953 thesis of Dr. H. W. Neill.

REFERENCES

ANANTHAKRISHNAN, R. 1936. Proc. Indian Acad. Sci. A, **4**: 82.
BAKER, A. B. and LORD, R. C. 1955. J. Chem. Phys. **23**: 1636.
BASTIANSEN, O. and HASSEL, O. 1946. Tidsskr. Kjemi, Bergvesen Met. **6**: 71.
BOYD, D. R. J. and LONGUET-HIGGINS, H. C. 1952. Proc. Roy. Soc. (London), A, **213**: 55.
DUNITZ, J. D. and SCHOMAKER, V. 1952. J. Chem. Phys. **20**: 1703.
GUENTHARD, H. H., LORD, R. C., and MCCUBBIN, T. K. 1956. J. Chem. Phys. **25**: 768.
HARRIS, L., ASHDOWN, A. A., and ARMSTRONG, R. T. 1936. J. Am. Chem. Soc. **58**: 852.
HERZBERG, G. 1945. Molecular spectra and molecular structure. Vol. II. Infrared and Raman spectra of polyatomic molecules. D. Van Nostrand Company, Inc., New York.

KISTIAKOWSKY, G. B. and RICE, W. W. 1940. J. Chem. Phys. **8**: 610.
LINNETT, J. W. 1938. J. Chem. Phys. **6**: 692.
LORD, R. C. and MERRIFIELD, R. E. 1952. J. Chem. Phys. **20**: 1348.
NEILL, H. W. 1953. Ph.D. Thesis, University of Michigan, Ann Arbor, Mich.
PLACZEK, G. and TELLER, E. 1933. Z. Physik, **81**: 209.
SAKSENA, B. D. 1939. Proc. Indian Acad. Sci. A, **10**: 449.
SINHA, S. P. 1950. J. Chem. Phys. **18**: 217.
SMITH, L. G. 1941. Phys. Rev. **59**: 924.
WELSH, H. L., STANSBURY, E. J., ROMANKO, J., and FELDMAN, T. 1955. J. Opt. Soc. Amer. **45**: 338.
WILSON, E. B., JR. 1935. J. Chem. Phys. **3**: 276.

THICKNESS CONTROL OF THIN LAYERS[1]

By A. C. S. van Heel

ABSTRACT

Observation of path differences by means of an interferometric arrangement making use of birefringent crystals has been described by M. Françon. Important advantages of the method are the fact that the interferometric part is concentrated in the eyepiece, and its ruggedness, the interference taking place within the crystal plates. It can therefore be adapted to other purposes than microscopic observation. Only those objects that are lying within the depth limits of the field give an observable effect. With the use of a large aperture object glass, this depth can be kept within narrow limits. Thus the effect of phase objects outside the sharp field is of no or slight influence. This means that the object to be studied can be placed between glass plates of bad quality. In consequence we can measure the thickness of coatings in a vacuum, that is, during the operation of evaporation. The light enters and leaves the vacuum vessel through windows of thick plate glass. The light source and the interference eyepiece are mounted outside the vessel. The measurement of the thickness of the coating is effected by means of a plane-parallel glass plate, placed in a non-parallel part of the light pencil. With white light the field is divided in sections of different colors, which may serve to measure the thickness of the layer (with reference to a screened part of the same surface on which no layer is formed). A better way is to observe in monochromatic light. It proved possible to measure simultaneously the thickness and the absorption of a layer.

1. Observations of path differences by an interferometric arrangement employing birefringent crystals has been described by M. Françon (1952, 1953, 1954). It has an advantage over the Michelson type of interferometer, that interference takes place within the crystal, thus obviating very accurate setting of the optical parts, and over both the Michelson and the Fabry-Pérot types, that the interferometer is concentrated in the eyepiece; its sensitivity is comparable to that of the Fabry-Pérot type.

There are two points that make further research with the crystal interferometer promising. In the first place a type of measurement other than matching or even remembrance of color must be introduced in order to make it acceptable for current use. In the second place it is clear that phase differences in the object space only produce an appreciable change of color in the otherwise one-colored field of view when the objects producing the phase differences are not too far from the plane on which focusing has taken place. The further the phase object recedes from the focusing plane, the more the irregularities of the wave front produced by it spread out. This implies that glass plates of non-optical quality may be introduced in the light path, provided they are not near the object being studied.

In the following a setup is described to measure the thickness of coatings in a vacuum vessel. The light enters and leaves the vacuum vessel through thick slabs of plate glass, and it is possible to follow the increasing thickness of a thin layer during the process of evaporation.

2. In Fig. 1, C is the source producing the vapor. A mirror M_3 is coated at the same time as the objects to be coated (not shown in the figure). By means

[1]Manuscript received July 13, 1956.
Contribution from the Laboratory for Technical Physics, Delft, Holland.

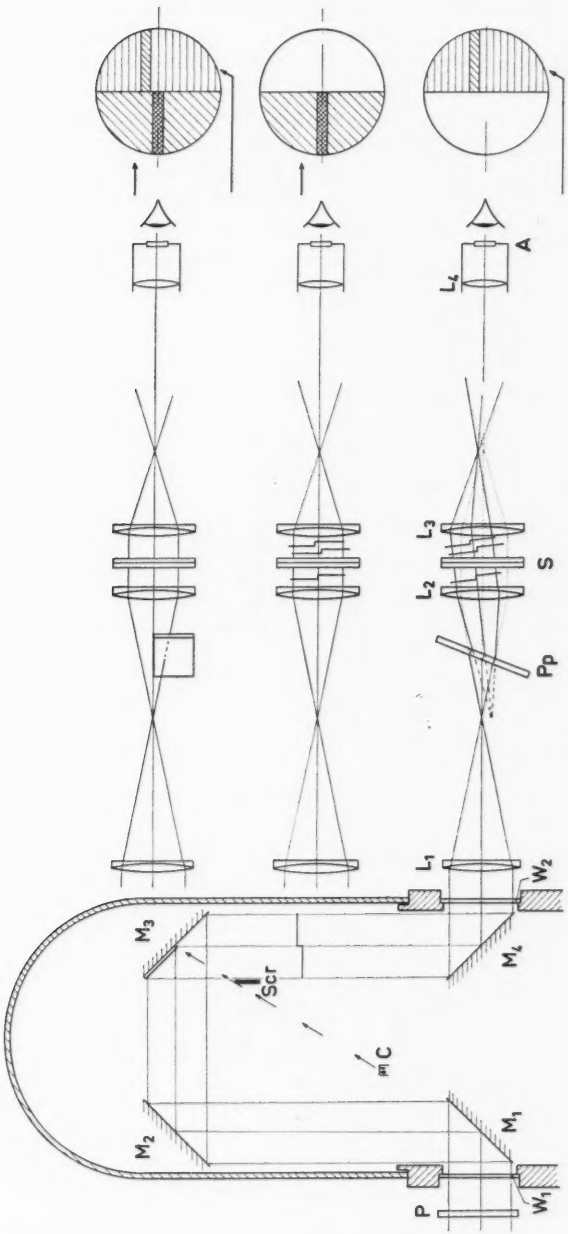

FIG. 1. The illuminating pencil.

of a screen Scr one-half of M_3 is prevented from being coated by the vapor stream. On this mirror a step is produced of which the thickness is a measure of the coatings on the other objects being treated. In order to get a sharp step, the vacuum must be good, a few parts in 10^{-6} mm. Hg. The distance CM_3 is about 0.5 meter and the screen is only a few millimeters from M_3.

Light entering the window W_1 leaves the vacuum vessel at W_2. The lens L_1 forms an image of the step at Pp where a plane-parallel plate is put, the use of which is explained below. The image of the step is projected by the lenses L_2 and L_3 to the front focal plane of the eyepiece L_4. Between L_2 and L_3 a Savart plate S is introduced. A polarizing filter is placed before this; another polarizing filter A, acting as an analyzer, is put before the eye. An auxiliary crystal plate can be placed between L_4 and A.

The illuminating pencil of light, coming from a slit and collimating lens, is shown in Fig. 1; it is a parallel pencil in the vacuum vessel. The lens L_1 forms an image of the slit in its back focal plane. Between the lenses L_2 and L_3 the beam is parallel again.

Half of the plane wave, reflected by M_3, is retarded by the step on M_3 with reference to the half from the uncoated part. Its form is illustrated by the stepped line between L_2 and S. The Savart plate S forms two waves of the same form. The path difference between these two is determined by the inclination of the pencil incident on S. At the same time the two waves are displaced with reference to one another in a lateral direction. This is illustrated by the two stepped lines between S and L_3. In the portion of the field containing the step an additional path difference is introduced by the step. Thus the "main" field has a certain color and is crossed by a strip of another color, as illustrated by Fig. 2, where the lenses are not shown and the directions of vibration have been indicated.

The inclination of the incident wave on S is altered in a way that is easily measured by means of the plane-parallel glass plate Pp, which shifts the image of the slit laterally, when it is not perpendicular to the axis of the pencil. This

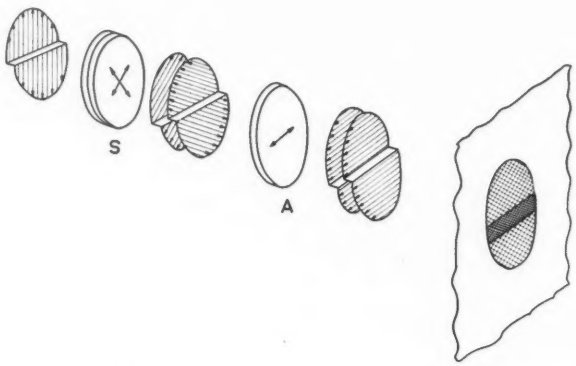

FIG. 2. Formation of the two interfering waves.

plate of thickness 1 mm. makes it possible to change the path difference between the two waves by, say, two wavelengths, when turned through an angle of 90°. In the lower part of Fig. 1 the plate Pp is to be imagined present behind the plane of the drawing. It gives rise to what is seen in the right half of the field of view (lowest circle, right half). The left half of the field of view has other colors, since it lacks the plane-parallel plate (see Fig. 1, center circle, with corresponding drawing of the light rays). The upper circle in Fig. 1 shows the combination of the two halves of the field of view; the (upper) drawing of the light rays gives a side view of the optics from L_1 to the eye.

3. Turning the plane-parallel plate Pp not only influences the colors but also shifts the strip, as can be seen from Figs. 4, 5, and 6, which show the field of view at different settings of the plane-parallel glass plate. In Fig. 4 the last plate is perpendicular to the pencil; both halves of the field are equal. In Fig. 5 the plane-parallel plate has been turned. It is possible to find a position of Pp such that the "main" field of one half of the field of view has the same color as the strip in the other half of the field of view (see Fig. 6). This way of matching gives very reproducible results when absorption of the coating is not appreciable; otherwise it fails because precision of matching is too much impaired.

4. It is easily possible to devise an instrument so that the path difference produced by the step is observable as a displacement in the field of view. For that purpose a second Savart plate followed by a polarizing filter replaces the analyzer, as has been suggested by Françon in 1951. Fig. 7 shows the results with a step of about $\lambda/4$. It is readily seen that precise measurements are practically excluded by the broadness of the maxima and minima. Attempts to improve this by introducing two, three, or even four auxiliary Savart plates

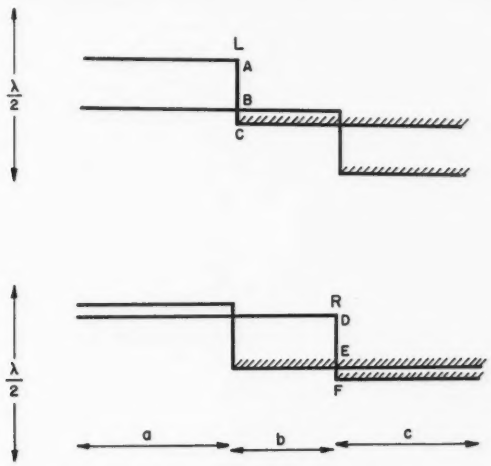

FIG. 3. Effect of absorption in the step.

instead of one and at the same time making the plane-parallel plate Pp cover the whole aperture—as in Figs. 8 and 9—failed to give satisfactory results.

5. In the end we returned to the first method but used monochromatic light (a super-high-pressure mercury lamp with green filter). At the same time we arranged for the plane-parallel plate Pp to cover the whole field of view. In this way the strip could be photometrically matched to the "main" field. It was immediately apparent that this could not be done at the same time for both the right and the left side of the strip, because absorption of the coating makes circumstances different at the right and left side.

This can be understood by inspection of Fig. 3, where the two waves are drawn in a particular case, the step being 0.1786 of a wavelength and the absorption of the step being 0.32. At L the left side *a* of the field is matched with the strip *b*. Those parts of the two interfering waves corresponding to the absorbing (or less reflecting) parts of the object have been indicated by hachures. If there had been no absorption the phase differences AB and BC would have been equal. In this case, however, for matching *a* and *b*, AB must be larger than BC. For matching *b* and *c*, that is the strip with the right-hand side of the field (see R), DE must be larger than EF. By matching the strip with each half of the main or free field, both the path difference and the absorption of the strip are found.

At path differences that are 0.5 wavelength either larger or less, the same general reasoning holds.

In the case given, the over-all intensity of the field of view is high; with 0.5 wavelength added or subtracted the field is much darker. Further consideration of the formulae not only makes this clear but also is in agreement with the observed fact that with "light" field the difference of setting left and right is larger than with "dark" field. There generally is one region (here "light" field) where the settings give more reliable values for the path difference and for the absorption.

For a step of ZnS on glass the following results were obtained. Two steps were made in Delft by evaporation in a good vacuum in January 1956. The thickness was measured shortly after the formation of the layer by means of a multiple beam interferometer. The result was 718±20 Å for each of the two steps. The measurements with a Savart plate in Ottawa gave 710±30 Å for each of the steps. The absorption found for one layer is 20.8±1.0%, while a Cary spectrophotometer gave 22% for the wavelength of 5460.7 Å. Putting the two steps together, their combined thickness appeared to be 1430±35 Å. The agreement is satisfactory, though small defects in the material and the mounting of the Savart plates seem to set a limit to precision, which can only be lowered by improving the Savart plates.

FIG. 4. Plane-parallel plate perpendicular to pencil.
FIG. 5. Plane-parallel plate turned in one direction.
FIG. 6. Plane-parallel plate turned in other direction until strip in right half is matched with "main" field in left half.
FIG. 7. Auxiliary Savart plate before the eye.
FIG. 8. Two auxiliary Savart plates; the fringes in the main field are symmetrical.
FIG. 9. Two auxiliary Savart plates; the setting aimed at symmetry in the strip.

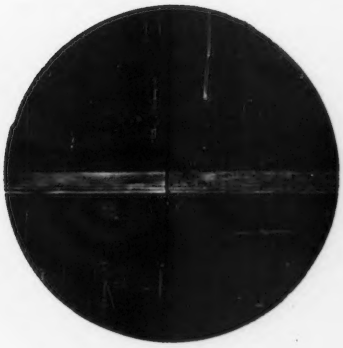

Figure 4

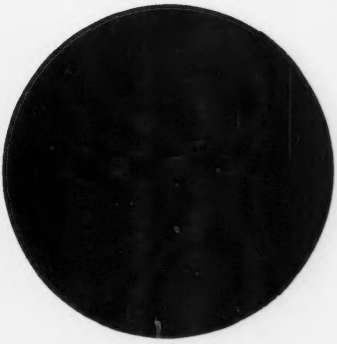

Figure 7

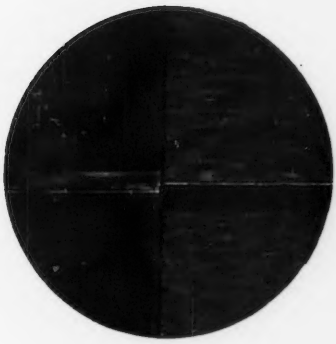

Figure 5

Figure 8

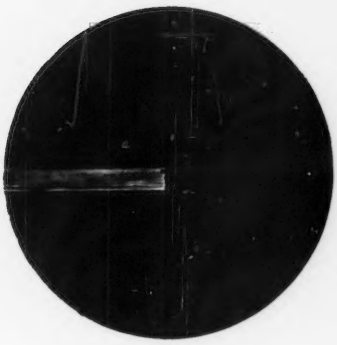

Figure 6

Figure 9

6. Experiments in Delft are proceeding in this direction. In the meantime a temporary stay at the laboratory of the National Research Council at Ottawa gave an opportunity to test the precision. Though these experiments have not been concluded, preliminary results show that a precision of a few per cent in the absorption or transmission of a step and of less than 0.005 of a wavelength in the thickness of the step can readily be measured.

It seems worth while to study the usefulness of the ingenious method of Françon for the determination of the changes of evaporated layers when air is admitted in the vacuum chamber.

In conclusion the author wishes to thank Mr. L. J. Leipoldt, who set up the measuring device in Delft and tested its practicability, Mr. K. von Morgen for the preparation of the steps and their testing by interferometric measurement, Mr. R. van Ligten for the taking of the Kodachrome pictures, and Mr. A. Walther for his help during the measurements in Ottawa. He tenders his thanks to the National Research Council of Canada for the opportunity of working in its laboratories, and especially to Dr. L. E. Howlett, Director of the Division of Applied Physics, for his invitation to do so and to him and his staff for their invaluable help.

REFERENCES

FRANÇON, M. 1952. Rev. opt. **31**: 65.
——— 1953. Rev. opt. **32**: 349.
——— 1954. Optica Acta, **1**: 50.

CATHODIC GLOW-TO-ARC TRANSITIONS[1]

By W. A. Gambling

ABSTRACT

One of the main factors determining the onset of a glow-to-arc transition is the electric field at the cathode surface. Because of the physical properties of the cathode dark space this field can only be measured at low pressures and hitherto only crude estimates of its value have been possible at high pressures. This paper develops a method whereby the cathode field strength can be determined at any pressure from a simple measurement of the cathode current density. This has been done for the typical cases of copper electrodes in hydrogen and air. The effect of cathode field strength and other parameters on glow-to-arc transitions is discussed.

INTRODUCTION

The cause of glow-to-arc transitions on low melting point cathodes has been the subject of many investigations and a large number of possible mechanisms have been put forward (Cobine 1941). For clean surfaces and pure gases perhaps the most likely explanation is that of enhanced emission from surface irregularities and it is interesting to note that two recent investigations also lead to this conclusion. Boyle and Haworth (1956) have reported that transitions take place when the field strength at the palladium cathode of an abnormal glow in air exceeds a critical value. Field emission from points on the surface then results in instability and a transition. In a study of the effects of impurities on the cathode Price *et al.* (1955) were able to show that, in the absence of low work function impurities, transitions did not occur unless the surface (clean or contaminated) was irregular.

The most important factor influencing glow-to-arc transitions thus appears to be the macroscopic or average field, E_m, at the cathode surface. It is possible to measure E_m at low pressures by means of electron probes, or by measuring the thickness of the cathode dark space, d, since $E_m = 2V_c/d$ where V_c is the cathode-fall voltage. At higher pressures the dark space is very thin and direct measurements cannot be made. Thus only relatively crude estimates of the cathode field at high pressures have been possible. This paper develops a method whereby the field at the cathode can be found at high pressures, independently of the temperature in the cathode dark space, from the simple measurement of the cathode current density.

THEORY

At low pressures the cathode dark space behaves in accordance with the principle of similarity and it has been shown (von Engel *et al.* 1933; Gambling, to be published) that when allowance is made for the temperature rise in the cathode dark space this principle also holds for the full pressure range from 1 mm. Hg up to atmospheric pressure and above.

[1]Manuscript received July 18, 1956.
Contribution from the Department of Electrical Engineering, University of British Columbia, Vancouver, B.C.

For the normal glow we thus have the following relations between the cathode current density, J, the pressure, p, the mean temperature in the cathode dark space, T, and E_m:

$$JT^2/p^2 = k_1 \tag{1}$$

and

$$E_mT/p = k_2. \tag{2}$$

T is not easily measured but the constants k_1 and k_2 may be found by measurements of J and E_m at a sufficiently low pressure (e.g. 1 mm. Hg) that T does not differ appreciably from room temperature. Thus for copper electrodes

$$k_1 = 5.2 \text{ and } 19.5 \text{ amp. cm.}^{-2}(\text{°K.})^2 \text{ (mm. Hg)}^{-2}$$

and

$$k_2 = 2.0\times10^5 \text{ and } 7.1\times10^5 \text{ volt cm.}^{-1}(\text{°K.}) \text{ (mm. Hg)}^{-1}$$

in hydrogen and air respectively.

Once these constants are known, then E_m can be found at any temperature and pressure by the simple process of measuring J, since T may be found from Eq. (1) and substituted in Eq. (2), or eliminating T we obtain

$$E_m = k_1^{-\frac{1}{2}}k_2J^{\frac{1}{2}}. \tag{3}$$

Although Eq. (3) enables E_m to be calculated without knowing T it should be emphasized that J (and E_m) does depend on T. This may well explain the discrepancies in the measurements of cathode current densities at high pressures (Gambling and Edels 1954).

Thus an important relation has been found which enables the electric field at the cathode of a normal glow at high pressures to be determined with a reasonable degree of accuracy. This has been done for the case of copper electrodes in hydrogen and air. Copper was chosen because it is a typical non-refractory type of metal which may be obtained in a high state of purity, hydrogen because the high-pressure glow is stable over a greater current range in this than in other gases, and air because of its practical importance in switching and other devices.

EXPERIMENT

The power density at the cathode of a glow discharge in hydrogen at atmospheric pressure is $\sim$2 kw./cm.^{2} so that to avoid overheating at high currents it is necessary to use a water-cooled cathode. Preliminary experiments also showed that with materials of normal commercial purity transitions occur very frequently over the current range proposed so that very pure electrodes were necessary. Accordingly a cathode 1 in. in diameter was constructed of spectroscopically pure copper sheet 1/16-in. thick and supported so that it could be cooled by a jet of cold water on the rear surface. The anode consisted of a $\frac{1}{4}$-in. diameter rod also of spectroscopically pure copper. After being cleaned and polished, the electrodes were mounted in the discharge vessel and further cleaned by operating each alternately as the cathode of a glow in

hydrogen at low pressure for several hours, the gas being changed frequently. Fresh hydrogen was then admitted to the required pressure, and with an electrode separation of ~1 mm. the cathode current density was obtained by photographic measurement of the diameter of the negative glow. This was done for decreasing currents so that the cathode surface conditions remained approximately constant, and at various pressures.

RESULTS

As would be expected from the similarity principle the cathode current density is independent of current. This is a good indication that the current is uniformly distributed across the cathode spot, and that there is no departure from similarity so that Eq. (3) can be applied. From these and other measurements at low pressures (von Engel *et al.* 1933) E_m has been evaluated for hydrogen and is shown in Fig. 1. Previous measurements (Gambling and Edels 1954; von Engel *et al.* 1933) are used to give the curve of E_m for copper electrodes in air.

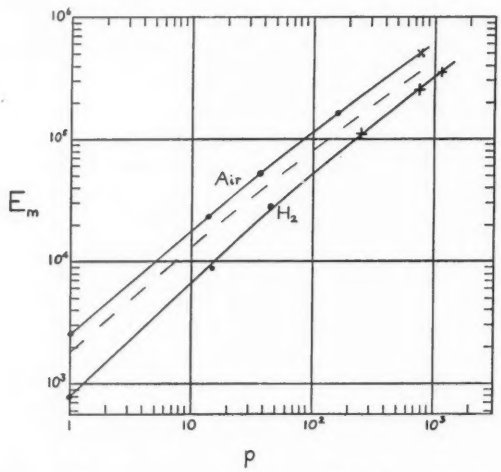

FIG. 1. Variation of E_m (volts/cm.) with p (mm. Hg). The experimental points were obtained as follows: + present measurements, ●von Engel *et al.* (1933), × Gambling and Edels (1954). The dashed curve is for air and was obtained using the approximate method based on Eq. (4).

Boyle and Haworth (1956) give an approximate expression for E_m in air which is based on the ion drift velocity equation for oxygen and nitrogen:

$$U_+ \simeq 10^4(E/p_0)^{\frac{1}{2}} \tag{4}$$

where U_+ is the drift velocity and p_0 is the pressure corrected to standard temperature. The values of E_m so obtained are also plotted and these are rather lower than those given by the method discussed above. The discrepancy may be due to the fact that Eq. (4) is known to hold only up to an E/p_0 of

1000 volts/cm.(mm. Hg) whereas over a large part of the cathode dark space in air E/p_0 is greater than this, falling from 2500 volts/cm.(mm. Hg) at the cathode to zero in the negative glow. Furthermore Eq. (4), which was obtained in a uniform field, is unlikely to hold accurately in a region where the field is varying rapidly.

DISCUSSION

The figure shows that the average field at the cathode is proportional to the pressure at low pressures, when the temperature rise is small, in accordance with Eq. (2). At the higher pressures E_m increases less rapidly owing to the rise in temperature in the cathode dark space. Since, for example, in air at $p = 1$ mm. Hg, $E_m = 2.5\times10^3$ volts/cm. when T may be taken as 293° K., the temperature at atmospheric pressure when $E_m = 5\times10^5$ volts/cm. may be found from Eq. (2) as 1080° K. This rise in temperature is a result of the increase in the power developed in the cathode dark space from 70×10^{-3} watts/cm.^{2} at 1 mm. Hg to 3×10^3 watts/cm.^{2} at atmospheric pressure. Because of the higher thermal conductivity and the lower current density the corresponding rise of temperature in hydrogen is much less.

In hydrogen and air respectively the field strength at the cathode at atmospheric pressure is 2.5×10^5 and 5×10^5 volts/cm. and is approaching values at which field emission may be expected from surface irregularities. The field enhancement factor, β, due to this cause is a matter of some doubt. For 'smooth' oxidized surfaces Llewellyn Jones and Perrelle (1953) obtained a value $\sim$10 which increased greatly when metal particles due to heavy-current sparking were present on the surface. It is possible to calculate a value of β from the field emission current measurements of Boyle and Haworth (1956). Using the nominal value of the work function, β comes out to be $\sim$65, and this seems rather high even considering the violent bombardment which the surface undergoes when it is sputtered clean in an abnormal glow. However, the effective value of the work function is unknown but will be less than the nominal value so that the β calculated in this way must be taken as an upper limit. Because of the uncertainty concerning the work function Boyle and Haworth themselves purposely avoid deducing a β value. The subject of field enhancement is still in debate (Lewis 1955) and it seems reasonable to assume that for a cathode that has been glow cleaned, β may be $\sim$10 or even higher depending on the treatment used. Another difficulty arises from the possible lowering of the work function due to irregularities (Lewis 1954). The work function and β appear in the exponential term in the field emission equation and may thus be expected to have a marked effect on the transition current. This is in accordance with observation.

An important consequence of the above analysis concerns the methods used to prevent glow-to-arc transitions and the resulting destruction of the cathode surface which occurs, in such applications as low current switches and the transmit–receive devices used in radar. It has generally been assumed that in order to avoid transitions on non-refractory cathodes it is necessary to provide adequate cooling. The above theory indicates, however, that cooling encourages

transitions since Eq. (2) shows that $E_m \propto T^{-1}$. Thus it is most interesting to note that with copper, silver, and iron electrodes in hydrogen and nitrogen (Cady 1916; Price *et al.* 1955) a glow may be obtained at currents between 1 and 2 amp. at pressures up to atmospheric even though the cathode becomes so hot that it melts and approaches boiling temperature. This behavior may now be readily understood. When the cathode is molten, not only is E_m reduced because of the high temperature, but surface irregularities disappear and $\beta \sim 1$. It seems likely that the transition which finally occurs is the result of local solidification and the formation of cold irregularities at the edge of the cathode. Thus transitions are more likely to be prevented if the cathode is allowed to remain hot.

So far the applicability of the similarity laws to the cathode dark space at high pressures has been reasonably demonstrated only for hydrogen and air, and departures from similarity will be observed in discharges in which certain fundamental mechanisms, such as the various cumulative processes, become appreciable. The above theory can be applied to any normal glow in which the similarity laws are obeyed in the cathode dark space. Two necessary properties of such a discharge are that the cathode-fall voltage shall be independent of pressure, current, and temperature, and the cathode current density independent of the current.

ACKNOWLEDGMENTS

The author would like to thank the Head of the Department of Electrical Engineering, University of British Columbia, Dr. F. Noakes, for the facilities provided, the National Research Council of Canada for the award of a Post-Doctorate Fellowship, and Professor J. M. Meek of the Department of Electrical Engineering, University of Liverpool, where the experimental results were obtained.

REFERENCES

BOYLE, W. S. and HAWORTH, F. E. 1956. Phys. Rev. **101**: 935.
CADY, W. G. 1916. Trans. Am. Electrochem. Soc. **29**: 593.
COBINE, J. D. 1941. Gaseous conductors. McGraw-Hill Book Company, Inc., New York.
VON ENGEL, A., SEELIGER, R., and STEENBECK, M. 1933. Z. Physik, **85**: 144.
GAMBLING, W. A. and EDELS, H. 1954. Brit. J. Appl. Phys. **5**: 36.
LEWIS, T. J. 1954. Proc. Phys. Soc. B, **67**: 187.
——— 1955. Proc. Phys. Soc. B, **68**: 504.
LLEWELLYN JONES, F. and DE LA PERRELLE, E. T. 1953. Proc. Roy. Soc. A, **216**: 267.
PRICE, W. L., GAMBLING, W. A., and EDELS, H. 1955. Nature, **176**: 28.

SPECTRUM OF THE C_3 MOLECULE BETWEEN 3600 Å AND 4200 Å[1]

By Norman H. Kiess and Herbert P. Broida

ABSTRACT

C_3 bands have been observed in the emission spectrum of an acetylene–oxygen flame with an excess of acetylene. In addition to the usually observed bands of the 4050 Å group, weak bands at wavelengths less than 4000 Å and greater than 4100 Å have been observed. Measured wavelengths are given of 40 band-heads superimposed on a strong continuum, extending from 3600 to 4200 Å. A rotational analysis of the two strongest bands with heads at 4050 Å and 4072 Å is given also. The relative simplicity of these two bands indicates that the complexity of the other C_2 bands is caused by lines of overlapping bands.

INTRODUCTION

The C_3 bands are a spectral group that have been known as the "4050 Å group" because of their intensity-maximum at 4050 Å. They have been observed in the spectra of comets and late N-stars. They have been produced in the laboratory in electric discharges, in acetylene–oxygen flames and explosions, and in carbon-tube furnaces. A rotational analysis of the strongest band with a head at 4050 Å was first obtained by Douglas (1951) and later extended by Kiess and Bass (1954). More complete summaries of the investigations on the C_3 molecule and the 4050 Å group are given by Rosen and Swings (1953) and by Herzberg (1955).

Recent work by Phillips and Brewer (1955) with a carbon-tube furnace and by Marr and Nicholls (1955) with an acetylene–oxygen flame has shown that the C_3 bands are associated with an intense continuum reaching a maximum near 4000 Å. This paper reports a new group of bands superimposed on this continuum.

The rotational analysis of the 4050 Å band has been extended to J values of about 110 in the P and R branches and to 137 in the Q branch. In addition an analysis is given of the 4072 Å band.

EXPERIMENTAL

The C_3 bands are emitted strongly in the luminous zone of an acetylene–oxygen flame with an acetylene-to-oxygen ratio (by volume) slightly greater than unity. The premixed gases were burned on a rectangular slot burner 50 mm. long with a width of 0.076 mm. First, the flame was observed end-on and optimum flame conditions were found by recording the spectrum from 3600 to 4200 Å by using a grating monochromator with photoelectric detection (Fastie 1952; Broida and Shuler 1952). Low-dispersion spectra were obtained with a quartz-prism spectrograph having a $f/4$ camera. In order to obtain the highest possible contrast, Eastman Kodak High Resolution plates were used; these required about 15 minutes exposure. Next, the spectrum was photographed in the first order of a 15,000 lines-per-inch grating spectrograph with

[1]Manuscript received August 27, 1956.
Contribution from the National Bureau of Standards, Washington 25, D.C. This research was supported in part by the U.S. Air Force through the Air Force Office of Scientific Research of the Air Research and Development Command under Contract CSO-680-56-30.

a dispersion of 5 Å per mm. Exposures from 15 to 90 seconds with Eastman Kodak Spectrum Analysis No. 1 plates were needed to cover the entire region from 3600 to 4200 Å. Finally, the same type of plate was used in the second order of a 30,000 lines-per-inch grating spectrograph with a dispersion of 0.88 Å per mm. Exposure times were from 10 to 30 minutes. The wavelengths of band heads and rotational lines were measured from these plates by comparison with iron-line standards.

RESULTS

Fig. 1 is a direct tracing of intensity versus wavelength obtained with the monochromator using photoelectric detection. A relatively wide slit (50 microns) and fast scan (100 Å per minute) were used. In order to show better the band-structure superimposed on the continuum, a biasing current equal to one-half the signal obtained near 4000 Å has been used. Thus the zero of intensity is twice as deep as the base of the figure. It will be seen that the strongest band-head at 4050 Å is only about 10% of the continuum beneath it. This spectrum was obtained from just above the inner cone of a flame with nearly a one-to-one mixture of acetylene-to-oxygen. The position in the flame was selected to give a compromise between strong CH and strong CN emission. In agreement with Phillips and Brewer (1955) and with Marr and Nicholls (1955), we observe that the continuum has a maximum near 4000 Å and

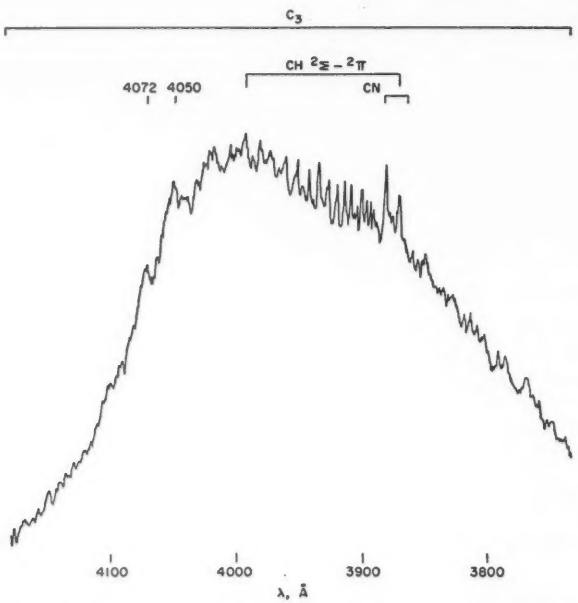

Fig. 1. Direct photoelectric recording of emission from luminous zone of a fuel-rich acetylene–oxygen flame.

PLATE I

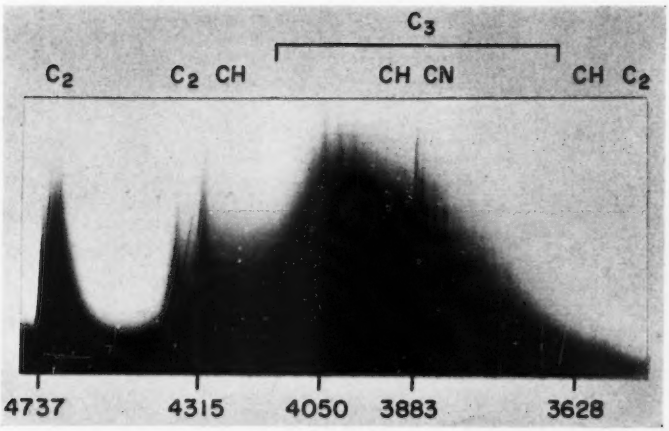

Fig. 2. Photographic spectrum from same flame as in Fig. 1. An $f/4$ quartz spectrograph was used with a 15 minute exposure on an Eastman Kodak High Resolution plate. The flame was imaged on the slit.

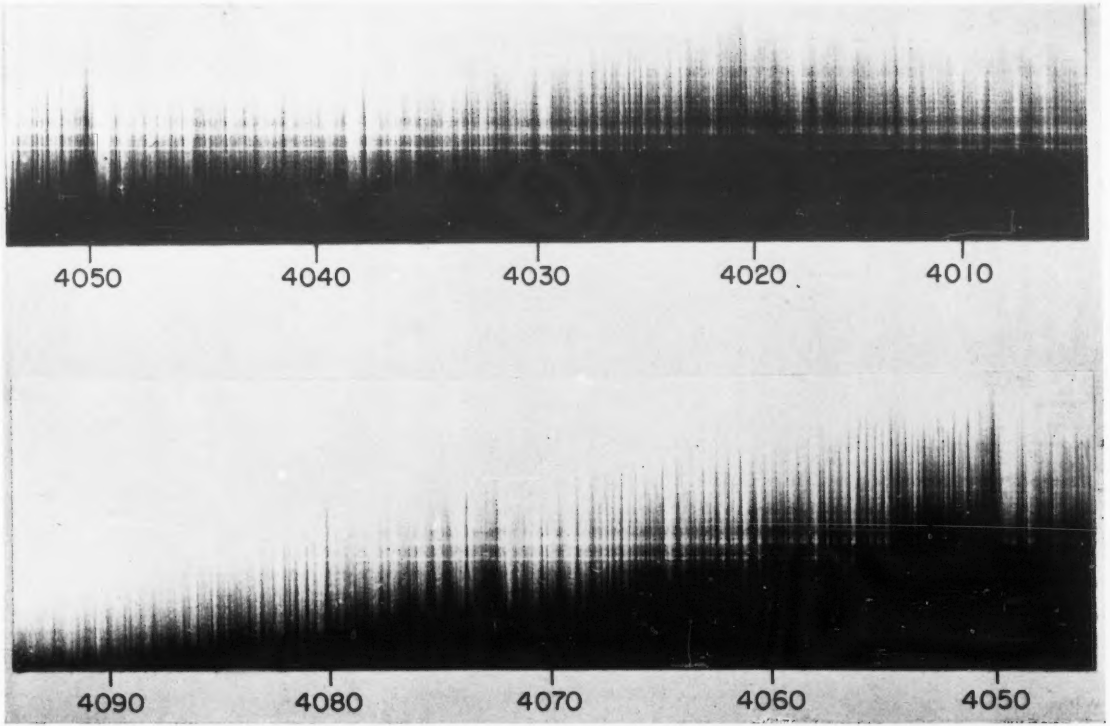

Fig. 3. Photographic spectrum from the same flame. A 30,000 lines-per-inch grating spectrograph was used in the second order. The flame was imaged on the slit.

extends from 3600 to 4200 Å. Also the continuum falls off more rapidly on the long-wavelength side of the maximum than on the short. It should be pointed out that a certain electrodeless discharge emits only the stronger bands near 4050 Å, with no continuum. This discharge was operated at 2450 megacycles with a mixture of about 1 part in 50 of methane in argon at a pressure near 1 mm. Hg.

The spectrum of Fig. 2, covering the same spectral region as Fig. 1, was taken from a high-contrast plate on the low-dispersion spectrograph. It brings out the banded structure shortward of 4000 Å. Under higher resolution these bands show structure similar to the stronger bands near 4050 Å. Since these bands occur under the same conditions as those of the 4050 group and its associated continuum, these new bands also are probably due to C_3. Wavelengths and wavenumbers of all band heads (omitting CN and CH) detected between 3600 and 4200 Å are given in Table I. The intensity column is the eye-estimate of the relative band-intensity above the continuum. The column marked "weight" is an estimate of the relative probability that the band is actually present, ascending numbers indicating a greater probability. This latter estimate was made necessary by the extreme difficulty of detecting and measuring the weak band heads superimposed on the strong continuum.

TABLE I

WAVELENGTHS AND WAVENUMBERS OF MEASURED BAND HEADS OF C_3

λ, Å	ν, cm^{-1}	Intensity	Weight	λ, Å	ν, cm^{-1}	Intensity	Weight
3634	27510	1	1	3966.918	25201.38	3	2
51.5	378	1	3	71.854	170.06	2	1
68.9	248	1	2	75.449	146.99	2	1
77.7	183	1	1	81.781	107.31	2	1
87.3	112	1	3	88.3	066	2	2
3705.8	26977	1	3	94.6	027	4	3
14.8	912	1	3	4007.589	24945.63	5	3
29.0	809	1	2	08.730	938.53	5	2
38.0	745	1	3	18.394	879.55	5	3
60.4	585	1	3	22.717	851.82	6	4
83.7	421	1	3	29.138	812.21	5	2
3802.5	291	1	3	38.043	757.50	5	4
14.2	210	1	1	41.676	735.25	4	2
24.1	143	1	3	49.754	685.90	10	5
33.3	080	1	1	64.963	593.55	4	3
44.8	002	1	2	72.373	549.80	7	5
93.8	25675	1	1	93.76	420.6	3	4
3925.0	471	2	3	4115.24	293.1	1	3
39.9	374	2	1	38.30	157.7	1	3
44.9	342	2	1	50.21	030.5	1	3

Fig. 3 shows the region 4005–4095 Å as photographed in the second order of a 30,000 lines-per-inch grating spectrograph. Wavelengths and relative intensities of all measured lines between 4007 and 4103 Å are given in Table II. Between 4007 and 4050 Å one set of measurements was used; between 4050 and 4103 Å the average of two sets of measurements was used. In this latter region most of the lines are identified as belonging to either of two bands—one forming a head at 4049.750 Å and the other at 4072.386 Å. With these identifications, 70% of the line-intensity above the continuum is explained in the region 4050–4094 Å. At 4094 Å lies the head of another band, which has not been analyzed.

TABLE II

MEASURED WAVELENGTHS OF ROTATIONAL LINES BETWEEN 4007 and 4104 Å

λ, Å	Intensity	λ, Å	Intensity	λ, Å	Intensity	λ, Å	Intensity
4007.589	3 bh	4018.311	1	4027.885	2	4038.349	3
.640	3	.394	2 bh	.974	2	.420	2
.704	3	.470	2	28.074	2	.539	2
.820	3	.565	2	.184	2	.654	2
.952	3	.644	2	.292	2	.792	2
08.106	3	.764	2	.350	1	.939	3
.261	3	.951	2	.430	2	39.085	3
.346	3	19.149	2	.586	3	.246	2
.447	3	.292	2	.844	3	.372	2
.579	3	.394	2	29.041	2	.450	2
.730	5 bh	.533	2	.138	1 bh	.605	4
.850	4	.599	2	.223	1	.774	1
.958	2	.743	2	.324	2	.860	1
09.037	1	.831	2	.439	2	.937	2
.146	1	20.200	2	.581	1	40.067	1
.311	3	.310	2	.738	2	.182	1
.472	2	.454	2	.884	3	.293	1
.552	2	.495	3	30.005	3	.354	3
.706	3	.625	2	.264	3	.479	2
.868	2	.745	1	.379	1	.604	2
.958	2	.924	2	.475	1	.730	2
10.125	2	21.055	2	.622	2	.840	4
.314	2	.140	2	.743	2	.961	2
.471	2	.286	2	.821	1	41.060	2
.621	2	.461	2	.932	2	.188	2
.810	2	.617	2	31.135	2	.310	1
.982	2	.745	1	.179	2	.452	1
11.057	2	.832	2	.351	1	.533	1
.244	2	22.019	2	.484	3	.579	2
.417	2	.098	1	.538	3	.676	1 bh
.485	2	.158	2	.676	2	.742	1
.678	3	.272	2	.727	2	.855	2
.805	3	.319	1	.933	3	.986	1
12.238	3	.392	2	32.010	1	42.169	2
.367	3	.475	1	.122	2	.369	2
.517	2	.544	1	.247	3	.528	2
.652	1	.717	3 bh	.394	2	.623	2
.778	1	.824	2	.478	3	.787	2
.920	3	.925	2	.577	1	.909	2
13.006	3	23.041	2	.657	2	43.056	2
.127	1	.169	3	.866	2	.198	1
.275	1	.287	3	.935	2	.263	1
.447	3	.394	3	33.090	2	.359	2
.558	2	.526	2	.343	1	.483	3
.671	1	.725	3	.499	1	.535	3
.778	1	.805	1	.613	2	.684	2
.881	1	.855	3	.684	2	.815	2
14.021	1	24.006	2	.837	2	.951	2
.201	2	.110	2	.949	2	44.221	3
.416	2	.225	2	34.098	2	.450	2
.552	2	.334	2	.247	2	.506	2
.687	3	.557	4	.385	2	.663	2
.898	3	.809	3	.495	1	.831	2
15.045	1	.915	1	.652	2	.947	2
.144	1	25.087	4	.746	1	45.041	1
.266	1	.287	2	.849	2	.172	2
.360	2	.345	4	.974	2	.258	2
.514	2	.588	3	35.079	2	.397	2
.667	2	.629	3	.246	1	.472	3
.745	2	.708	2	.348	2	.622	1
.793	1	.785	2	.486	3	.696	1
.942	2	.857	3	.705	2	.790	1
16.074	2	.954	1	.945	3	.918	2
.251	2	26.021	1	36.100	2	46.005	2
.377	1	.132	3	.298	2	.228	1
.513	2	.199	3	.398	2	.326	1
.633	2	.284	1	.542	2	.471	1
.805	2	.389	2	.696	2	.570	2
.905	1	.535	2	.794	1	.645	2
17.023	1	.581	3	.873	2	.777	1
.106	1	.646	1	.969	1	.906	1
.181	2	.695	2	37.142	6	47.128	3
.235	2	.770	3	.276	1	.231	2
.381	2	.834	1	.418	1	.383	1
.508	2	.989	3	.585	1	.505	2
.597	1	27.117	1	.707	1	.648	2
.684	1	.223	3	.809	2	.735	2
.760	1	.357	2	.949	2	.879	2
.884	2	.431	1	38.043	3 bh	48.013	2
18.018	1	.539	3	.109	3	.120	2
.143	1	.721	2	.177	3	.265	1
.211	1	.833	2	.270	2	.337	3

TABLE II (*continued*)

MEASURED WAVELENGTHS OF ROTATIONAL LINES BETWEEN 4007 AND 4104 Å (*continued*)

λ, Å	Intensity	Identification
4048.477	4	
.693	3	
.991	1	
49.457	1	
.582	3	
.672	1	
.750	5	$R(26)$
.851	3	$R(30)$
.902	3	$R(32)$
.975	1	$R(34)$
50.216	2	$R(38)$
.320	2	$R(40)$
.379	1	
.472	2	$R(42)$
.608	2	$R(44)$
.700	1	
.789	2	$R(46)$
.958	4	$R(48)$
51.168	2	$R(50)$
.364	2	$R(52)$
.585	4	$R(54)$, $Q(7)$
.654	3	$Q(9)$
.811	3	$R(56)$, $Q(11)$
.899	1	$Q(13)$
52.073	3	$R(58)$, $Q(15)$
.308	3	$R(60)$, $Q(17)$
.524	1	
.599	1	$R(62)$
.680	1	$Q(21)$
.795	1	
.904	3	$R(64)$, $Q(23)$
.988	2	
53.173	3	$R(66)$, $Q(25)$
.281	2	
.477	4	$R(68)$, $Q(27)$
.688	1	
.788	4	$R(70)$, $Q(29)$
.921	2	
54.090	3	$Q(31)$, $R(72)$
.192	2	
.437	6	$Q(33)$, $P(16)$, $R(74)$
.620	1	
.787	3	$Q(35)$, $R(76)$
.881	1	$P(18)$
55.002	1	
.159	4	$Q(37)$, $R(78)$
.233	1	
.342	1	$P(20)$
.540	4	$Q(39)$, $R(80)$
.598	1	
.757	2	
.853	1	$P(22)$
.934	4	$Q(41)$, $R(82)$
56.015	1	
.203	1	
.368	5	$Q(43)$, $P(24)$, $R(84)$
.558	1	
.715	2	$R(86)$
.813	3	$Q(45)$
.938	1	$P(26)$
57.116	2	$R(88)$
.243	3	$Q(47)$
.324	1	
.464	2	
.548	3	$P(28)$, $R(90)$
.709	4	$Q(49)$
.782	1	
.864	1	
.978	2	$R(92)$
58.091	1	$P(30)$
.174	3	$Q(51)$
.247	3	
.402	1	$R(94)$
.517	2	
.660	3	$Q(53)$, $P(32)$
.736	1	
.899	1	$R(96)$
59.043	2	
.164	2	$Q(55)$
.319	1	$P(34)$, $R(98)$
.404	1	
.551	1	
4059.670	3	$Q(57)$
.831	2	$R(100)$
.965	1	$P(36)$
60.072	1	
.195	3	$Q(59)$
.290	2	$R(102)$
.395	1	
.591	3	$P(38)$
.731	3	$Q(61)$
.883	2	
61.287	4	$Q(63)$, $P(40)$, $R(106)$
.416	1	
.518	1	
.671	2	
.836	3	$Q(65)$, $R(108)$
.985	2	$P(42)$
62.208	1	
.353	2	$R(110)$
.419	3	$Q(67)$
.674	2	$P(44)$
.997	3	$Q(69)$
63.104	1	
.212	1	
.379	2	$P(46)$
.456	2	$R(114)$
.589	3	$Q(71)$
.782	1	
64.097	3	$P(48)$
.195	3	$Q(73)$
.420	1	
.627	1	
.833	3	$Q(75)$, $P(50)$
.955	1	bh
65.032	1	
.120	1	
.250	1	
.444	3	$Q(77)$
.620	3	$P(52)$
.846	1	
.971	1	
66.068	3	$Q(79)$
.148	1	
.385	3	$P(54)$
.495	1	
.599	1	
.746	3	$Q(81)$
67.047	1	
.131	3	$P(56)$
.378	3	$Q(83)$
.517	1	
.655	2	
.738	1	
.931	2	$P(58)$
68.051	3	$Q(85)$
.193	2	
.365	1	
.613	1	
.720	3	$Q(87)$, $P(60)$
.788	1	
69.412	2	$Q(89)$
.537	2	$P(62)$
.694	1	
.861	1	
.990	1	
70.116	2	$Q(91)$
.359	2	$P(64)$
.486	1	
.689	1	
.811	2	$Q(93)$
71.029	1	
.112	1	
.193	2	$P(66)$
.318	1	
.425	1	
.536	2	$Q(95)$
.671	1	
72.027	2	$P(68)$
.260	2	$Q(97)$
.386	3	$r(24)$
.438	3	$r(26)$
.585	1	$r(30)$
.715	1	$r(32)$
4072.898	2	$P(70)$, $r(36)$
73.006	1	$Q(99)$, $r(38)$
.114	1	$r(40)$
.242	1	$r(42)$
.412	2	$r(44)$
.557	1	$r(46)$
.660	1	
.765	4	$Q(101)$, $P(72)$, $r(48)$
.963	1	$r(50)$
74.115	1	
.246	1	$r(52)$
.403	1	
.460	1	$r(54)$
.527	2	$Q(103)$
.658	2	$P(74)$, $r(56)$
.792	1	$q(17)$
.869	1	
75.038	1	$q(19)$
.154	1	
.235	1	$r(60)$
.303	2	$Q(105)$, $q(21)$
.384	2	
.430	2	
.523	1	$P(76)$, $q(23)$
.630	1	
.753	1	$r(64)$
.891	1	$q(25)$
76.104	2	$Q(107)$, $r(66)$
.248	1	
.387	2	$P(78)$, $r(68)$
.455	2	
.622	1	
.771	1	$r(70)$
.879	1	$Q(109)$, $q(31)$
.967	1	
77.059	1	$r(72)$
.275	2	$q(33)$
.367	3	$P(80)$
.509	1	$r(74)$
.615	2	$q(35)$
.701	2	$Q(111)$
.774	1	
.887	1	$r(76)$
.976	1	$p(20)$
78.041	1	$q(37)$
.113	1	
.239	1	$P(82)$
.344	1	$r(78)$
.434	1	$q(39)$
.487	1	$Q(113)$
.629	1	
.734	1	$r(80)$
.843	2	$q(41)$
79.070	2	$p(24)$
.171	1	$P(84)$, $r(82)$
.238	1	$q(43)$
.312	1	$Q(115)$
.413	1	
.670	1	$q(45)$, $p(26)$
.758	1	
80.143	4	$Q(117)$, $P(86)$, $q(47)$
.416	1	
.488	1	
.598	2	$q(49)$
.712	2	
81.078	3	$q(51)$, $P(88)$
.304	2	
.548	3	$q(53)$, $p(32)$
.866	3	$Q(121)$
82.056	3	$q(55)$, $P(90)$
.233	1	
.357	1	
.458	1	
.565	2	$q(57)$
.717	1	$Q(123)$
.880	1	$p(36)$
.976	1	
83.033	1	$P(92)$
.108	2	$q(59)$
.333	1	
.413	1	

TABLE II (*concluded*)

MEASURED WAVELENGTHS OF ROTATIONAL LINES BETWEEN 4007 AND 4104 Å (*concluded*)

λ, Å	Intensity	Identification
4083.482	1	
.613	2	$Q(125)$
.667	2	$q(61)$
.735	1	
.895	1	
84.002	1	$P(94)$
.107	1	
.226	2	$q(63)$, $p(40)$
.362	1	
.501	1	$Q(127)$
.613	2	
.813	2	$q(65)$
85.160	1	
.405	3	$q(67)$, $Q(129)$
.569	1	$p(44)$
.716	1	
.839	1	
.898	1	
86.026	3	$q(69)$, $P(98)$
.255	1	$p(46)$
.418	2	
.606	2	
.661	2	$q(71)$
.809	1	
.864	1	
87.002	1	$p(48)$, $P(100)$
.099	1	
.286	2	$q(73)$
.421	1	
.696	2	$p(50)$
.864	1	
.956	2	$q(75)$
88.030	1	$P(102)$
.199	1	$Q(135)$
4088.300	1	
.480	2	$p(52)$
.630	2	$q(77)$
.824	2	
89.098	2	$P(104)$
.336	2	$q(79)$, $p(54)$
.579	1	
.720	1	
.817	1	
.932	1	
90.014	2	$q(81)$
.131	2	$p(56)$
.326	1	
.423	1	
.544	1	
.716	2	$q(83)$
.946	2	$p(58)$
91.163	2	$P(108)$
.455	2	$q(85)$
.546	2	
.750	2	$p(60)$
92.072	1	
.155	1	$q(87)$
.257	1	$P(110)$
.368	2	
.542	2	$p(62)$
.703	1	
.809	1	
.947	1	$q(89)$
93.088	1	
.187	1	
.288	1	
.381	1	$p(64)$
.698	2	$q(91)$
.807	1	bh
4094.442	1	$q(93)$
.832	1	
95.241	1	$q(95)$
.481	1	
.940	1	
96.040	1	$p(70)$, $q(97)$
.105	1	
.810	1	
.882	1	$q(99)$
97.723	1	
98.545	1	
.609	1	
.761	1	
.953	1	
99.227	1	
.505	1	
.939	1	
4100.113	1	
.361	1	
.441	1	
01.172	1	
.665	1	
.995	1	
02.075	1	
.573	1	
03.083	1	
.326	1	
.376	1	
.501	1	
.556	1	
.642	1	
.730	1	
.816	1	

Wavenumbers of the lines of the two analyzed bands are given in Tables III and IV. Small differences between wavenumbers given in these tables and wavenumbers computed from the wavelengths of Table II exist because the wavenumbers of Tables III and IV are averages of more than two sets of measurements. These measurements, however, usually agreed to within 0.01 Å.

Rotational constants B and D were obtained for the combining states of both bands by the usual plots of $\Delta_2F/(J+\frac{1}{2})$ versus $(J+\frac{1}{2})^2$ (Herzberg 1950). The band origin ν_0 was obtained for each band by the usual plots of $Q(J)$ versus $J(J+1)$ (Herzberg 1950). The rotational constants and the band origins are given in Table V. The estimates of the precision of these numbers are based on the scatter of points in the plots used to determine them.

CONCLUSION

Our spectra, illustrated in Figs. 1, 2, and 3, confirm the results of Marr and Nicholls (1955) on the presence in the acetylene–oxygen flame of a continuum associated with the C_3 bands. However, in addition to the continuum, we find a band structure throughout the region of the continuum. These bands are extremely weak compared to the continuum (about 1%), except between 4000 and 4100 Å. A combination of low dispersion and high contrast was required to obtain plates on which the bands were readily discernible.

Although an effort was made to fit the band heads into a vibrational scheme, no particularly useful arrangement was found. Several band-head differences

were repeated often. For example, some 21 differences of approximately 523 cm^{-1}, 19 differences of 264 cm^{-1}, and 14 differences of 133 cm^{-1} were found. The 523 cm^{-1} frequency is close to what can be expected for a carbon–carbon double-bond bending frequency.

The rotational analysis (Tables III and IV) is considered to be fairly certain, insofar as the branches of the bands have been picked out. The 4050 and 4072 Å bands have similar structure. Although the rotational constants indicate that the lower states may be the same for these two bands, we feel that the combination differences render this conclusion uncertain. The following unusual

TABLE III

WAVENUMBERS OF MEASURED LINES OF THE 4050 Å BAND

J	$P(J)$	$Q(J)$	$R(J)$	J	$P(J)$	$Q(J)$	$R(J)$
3		24675.38		65		24612.46	
4	24671.76			66	24555.85		24665.06
5		75.14		67		08.93	
6	69.59			68	50.85		63.19
7		74.75		69		05.43	
8	67.32			70	45.61		61.46
9		74.33		71		01.85	
10	65.03			72	40.41		59.50
11		73.32		73		598.17	
12	62.53			74	35.14		57.50
13		72.79		75		94.53	
14	60.02			76	29.72		55.28
15		71.76		77		90.83	
16	57.34			78	24.50		53.01
17		70.60		79		86.88	
18	54.71			80	18.88		50.69
19		69.40		81		83.00	
20	51.89		24685.65	82	13.48		48.30
21		68.06		83		78.95	
22	48.76		85.91	84	07.82		45.78
23		66.59		85		74.89	
24	45.53		85.91	86	02.04		43.55
25		65.04		87		70.83	
26	42.25		85.91	88	496.43		41.08
27		63.19		89		66.66	
28	38.48		85.65	90	90.58		38.48
29		61.29		91		562.42	
30	35.22		85.33	92	484.78		35.84
31		59.32		93		58.26	
32	31.68		84.97	94	78.92		33.27
33		57.27		95		53.88	
34	27.72		84.58	96	72.82		30.48
35		55.13		97		49.48	
36	23.79		83.94	98	66.79		27.70
37		52.97		99		44.99	
38	20.01		83.18	100	60.88		24.59
39		50.69		101		40.41	
40	15.75		82.42	102	54.60		21.81
41		48.25		103		35.78	
42	11.56		81.51	104	48.32		18.74
43		45.73		105		31.16	
44	07.34		80.69	106	42.02		15.75
45		42.98		107		26.45	
46	03.09		79.56	108	36.04		12.46
47		40.31		109		21.66	
48	598.73		78.52	110	29.53		09.31
49		37.52		111		16.76	
50	94.42		77.24	112			05.97
51		34.66		113		12.00	
52	89.58		76.03	114			02.68
53		31.72		115		06.97	
54	84.93		74.70	117		02.04	
55		28.63		119		496.88	
56	80.26		73.32	121		91.66	
57		25.55		123		86.50	
58	75.56		71.81	125		81.25	
59		22.38		127		75.94	
60	70.81		70.32	129		70.43	
61		19.13		131		64.97	
62	65.89		68.56	133		59.55	
63		15.75		135		53.74	
64	60.88		66.67	137		48.02	

TABLE IV

WAVENUMBERS OF MEASURED LINES OF THE 4072 Å BAND

J	$P(J)$	$Q(J)$	$R(J)$	J	$P(J)$	$Q(J)$	$R(J)$
16	24521.37		24548.38	58	24437.34		24533.33
17		24534.23		59		24484.22	
18	18.27		48.60	60	32.51		31.74
19		32.74		61		80.90	
20	15.09		48.80	62	27.74		30.02
21		31.16		63		77.50	
22	11.85		48.80	64	22.81		28.17
23		29.56		65		74.02	
24	08.51		48.60	66	17.64		26.29
25		27.71		67		70.42	
26	04.96		48.38	68	12.28		24.20
27		25.82		69		66.79	
28	01.27		48.05	70	06.90		22.32
29		23.72		71		62.98	
30	497.54		47.61	72	01.47		20.19
31		21.66		73		59.17	
32	93.74		47.01	74	396.17		17.88
33		19.38		75		55.22	
34	89.80		46.21	76	90.75		15.40
35		16.98		77		51.22	
36	85.69		45.61	78			12.98
37		14.67		79		46.97	
38	81.52		44.96	80			10.31
39		12.32		81		43.03	
40	77.50		44.29	82			07.83
41		09.85		83		38.80	
42	73.52		43.47	84			05.31
43		07.44		85		34.47	
44	69.51		42.55	86			02.62
45		04.82		87		30.08	
46	65.40		41.50	88			
47		02.04		89		25.45	
48	60.88		40.41	90			
49		499.33		91		21.00	
50	56.48		39.09				
51		96.50		93		16.49	
52	52.07		37.63				
53		93.54		95		11.72	
54	47.22		36.24				
55		90.58		97		06.96	
56	42.25		34.89				
57		87.43		99		01.94	

TABLE V

ROTATIONAL CONSTANTS (cm^{-1})

A. 4050 Å Band	B. 4072 Å Band
$B' = 0.4125 \pm 0.0005$	$B' = 0.4110 \pm 0.0005$
$B'' = 0.4280 \pm 0.0005$	$B'' = 0.428 \pm 0.001$
$\nu_0 = 24675.78 \pm 0.08$	$\nu_0 = 24539.8 \pm 0.2$
$D' = (0.22 \pm 0.03) \times 10^{-6}$	$D' = (0.22 \pm 0.06) \times 10^{-6}$
$D'' = (0.46 \pm 0.05) \times 10^{-6}$	$D'' = (0.7 \pm 0.2) \times 10^{-6}$

features should be noted, however. In agreement with Douglas (1951), we find that the Λ-doubling follows no simple formula, and is large even for low values of J. Following a suggestion by Douglas (1953), the quantity $[\nu_0 - Q(J)]/[J(J+1)]$ was plotted versus $J(J+1)$. According to the relation

$$Q(J) = \nu_0 + (B' - B'')J(J+1) - (D' - D'')J^2(J+1)^2 \text{ (Herzberg 1950),}$$

this plot should give a straight line whose slope is $D' - D''$. For each band, however, a smooth curve was obtained, the initial slope of which was four times and the final slope of which was one-half the value of $D' - D''$ obtained from the $\Delta_2 F$ combination differences. As the lines near the origins of both

bands were difficult to measure, these features may be due to the J-numbering of the lines being off by a unit. Attempts to analyze other bands of the system were not successful. Although the locations of the band heads were measureable, the closeness of the rotational structure and the overlapping of the many bands of nearly equal intensity make the analysis very difficult.

We wish to thank the Spectroscopy Section of the National Bureau of Standards for the use of their large grating spectrographs. Also, we wish to express our indebtedness to Dr. R. E. Ferguson for his suggestion to look for the 4050 Å bands in the emission from acetylene–oxygen flames.

REFERENCES

BROIDA, H. P. and SHULER, K. E. 1952. J. Chem. Phys. **20**: 168.
DOUGLAS, A. E. 1951. Astrophys. J. **114**: 466.
——— 1953. Private communication.
FASTIE, W. G. 1952. J. Opt. Soc. Amer. **42**: 641.
HERZBERG, G. 1950. Molecular spectra and molecular structure. Vol. I. 2nd ed. D. Van Nostrand Company, Inc., New York. pp. 181, 187.
——— 1955. Mém. soc. roy. sci. Liège. **15** (4): 291.
KIESS, N. H. and BASS, A. M. 1954. J. Chem. Phys. **22**: 569.
MARR, G. V. and NICHOLLS, R. W. 1955. Can. J. Phys. **33**: 394.
PHILLIPS, J. G. and BREWER, L. 1955. Mém. soc. roy. sci. Liège, **15** (4): 341.
ROSEN, B. and SWINGS, P. 1953. Ann. astrophys. **16**: 82.

ENERGY AND ANGULAR DISTRIBUTIONS OF PHOTOPROTONS PRODUCED BY 70 MEV. X-RAYS[1]

By W. K. Dawson[2]

ABSTRACT

Thin foils of aluminum, copper, rhodium, and gold were bombarded with the X-ray beam from the 70 Mev. synchrotron. The resulting photoprotons were detected by means of 200μ Ilford C-2 emulsions in a moving-plate camera which enabled energy distributions up to about 16 Mev. and angular distributions from 20 to 160 degrees with respect to the X-ray beam to be determined. At least 3500 tracks from each of aluminum, copper, and rhodium and about 2000 tracks from gold were measured. The experimental energy distributions have been compared to evaporation theory with a nuclear temperature independent of excitation energy and a photoelectric formula varying as $E^{-7/2}$. The evaporated component of the observed photoproton energy distributions can be fitted with constant nuclear temperatures of 2.1, 1.1, and 1.0 Mev. for aluminum, copper, and rhodium respectively. It has not been possible to give an interpretation of the energy distribution of photoprotons from gold. The angular distribution of photoprotons of energies greater than 8 Mev. from aluminum shows a pronounced forward asymmetry while those of lesser energy, as well as photoprotons of all observed energies from copper, appear to have isotropic angular distributions. Higher energy photoprotons from rhodium ($E_p > 7$ Mev.) and gold ($E_p > 11$ Mev.) have angular distributions which are well represented by $I(\theta) = a + b(\sin\theta + p \sin\theta \cos\theta)^2$. This angular distribution is attributed to interference between electric dipole and electric quadrupole absorption.

INTRODUCTION

The present paper describes some measurements made on the energy and angular distributions of photoprotons produced by bombarding various metallic foils with 70 Mev. X-rays. The elements used were aluminum, copper, rhodium, and gold, which roughly span the periodic table. While similar measurements have been made elsewhere on the first three named elements using lower bombarding energies (about 24 Mev.) and on aluminum up to 65 Mev., it was decided to repeat these measurements with a greater statistical accuracy and, with the exception of aluminum, at a higher energy.

Detection of the photoprotons was effected by means of nuclear emulsions in a moving-plate camera, which is described in the next section. The section on experimental results is preceded by a short discussion of some theoretical aspects of the problem and is followed by a comparison of the present results with those obtained by other authors.

APPARATUS

Fig. 1 shows in outline the construction of the nuclear plate camera used in the present experiments. A metal foil, a few thousandths of an inch thick and one inch long, placed at the center of a well-collimated beam of X-rays, is tilted to make a small angle with the beam. A nuclear plate (1 in. by 3 in.) is placed vertically with its long side parallel to the beam. The plate is slightly

[1]Manuscript received July 26, 1956.
Contribution from the Department of Physics, Queen's University, Kingston, Ontario. This work was reported at the Toronto Meeting of the American Physical Society on June 23, 1955.

[2]Present address: Suffield Experimental Station, Ralston, Alberta.

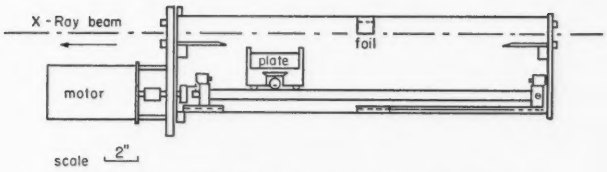

FIG. 1. Main features of the moving-plate camera used for the determination of the energy and angular distributions of photoprotons.

below the beam and off to one side, with the emulsion facing the beam. The plate-holding carriage rests on two tracks and is driven back and forth in a regular fashion by a motor outside the camera, allowing some of the protons leaving the foil at various angles to be recorded. Actually two plates placed symmetrically with respect to the beam are exposed simultaneously. The angular range covered by the camera is from 20 to 160 degrees with respect to the incident beam, and angles are determined by the angle included between the particle track and the long edge of the plate. The plates are outside the 20 to 160 degree angular interval when reversal of the direction of motion takes place.

Collimation of the X-ray beam to a width of about 0.5 in. at the target foil is effected by means of a lead collimator 8 in. thick. The X-ray beam enters and leaves the vacuum-tight camera through 0.005-in.-thick aluminum windows. Protons (or any other particles) ejected from the windows are prevented from entering the emulsion in such a way as to appear as though they came from the target foil by means of a brass baffle placed beneath each window. The air pressure inside the camera was usually less than 75 microns.

EXPERIMENTAL PROCEDURE

Centering of the camera in the X-ray beam was carried out using X-ray film, and the results from plates irradiated simultaneously on either side of the beam showed no significant differences in either the numbers of protons or their distributions. All irradiations were monitored with an ionization chamber placed directly in the beam and connected to a direct-current amplifier. The output of the amplifier was fed to an Esterline-Angus chart recorder, giving a permanent record of the beam intensity during an irradiation. The reading of this monitor has been compared with that given by a Victoreen thimble behind 7.3 cm. of lucite at a distance of 1 meter from the synchrotron target (Janzen 1953).

Ilford C-2 nuclear research emulsions, 200 microns thick, coated on 1 in. by 3 in. glass backings, were used for all the irradiations. With the particular geometry used, emulsions of this thickness allowed proton energy distributions up to about 16 Mev. to be determined. A temperature-change method was used for processing the plates (Dawson and Livesey 1956) and particular care was taken with the shrinkage factor measurements.

The majority of the scanning and track measurements were carried out using a combination of objective and eyepieces which gave a field of view of about 200 microns. During the reduction of the data obtained from track measurements comparisons were made between the tracks found on one transit and those found on neighboring (overlapping) transits in order to eliminate any duplications in measurement. Also the angle and dip measurements were used to discard tracks which could not have originated in the irradiated part of the foil.

Each accepted proton track was corrected for its range loss in the foil according to its angle of emission. The corrected ranges were converted to energies using Wilkins' (1951) range–energy relations for protons in Ilford C-2 emulsions. A further correction was applied to the number of observed protons with energies greater than 12 Mev. in order to allow for those tracks which were not measured because they did not end in the emulsion.

An experimental verification of the calculated variation of the camera's collection efficiency with angle was made using a radioactive source of alpha-particles which are emitted isotropically. Actinium active deposit was collected on a brass plate of size approximately that of the irradiated part of the foil. This source was placed in the camera which was then pumped down to 100 microns before the motion of the plates was started. Equivalent areas of the two plates exposed on either side of the source were scanned, and over 8000 tracks of alpha-particles were recorded. The numbers of tracks observed on the two plates agreed within the statistical limits, and the angular distributions when corrected for the calculated angular dependence of the camera's collection efficiency were isotropic in both plates.

THEORY

Two different types of process have been invoked in attempts to explain the observed energy and angular distributions of photoprotons from various elements. They are compound-nucleus formation, which will be discussed first, and a direct process in which no intermediate state is formed.

Energy Distribution of Evaporated Protons

Assuming compound-nucleus formation Weisskopf and Ewing (1940) have given an expression for the energy distribution of protons resulting from the absorption of monoenergetic gamma-rays. Diven and Almy (1950) and others (Toms and Stephens 1951; Byerly and Stephens 1951; Butler and Almy 1953) have used this expression in the calculation of the energy distribution of protons resulting from the bombardment of an element by high energy bremsstrahlung with the following result:

$$(1) \qquad I(\epsilon)d\epsilon = \epsilon\,\sigma_c(\epsilon)d\epsilon \int_{B_p+\epsilon}^{E\max} \frac{N_\gamma(E)\sigma_{\gamma,n}(E)\omega(E_Y)dE}{\int_0^{E-B_n} \epsilon'\sigma_c(\epsilon')\omega(E_Y)d\epsilon'},$$

where $I(\epsilon)d\epsilon$ = relative number of protons with energies between ϵ and $\epsilon+d\epsilon$,

B_p (B_n) = binding energy of a proton (neutron) in the target nucleus,

E_Y = excitation energy of residual nucleus = $(E-B-\epsilon)$,

$\sigma_c(\epsilon)$ = capture cross section for protons of energy ϵ on the residual nucleus having energy E_Y,

$N_\gamma(E)$ = number of photons of energy E per unit energy interval in the bremsstrahlung spectrum,

$\sigma_{\gamma,n}(E)$ = cross section for the (γ, n) reaction at photon energy E for the target nucleus,

$\omega(E_Y)$ = level density of the residual nucleus with excitation energy E_Y,

$E_{\max}$ = maximum bremsstrahlung energy.

Three of the quantities used in equation (1) are based on theoretical estimates. They are $\sigma_c(\epsilon)$, $N_\gamma(E)$, and $\omega(E_Y)$. The first two are usually considered as known and the observed energy distribution used to derive information about $\omega(E_Y)$. The values of $\sigma_c(\epsilon)$ for a nuclear radius of $1.3\times10^{-13}\,A^{1/3}$ cm. given by Blatt and Weisskopf (1952) and Schiff's (1946, 1951) calculation of $N_\gamma(E)$ modified for absorption of the X-ray beam in the material between the synchrotron target and the target foil were used. The present experimental energy distributions are best reproduced by equation (1) when a level density of the form $\omega(E_Y) = Ce^{E_Y/T}$ (where C is a constant and T the nuclear temperature in Mev.) due to Livesey (1955) is used. This choice of level density is discussed more fully below. With this substitution equation (1) becomes

$$I(\epsilon)d\epsilon = \epsilon\,\sigma_c(\epsilon)e^{-\epsilon/T}d\epsilon \int_{B_p+\epsilon}^{E\max} N_\gamma(E)\sigma_{\gamma,n}(E)dE. \tag{2}$$

Equation (2) was used to calculate the expected energy distribution of photoprotons resulting from compound nucleus formation.

A form of the level density that has been used by a number of authors is that resulting from the assumption that the particles in the nucleus may be considered as a degenerate Fermi–Dirac gas, i.e.

$$\omega(E_Y) = \omega_0 \exp(aE_Y)^{\frac{1}{2}}, \tag{3}$$

where ω_0 is the level density at zero excitation and a is a constant which is usually taken as $1.6(A-40)^{\frac{1}{2}}$ Mev.$^{-1}$. However, Toms and Stephens (1951) and Butler and Almy (1953) have found that a level density which increases more slowly than the predictions of equation (3) with increasing excitation energy was required to explain their observed photoproton energy distributions from Mg^{25} and Mo^{90} respectively. Livesey's assumption that at excitation energies less than about 10 Mev. the nuclear temperature is independent of excitation energy yields a level density of the form

$$\omega(E_Y) = C \exp(E_Y/T), \tag{4}$$

where C is a constant determined from the conditions at 10 Mev. and T is the nuclear temperature measured in energy units and is approximately given by $(100/A)^{\frac{1}{2}}$ Mev. With appropriate values of C and T equation (4) predicts a much slower rise in level density over the first 10 Mev. than equation (3), a prediction which, as Livesey has pointed out, is in accord with a number of experiments.

Energy Distribution of Direct Protons

Measurements of the cross sections for the production of photoprotons as well as the energy and angular distributions of the ejected protons have shown that the compound-nucleus picture only partially explains the features of these reactions. Courant (1951) found that several discrepancies could be greatly reduced by postulating that photoprotons could be ejected by a direct photoelectric process. According to this view the ejected particle gains sufficient energy directly from the incident photon to overcome the potential barrier and to leave the nucleus without any intermediate state being formed.

A calculation of the cross section for photon absorption by the direct process has been made by Courant (1951) and the cross section turns out to be a complicated function of the photon energy. Toms and Stephens (1953) have found that the energy dependence of the cross section may be considered as E^{-3}, which is close to the $E^{-7/2}$ dependence of the photoelectric effect. Because of the relatively large exponents in these expressions the particular value of the exponent chosen does not appreciably affect the calculated energy distribution. The energy distribution of the photoprotons resulting from the direct effect has been taken as

$$I(\epsilon)d\epsilon = f(\epsilon)d\epsilon \int_{B_p+\epsilon}^{E\max} N_\gamma(E)E^{-7/2}dE, \tag{5}$$

where $f(\epsilon)$ is a coulomb-barrier penetration factor. The integral is proportional to the number of nuclei capable of emitting a proton of energy ϵ. This very approximate formula has neglected the presence of competition between the various possible reactions and its effect on the energy distribution of the direct photoprotons.

Angular Distributions of Photoprotons

During the lifetime of the compound nucleus a large number of collisions between nucleons occur before a particle is ejected. Thus it is expected that there will be no preferred direction of emission, i.e., that the angular distribution of the outgoing particles will be isotropic, or nearly so (see Wolfenstein 1951).

Protons resulting from the direct photodisintegration process should have an angular distribution of the form $A+B\sin^2\theta$ if the process occurs by electric dipole absorption of the incident photon (Courant 1951). The ratio B/A depends on the angular momentum of the outgoing particle before and after emission. Electric quadrupole absorption results in an angular distribution having a $\sin^2\theta\cos^2\theta$ angular dependence. Interference between electric dipole and electric quadrupole absorption gives an angular distribution of the form

$$I(\theta) = a+b(\sin\theta+p\sin\theta\cos\theta)^2, \tag{6}$$

where $p^2/5$ is equal to the cross section for electric quadrupole absorption divided by that for electric dipole absorption. Angular distributions of this form have been found, and the values of p determined from them range from about 0.5 to 2 (Mann *et al.* 1952; Toms and Stephens 1953; Johansson 1955).

EXPERIMENTAL RESULTS

Energy Distributions

(*a*) *Aluminum*

The measured energy distribution of photoprotons from aluminum is shown by the histogram in Fig. 2 and is based on 3885 tracks. The aluminum target foil was 0.0020 in. thick.

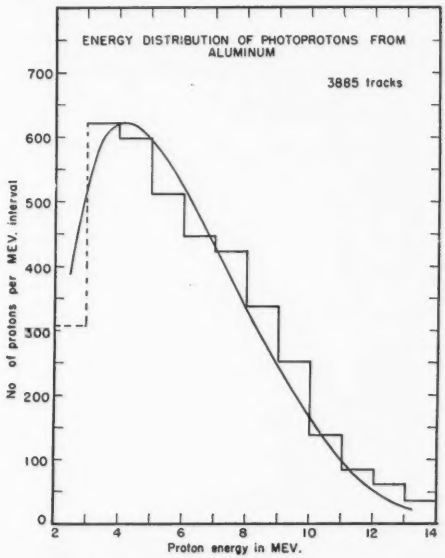

FIG. 2. The smooth curve is the energy distribution calculated assuming compound-nucleus formation only and a constant nuclear temperature of 2.1 Mev. The histogram represents the experimental results.

The smooth curve is the energy distribution calculated from equation (2) using the $Al^{27}(\gamma, n)Al^{26}$ cross section of Katz and Cameron (1951*b*). A nuclear temperature of 2.1 Mev. was used. This compares favorably with the value 1.9 Mev. obtained from $T = (100/A)^{\frac{1}{2}}$ Mev. (Livesey 1955).

The present comparison between theory and experiment makes use of evaporated protons only. However, the presence of up to 10% direct protons would still be consistent with the experimental results. The statistical accuracy at the high energy end of the distribution does not warrant any closer estimate than this.

The yield of photoprotons with energies less than 14 Mev. from aluminum was found to be 4.0×10^5 protons/r-mole at 70 Mev. Using nuclear emulsions Diven and Almy (1950) found a yield of 1.7×10^5 protons/r-mole at 21 Mev., while Halpern and Mann (1951) using scintillation counters found a yield of $(4.0\pm0.8)\times10^5$ protons/r-mole at 23.5 Mev. and an integrated cross section of 0.12 ± 0.03 Mev.-barn. Calculations made using Halpern and Mann's

$Al^{27}(\gamma, p)Mg^{26}$ cross section as a function of photon energy and the yield measured here result in a value of 0.15 Mev.-barn for the integrated cross section.

(*b*) *Copper*

When all the measured 3554 tracks from copper were assumed to be protons the full line histogram in Fig. 3 was obtained for their energy distribution. Uncertainty in the experimental point below 3 Mev. due to energy loss in the

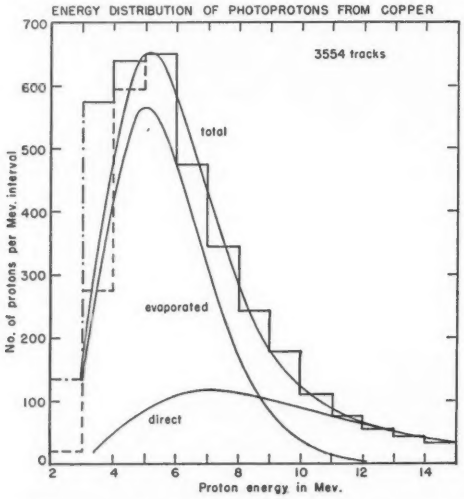

FIG. 3. The calculated energy distribution (smooth curve marked total) contains both evaporated and direct protons in a 7 to 3 ratio. The separate distributions are also shown. A constant nuclear temperature of 1.1 Mev. was used for the evaporated proton energy distribution.

foil (0.00123 in. thick) and the selection criterion for tracks is indicated by the dash–dot line. Byerly and Stephens (1951) have shown that the bombardment of copper with high energy bremsstrahlung leads to the production of an appreciable number of deuterons. The only reasonably certain way of distinguishing between protons and deuterons is to grain count every track. Rather than following this long and tedious process the deuteron component found by Byerly and Stephens was subtracted from the present results giving the dashed line below 9 Mev. This subtraction was carried out assuming that the deuteron energy distribution does not change appreciably when the bombarding energy is increased from 24 Mev. (the energy used by Byerly and Stephens) to 70 Mev. Some error may be introduced by this assumption.

Both evaporated and direct protons were required to explain the observed energy distribution. The normal copper (γ, n) cross section was obtained by multiplying Katz and Cameron's (1951*a*) cross sections for the individual isotopes by the isotopic abundance and then adding. A nuclear temperature

of 1.1 Mev. was used for the evaporated protons. The theoretical fit to the experimental data requires that approximately 30% of the total number of protons emitted be attributed to the direct emission process.

The calculated yield of 10×10^5 protons/r-mole at 70 Mev. for protons with energies less than 15 Mev. happens to agree almost exactly with the value 10.7×10^5 protons/r-mole found by Byerly and Stephens (1951) at 24 Mev.

(*c*) *Rhodium*

A total of 3696 proton tracks were observed from rhodium and their energy distribution is given by the histogram in Fig. 4. A target foil 0.00123 in. thick was used. As in the case of copper, both evaporated and direct protons were

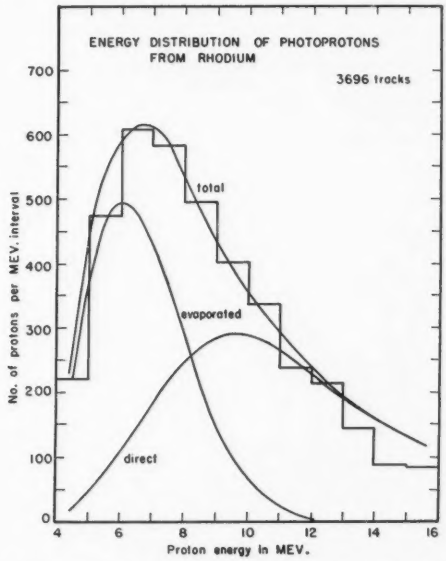

FIG. 4. The calculated energy distribution (smooth curve marked total) contains both evaporated and direct protons in a 1 to 1 ratio. The separate distributions are also shown. A constant nuclear temperature of 1.0 Mev. was used for the evaporated proton energy distribution.

required to explain the observed energy distribution. Nathans and Halpern's (1954) rhodium (γ, n) cross section and a nuclear temperature of 1.0 Mev. were used to calculate the expected energy distribution of the evaporated protons. Direct and evaporated protons appear to be present in approximately equal numbers.

The discrepancy between theory and experiment at the high energy end of the distribution may be caused by the poor statistical accuracy in this region or by too small a correction for tracks not measured because they did not terminate in the emulsion.

The calculated yield of 2.6×10^5 protons/r-mole for protons with energies

up to 16 Mev. agrees with yields measured in this region of Z at about 23 Mev. For example, Weinstock and Halpern's (1954) results indicate a value of about 2.5×10^5 protons/r-mole.

(*d*) *Gold*

Approximately 50 cm.^{2} of nuclear emulsion were scanned in order to obtain the 1989 photoproton tracks shown in Fig. 5. The gold target foil was 0.00098 in. thick. It has not been possible to fit the experimental energy

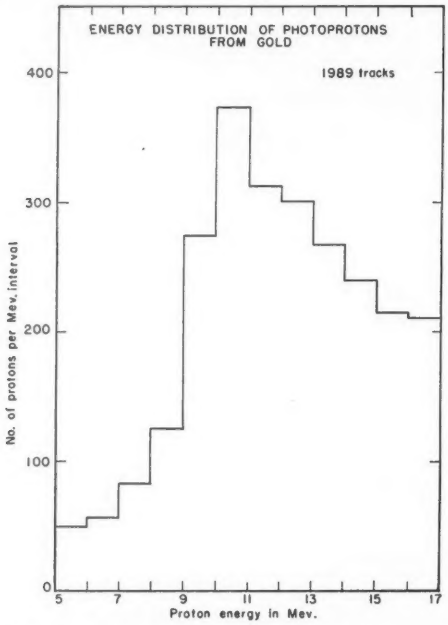

FIG. 5. The energy distribution of photoprotons from gold shown here cannot be explained on the basis of the theories outlined in the text.

distribution with any combination of direct and evaporated protons as was done for the previous elements. The difficulty lies in obtaining a curve which reproduces the extremely rapid rise in the energy distribution between about 8 and 10 Mev. The shape of this energy distribution is remarkably similar to that obtained by Toms and Stephens (1953) for photoprotons from bismuth.

The measured yield of photoprotons with energies less than 17 Mev. from gold is 6.8×10^4 protons/r-mole. Weinstock and Halpern (1954) give $(1.9\pm1.6)\times10^4$ protons/r-mole as the yield of photoprotons from gold at 22 Mev.

Angular Distributions

(*a*) *Aluminum*

The angular distributions of the photoprotons from aluminum are shown in Fig. 6. The decrease in the number of protons in the 2 to 4 Mev. group at small

and large angles is attributed to the track-length selection criterion and the large energy loss of low energy particles at these angles. Thus it is considered that the protons in this energy group are emitted isotropically. Protons with energies between 4 and 6 Mev. also appear to be emitted isotropically. There is an excess of particles in the 20 to 30 degree interval and all of these are in the 4 to 5 Mev. energy range. This excess might merely be a statistical fluctua-

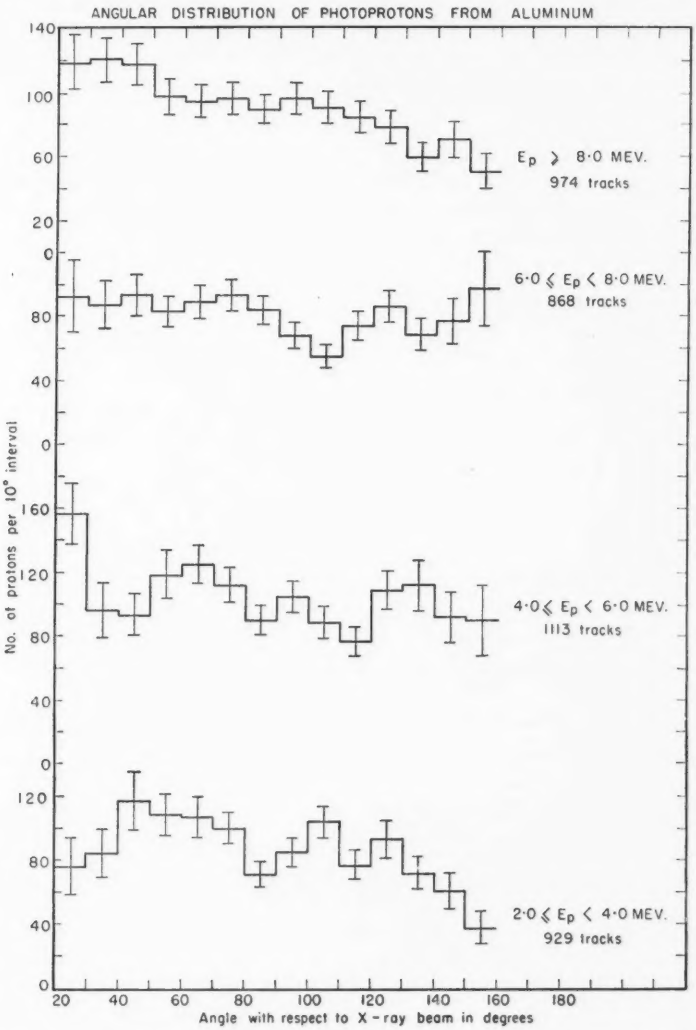
ANGULAR DISTRIBUTION OF PHOTOPROTONS FROM ALUMINUM
$E_p \geq 8{\cdot}0$ MEV.
974 tracks
$6{\cdot}0 \leq E_p < 8{\cdot}0$ MEV.
868 tracks
$4{\cdot}0 \leq E_p < 6{\cdot}0$ MEV.
1113 tracks
$2{\cdot}0 \leq E_p < 4{\cdot}0$ MEV.
929 tracks
No. of protons per 10° interval
Angle with respect to X-ray beam in degrees

FIG. 6. The angular distributions of photoprotons of various energies from aluminum. Standard deviations are shown.

tion. An isotropic angular distribution was obtained for protons with energies between 6 and 8 Mev.

Above a proton energy of 8 Mev. the angular distribution changes markedly from the isotropic ones obtained for protons of lower energies. There is a pronounced forward asymmetry. The number of protons between 20 and 30 degrees is approximately twice the number between 150 and 160 degrees. As the number of protons per 10-degree angular interval is still increasing at 20 degrees and the measurements do not extend to smaller angles, it is impossible to say whether the angular distribution goes through a maximum at small angles or whether it keeps on rising as the angle of emission decreases to zero.

(*b*) *Copper*

As shown by Fig. 7 the angular distributions of the photoprotons from copper do not show any significant deviations from isotropy. The possible presence of a small anisotropic component in the high energy group cannot be excluded on the basis of the present statistical accuracy.

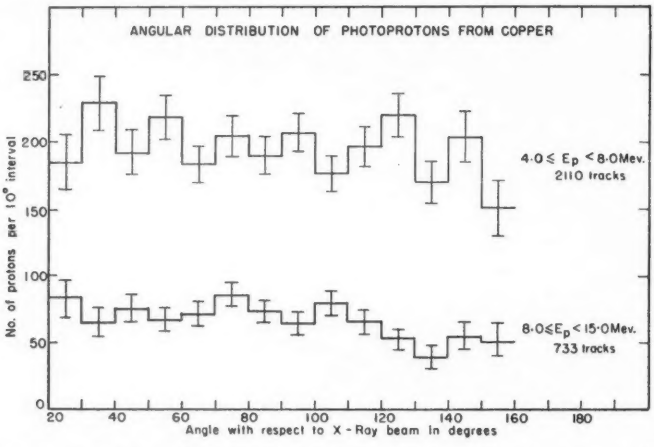

FIG. 7. The angular distributions of photoprotons of various energies from copper. Standard deviations are shown.

(*c*) *Rhodium*

The photoprotons from rhodium in the energy range from 4 to 7 Mev. are emitted isotropically as shown in Fig. 8. The decrease in the number of protons at large and small angles is attributed to the track-length selection criterion. Protons of energies greater than 7 Mev. have been divided into two groups and their angular distributions compared with that given by equation (6). The value of the ratio b/a increases from 0.8 for the 7 to 10 Mev. group to 1.5 for the 10 to 16 Mev. group. At the same time the value of p increases from 0.2 to 0.3. It is interesting to note that in going from the lower energy group to the higher energy group the peak in the angular distribution becomes more pronounced and moves forward slightly.

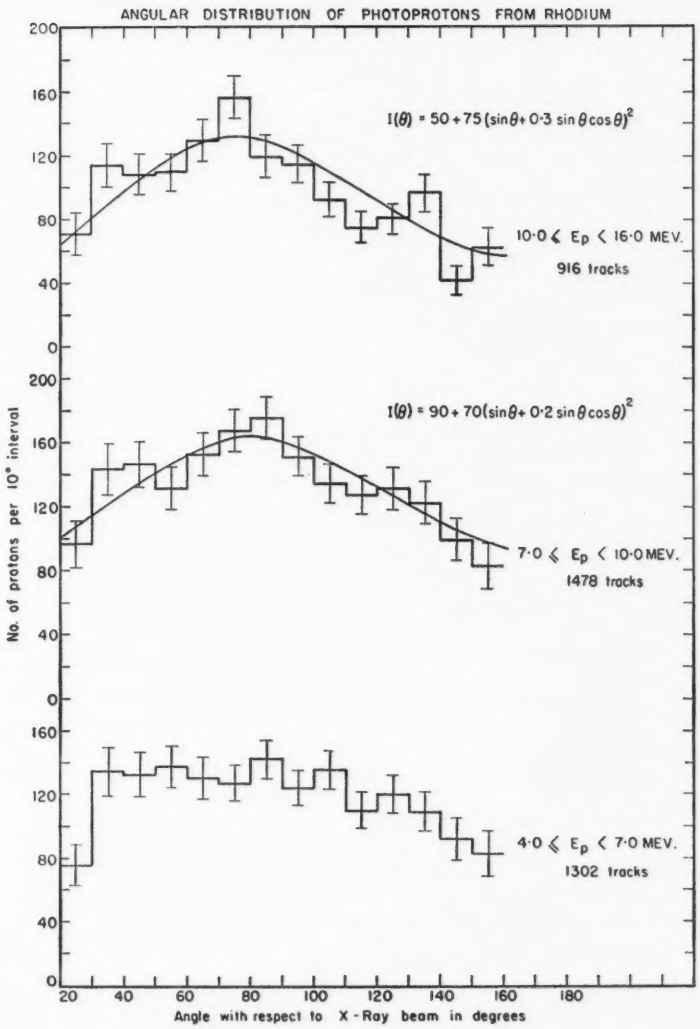
ANGULAR DISTRIBUTION OF PHOTOPROTONS FROM RHODIUM
I(θ) = 50 + 75 (sinθ + 0·3 sinθ cosθ)²
10·0 ≤ Ep < 16·0 MEV.
916 tracks
I(θ) = 90 + 70(sinθ + 0·2 sinθ cosθ)²
7·0 ≤ Ep < 10·0 MEV.
1478 tracks
4·0 ≤ Ep < 7·0 MEV.
1302 tracks
No. of protons per 10° interval
Angle with respect to X-Ray beam in degrees

FIG. 8. The angular distributions of photoprotons of various energies from rhodium. Standard deviations are shown. The smooth curves were calculated from equation (6).

(*d*) *Gold*

The angular distribution of photoprotons from gold with energies between 11 and 17 Mev. is shown by the upper histogram in Fig. 9. The solid line was obtained from equation (6) using a value of 1.0 for both b/a and p. This energy group was chosen as it contains all the protons past the peak in the energy

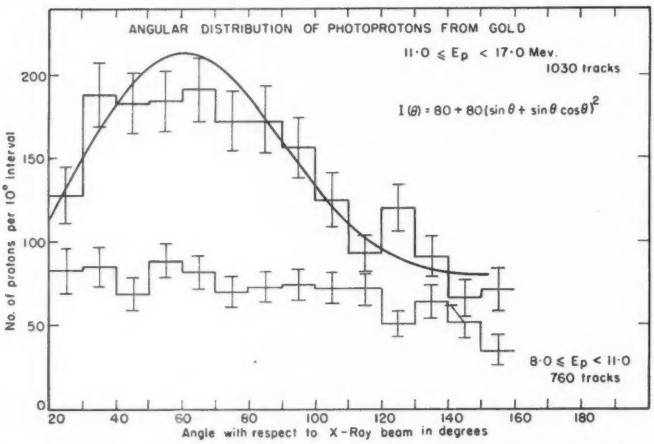
ANGULAR DISTRIBUTION OF PHOTOPROTONS FROM GOLD
11·0 ≤ Ep < 17·0 Mev.
1030 tracks
I(θ) = 80 + 80(sin θ + sin θ cosθ)²
8·0 ≤ Ep < 11·0
760 tracks
No. of protons per 10° interval
Angle with respect to X-Ray beam in degrees

FIG. 9. The angular distributions of photoprotons of various energies from gold. Standard deviations are shown. The smooth curve for the higher energy group ($11.0 \leqslant E_p < 17.0$ Mev.) was calculated from equation (6).

distribution. Protons in the 8 to 11 Mev. region (the rapidly rising part of the energy distribution) have an angular distribution which is not far from being isotropic. There may be a slight forward asymmetry.

DISCUSSION OF RESULTS

The preceding section shows that the theory outlined previously fits the experimental results in a satisfactory manner. The gold energy distribution forms a notable exception. Various aspects of the comparison between the theory, the present experimental results, and other data will now be considered.

Nuclear Temperatures

Table I summarizes some measurements of nuclear temperatures made here and elsewhere. No errors have been assigned to the present results as the

TABLE I

COMPARISON OF EXPERIMENTAL AND THEORETICAL VALUES OF NUCLEAR TEMPERATURE

Reaction	Incident energy	Reference	Nuclear temperature in Mev. Al	Cu	Rh
(p, n)	16 Mev.	Gugelot (1951)	1.3±0.1		0.85±0.1
(n, n')	14 Mev.	Graves and Rosen (1953)	1.01±0.10	0.77±0.08	
(n, n')	14 Mev.	Stelson and Goodman (1951)	1.1		
(n, n')	14.8 Mev.	O'Neill (1954)	1.06±0.16	0.82±0.12	
(γ, n)	70 Mev. X-rays	Dixon (1955)		1.2	
(γ, p)	70 Mev. X-rays	Present work	2.1	1.1	1.0
Calculated from $T = (100/A)^{\frac{1}{2}}$ Mev.		Livesey (1955)	1.9	1.2	1.0

nuclear temperature used depends somewhat on the interpretation of the energy distribution. It is believed that the nuclear temperatures given for copper and rhodium represent minimum values.

Copper is the only element for which both the photoneutron and photoproton energy distributions have been measured. Dixon's (1955) value of 1.2 Mev. for the nuclear temperature of copper derived from the photoneutron energy distribution is in excellent agreement with the nuclear temperature of 1.1 Mev. obtained from the photoproton energy distribution. Livesey's (1955) estimate of the nuclear temperature, $T = (100/A)^{\frac{1}{2}}$ Mev., is in good agreement with the values inferred from the present experimental results.

Nuclear temperatures determined from the energy distribution of neutrons resulting from nuclei formed by particle capture are definitely lower than those determined from the energy distributions of particles resulting from photon-induced reactions. Such a difference may arise as follows.

Since nuclear absorption of photons occurs mainly by an electric dipole process, the majority of the compound nuclei formed have a total angular momentum which differs from the ground state angular momentum by one unit. Compound nuclei formed by particle absorption can, however, have angular momenta differing from the ground state angular momentum by a wide range of values. Therefore more levels of the compound nuclei can be excited when they are formed by particle absorption than when they are formed by photon absorption. It then follows that particle-induced reactions lead to a larger number of levels of the residual nucleus than photon-induced reactions. A decrease in nuclear temperature is required to explain an increase in level density and, experimentally, a decrease in nuclear temperature is found.

Direct and Evaporated Protons

The comparison of the experimental results with the theory shows that as the atomic number increases an increasing fraction of the observed photoprotons must be attributed to the direct emission process. The fraction increases from roughly 10% in aluminum to 30% in copper and 50% in rhodium. Such a variation indicates that the direct emission process should account for practically all the observed photoprotons from gold. Toms and Stephens (1953, 1955) show that only about 5% of the observed photoprotons from Bi, Ta, and Pb^{208} can be explained by compound-nucleus formation.

According to the above evidence it should be possible to fit the observed gold photoproton energy distribution by a curve obtained from equation (5). However, equation (5) predicts an energy distribution which rises almost linearly from 7 to 13 Mev. and then rounds off and decreases slowly. If this curve is normalized to the experimental results at 15 Mev. and then subtracted from them a curve which peaks sharply at 10.5 Mev. is obtained. A nuclear temperature of 2.0 Mev. is required to place the evaporated photoproton energy distribution peak at this energy and, on this basis, about 35% of the protons must be considered as resulting from evaporation from the compound nucleus. The fit to the experimental data thus obtained, besides being a very

poor one, requires the use of values of the nuclear temperature and ratio of evaporated to direct protons which are neither expected from existing theories nor supported by other experiments.

The source of the discrepancy between theory and experiment may lie either in the coulomb-barrier penetration factors used or in the presence of another mechanism for the ejection of protons from heavy nuclei. Dixon (1955) has obtained some experimental evidence which, although not very conclusive, indicates that there may be a "very direct" emission of particles. In this process all the incident energy is given to the outgoing particle and the residual nucleus is left in its ground state. Thus the energy distribution of the ejected particles should have the same shape as the photon-absorption cross section. Because of the low yield of photoprotons no measurements of the (γ, p) cross section shapes have been made for heavy elements although they are of great interest. It is therefore impossible at present to shed any further light on Dixon's tentative hypothesis.

Yields of Photoprotons

The measured yields of photoprotons at 70 Mev. are as follows:

Aluminum, 4.0×10^5 protons up to 14 Mev./r-mole;
Copper, 10.0×10^5 protons up to 15 Mev./r-mole;
Rhodium, 2.6×10^5 protons up to 16 Mev./r-mole;
Gold, 6.8×10^4 protons up to 17 Mev./r-mole.

It is believed that the yields given are accurate to within about 30%. With the exception of gold, the measured yields are approximately the same as those determined elsewhere at 24 Mev.

If the (γ, p) cross section as a function of photon energy is known, then the photoproton yields at various maximum bremsstrahlung energies may be calculated. This has been done for aluminum using the (γ, p) cross section given by Halpern and Mann (1951). The calculated yields of 4.0×10^5 protons/r-mole at 30 Mev. and 3.4×10^5 protons/r-mole at 70 Mev. are to be compared with the measured yield of 4.0×10^5 protons/r-mole at both 25 and 70 Mev. The difference in the calculated yields is caused by the different photon spectra and the resulting effect on the dose measurements. Thus the measured yield at 70 Mev. is higher than the calculated one. If this difference is significant it is probably due to a contribution to the 70 Mev. yield by photons with energies greater than 26 Mev., above which energy the cross section was assumed to be zero.

Unfortunately, the (γ, p) cross sections as functions of photon energy are not known for copper, rhodium, and gold. The yields at 70 Mev. listed above are lower limits, as the energy spectra indicate the presence of protons with energies above the working range. As the measured yields at 70 Mev. in these elements are either approximately equal to or larger than those measured by others at 25 Mev., significant (γ, p) cross sections above 26 Mev. are indicated.

Angular Distributions

The low energy proton groups from each of the four elements irradiated are emitted isotropically, or very nearly so. With the exception of gold, the low

energy proton groups have been considered as largely consisting of evaporated protons for which isotropic angular distributions are expected. On the basis of other results for heavy elements nearly all the gold photoprotons should have an angular distribution given by equation (6). The isotropy, or apparent isotropy, of the 8 to 11 Mev. group is puzzling. The experimental angular distribution does show some signs of a forward asymmetry and it is possible that a small value of b/a accounts for the apparent isotropy. A somewhat analogous situation occurs for the high energy proton group from copper. Experimentally a very nearly isotropic angular distribution is found for these protons which, on the basis of their energy distribution, has been attributed to the direct effect.

The energy and angular distributions of photoprotons from aluminum have also been measured by Diven and Almy (1950) who used a maximum bremsstrahlung energy of 20.8 Mev. Allowing for the difference in bombarding energies their results are very similar to the present ones. They found essentially isotropic angular distributions for protons of up to 12 Mev. in energy. However, only about 100 protons with energies greater than 8 Mev. were observed. The higher bombarding energy used in the present experiment has permitted the measurement of a much larger number of protons with energies greater than 8 Mev., and these protons have been found to have a pronounced forward asymmetry in their angular distribution. Hoffman and Cameron (1953) have made similar measurements using energies up to 65 Mev. The emphasis in their work is on protons with energies greater than 20 Mev. whose angular distributions were found to be well represented by equation (6) with $a = 0$.

The copper photoproton energy distribution measured by Byerly and Stephens (1951) is in good agreement with the present results. Their angular distribution for protons with energies greater than 10 Mev. shows a pronounced peak at 90 degrees, whereas the data obtained here indicate a very nearly isotropic angular distribution for these protons.

Curtis *et al.* (1950) measured the energy and angular distributions of photoprotons ejected from rhodium by 20 Mev. bremsstrahlung. Their angular measurements indicated a symmetry about 90 degrees with the peak becoming more pronounced as the proton energy increased. The symmetry about 90 degrees was deduced from measurements made at 20, 90, and 160 degrees. The b/a ratio required to fit the angular distribution of the 10 to 16 Mev. proton group obtained here is larger than that used for the 7 to 10 Mev. group in accord with the interpretation of the energy distribution. The former group is considered to consist mainly of direct protons while the latter contains a large fraction of evaporated protons. The angular distributions also indicate that about 1% of the protons in the 7 to 10 Mev. group and 2% in the 10 to 16 Mev. group result from electric quadrupole absorption of the incident photons.

No previous measurements have been made of the energy and angular distributions of photoprotons from gold. The angular distribution of the 8 to 11 Mev. group has been discussed above. The higher energy group (11 to 17 Mev.) appears to be well described by equation (6) with $b/a = p = 1$. This value of p implies that the electric quadrupole cross section is one-fifth the electric dipole cross section.

ACKNOWLEDGMENTS

It is a pleasure to thank Professor B. W. Sargent for his encouragement and helpful advice throughout the course of this project. I am also greatly indebted to Dr. L. E. H. Trainor, Dr. D. L. Livesey, Mr. H. Janzen, and Mr. R. D. Bradfield, who contributed generously of their time and advice. Sincere thanks are due Mrs. E. MacPhail who ably measured a large portion of the proton tracks. Financial assistance from the National Research Council is gratefully acknowledged. This project was part of the synchrotron program at Queen's University receiving financial aid from the Atomic Energy Control Board.

REFERENCES

BLATT, J. M. and WEISSKOPF, V. F. 1952. Theoretical nuclear physics. John Wiley & Sons, Inc., New York.
BUTLER, W. A. and ALMY, G. M. 1953. Phys. Rev. **91**: 58.
BYERLY, P. R. and STEPHENS, W. E. 1951. Phys. Rev. **83**: 54.
COURANT, E. D. 1951. Phys. Rev. **82**: 703.
CURTIS, N. W., HORNBOSTEL, J., LEE, D. W., and SALANT, E. O. 1950. Phys. Rev. **77**: 290.
DAWSON, W. K. and LIVESEY, D. L. 1956. Can. J. Phys. **34**: 241.
DIVEN, B. C. and ALMY, G. M. 1950. Phys. Rev. **80**: 407.
DIXON, W. R. 1955. Can. J. Phys. **33**: 785.
GRAVES, E. R. and ROSEN, L. 1953. Phys. Rev. **89**: 343.
GUGELOT, P. C. 1951. Phys. Rev. **81**: 51.
HALPERN, J. and MANN, A. K. 1951. Phys. Rev. **83**: 370.
HOFFMAN, M. M. and CAMERON, A. G. W. 1953. Phys. Rev. **92**: 1184.
JANZEN, H. 1953. Thesis, Queen's University, Kingston, Ont.
JOHANSSON, S. A. E. 1955. Phys. Rev. **97**: 434.
KATZ, L. and CAMERON, A. G. W. 1951*a*. Can. J. Phys. **29**: 518.
——— 1951*b*. Phys. Rev. **84**: 1115.
LIVESEY, D. L. 1955. Can. J. Phys. **33**: 391.
MANN, A. K., HALPERN, J., and ROTHMAN, M. 1952. Phys. Rev. **87**: 146.
NATHANS, R. and HALPERN, J. 1954. Phys. Rev. **93**: 437.
O'NEILL, G. K. 1954. Phys. Rev. **95**: 1235.
SCHIFF, L. I. 1946. Phys. Rev. **70**: 87.
——— 1951. Phys. Rev. **83**: 252.
STELSON, P. H. and GOODMAN, C. 1951. Phys. Rev. **82**: 69.
TOMS, M. E. and STEPHENS, W. E. 1951. Phys. Rev. **82**: 709.
——— 1953. Phys. Rev. **92**: 362.
——— 1955. Phys. Rev. **98**: 626.
WEINSTOCK, E. V. and HALPERN, J. 1954. Phys. Rev. **94**: 1651.
WEISSKOPF, V. F. and EWING, D. H. 1940. Phys. Rev. **57**: 472.
WILKINS, J. J. 1951. Atomic Energy Research Establishment Report G/R 664, Harwell.
WOLFENSTEIN, L. 1951. Phys. Rev. **82**: 690.

SOME UPPER LIMITS OF ISOTOPIC ABUNDANCE—II: Ne, Cl, and Ga

By Larkin Kerwin and D. E. McElcheran

Continuing the search for possible rare isotopes of elements which do not appear to have been closely scrutinized (Kerwin 1956), we have been able to establish some upper limits of abundance for isotopes of the elements neon, chlorine, and gallium. The present status of the isotopic abundance of these elements is therefore as follows:

Isotope	Abundance, %	Reference
	Neon	
Ne 18	<0.05	This note
Ne 19	<0.01	This note
Ne 20	90.92	Nier (1950)
Ne 21	0.257	Nier (1950)
Ne 22	8.82	Nier (1950)
Ne 23	<0.01	Bleakney (1933), this note
Ne 24	<0.01	This note
Ne 25	<0.01	This note
	Chlorine	
Cl 31	<0.02	This note
Cl 32	<0.02	This note
Cl 33	<0.02	This note
Cl 34	<0.02	This note
Cl 35	75.4	Nier and Hanson (1936)
Cl 36	<0.07	This note
Cl 37	24.6	Nier and Hanson (1936)
Cl 38	<0.07	This note
Cl 39	<0.004	Nier and Hanson (1936)
	Gallium	
Ga 66	<0.04	This note
Ga 67	<0.04	This note
Ga 68	<0.04	This note
Ga 69	60.2	Inghram *et al.* (1948)
Ga 70	<0.07	This note
Ga 71	39.8	Inghram *et al.* (1948)
Ga 72	<0.2	This note
Ga 73	<0.04	This note
Ga 74	<0.04	This note

It is a pleasure to acknowledge the support of the Defence Research Board (Grant No. DRB-9510–13) during the progress of this work.

Bleakney, W. 1933. Phys. Rev. **43**: 1056A.
Inghram, M. G., Hess, D. C., Brown, H. S., and Goldberg, E. 1948. Phys. Rev. **74**: 343L.
Kerwin, L. 1956. Can. J. Phys. **34**: 1080.
Nier, A. O. 1950. Phys. Rev. **79**: 450.
Nier, A. O. and Hanson, E. E. 1936. Phys. Rev. **50**: 722.

Received September 19, 1956.
Département de Physique,
Université Laval,
Quebec, Que.

MECHANISM OF DISLOCATION LOCKING IN ATTENUATION OF HIGH FREQUENCY SOUND AT LOW TEMPERATURES

By T. S. Hutchison and G. J. Hutton

In a recent article Hutchison and Filmer (1956) describe low temperature internal friction peaks found at 155° K. with 5 Mc. sound waves in 99.99$_4$% pure aluminum of grain size 3–4 mm. The height of these peaks was markedly increased by small amounts of cold work of the order of 1.0–1.5%, and decreased by subsequent low temperature annealing. The activation energy of the peak is similar to that calculated for the low temperature internal friction peak in aluminum by Mason (1955), using results obtained from high frequency sound attenuation measurements by Bömmel (1954) and Bordoni (1954). Mason's dislocation relaxation mechanism proposed locking of the dislocations at irregular intervals with a maximum in the distribution at loop lengths of the order of 10^{-4} cm. It was assumed that the locking was by Cottrell impurity atmospheres. The present note describes experiments carried out to test the time dependence at room and lower temperatures of the internal friction peak produced by cold working.

The material used for these experiments was 99.99$_4$% aluminum containing 0.004% Fe, 0.002% Cu, <0.001% Mg, <0.001% Si, <0.001% Zn. A uniform, fine-grained specimen was prepared by two successive 30% compressions followed by anneals at 350° C. for one-half hour and 400° C. for one hour respectively. This gave a final grain size of the order of 0.25 mm. and eliminated all preferred orientation arising from the original rolling texture. The internal friction was measured, using 5 Mc. sound waves, over the range 250° K.–100° K., with an average rate of cooling of about 3° K. per minute. The result is shown in Fig. 1, case A. The specimen was then warmed to room tempera-

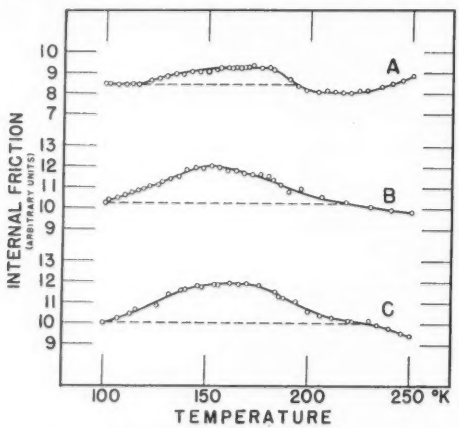

Fig. 1. Internal friction in pure aluminum.
A. As annealed.
B. Cold worked 1.16% and measured immediately.
C. Measured after 30 hr. at room temperature.

ture, cold worked 1.16% in compression in four seconds, and cooled to 250° K. within one minute from the time of compression. The internal friction measurements were then repeated immediately in precisely the same manner as in case A and over the same temperature range—case B. Lastly the specimen was allowed to return to room temperature (23° C.), held there for 30 hr., and again tested as before—case C.

The nature of the dependence of acoustic losses on temperature using this method of measurement is discussed in the previous paper by Hutchison and Filmer (1956). It can be seen from Fig. 1 that the height of the internal friction peak is almost doubled, and the background attenuation increased, immediately after cold work, and that both peak height and background remain unchanged by the subsequent room temperature aging. A similar series of measurements on a sample cold worked 1.7% and measured after 5 min. and 40 hr. at room temperature produced the same result, i.e., no change in the height of the deformation-induced internal friction peak during room temperature aging.

Cottrell and Bilby (1949) have derived the following expression for $n(t)$, the number of impurity atoms which would segregate to unit length (1 cm.) of dislocation in time t:

$$n(t) = n_0\, 3(\pi/2)^{1/3}(A\ Dt/kT)^{2/3}$$

where n_0 is the initial number of atoms in solution per unit volume, D is the diffusion coefficient for these atoms, and A, derived by Cottrell (1948), is a constant characteristic of a given system. For the system under consideration here, calculation of $n(t)$ at time $t = 60$ sec. gives values between 2.4×10^7 and 5×10^6, depending on the assumptions made in deriving A and in extrapolating to values of D for such low impurity concentrations and for such a low temperature. If we take the latter value of $n(t)$ and assume uniform spacing of impurity atoms in condensed atmospheres along the dislocation lines, then the loop lengths between locking points would be of the order of 10^{-7} cm. This length, a *maximum* loop length after 60 sec. aging at room temperature, is far too small to account for the observed internal friction peak on the basis of a dislocation relaxation mechanism.

Also, both calculations based on the Cottrell mechanism, and experimental observation by Smallman, Williamson, and Ardley (1953) of the time dependence of the appearance of a yield point in commercially pure aluminum and by McReynolds (1949) and Cupp *et al.* (1956) of a time dependent yield point phenomenon in superpure aluminum, indicate that aging is by no means complete after 60 sec. Thus, if the internal friction peak found one minute after cold working were indeed due to impurity locking, it would change in height and position as aging progressed and the average loop length changed. As we have seen, it does not.

In any case the ratio of impurity concentration to dislocation density in the system under consideration is such that after 30 hr. aging at room temperature (or probably much less) far more than enough impurity atoms would have segregated to the dislocations to lock them along their entire lengths (Cottrell 1953).

It therefore seems unlikely that a distribution of dislocation loop lengths necessary for the observed relaxation peak phenomena can be explained on the basis of an impurity locking mechanism. If, however, the dislocations produced by the cold work are on intersecting slip planes the locking may well be predominantly by the network so formed. This would account for the observed fact that the peak height does not change appreciably with room temperature aging.

Further experiments by the authors on other characteristics of the attenuation maxima also indicate that the locking is by other dislocations or arrays.

This work was supported by Defence Research Board of Canada, Grant Number 7510–14, Project D44–75–10–14.

BÖMMEL, H. E. 1954. Phys. Rev. **96**: 220.
BORDONI, P. G. 1954. J. Acoust. Soc. Amer. **26**: 495.
COTTRELL, A. H. 1948. Report of a Conference on the Strength of Solids. Physical Society, London. p. 30.
——— 1953. Dislocations and plastic flow in crystals. Clarendon Press, Oxford. p. 139.
COTTRELL, A. H. and BILBY, B. A. 1949. Proc. Phys. Soc., A, **62**: 49.
CUPP, C. R., DAVIS, R. S., ELBAUM, C., and HUTTON, G. J. 1956. Acta Met. In press.
HUTCHISON, T. S. and FILMER, A. J. 1956. Can. J. Phys. **34**: 159.
MCREYNOLDS, A. W. 1949. Trans. Am. Inst. Mining Met. Engrs. **185**: 32.
MASON, W. P. 1955. J. Acoust. Soc. Amer. **27**: 643.
SMALLMAN, R. E., WILLIAMSON, G. K., and ARDLEY, G. 1953. Acta Met. **1**: 126.

RECEIVED JULY 31, 1956.
DEPARTMENT OF PHYSICS,
ROYAL MILITARY COLLEGE OF CANADA,
KINGSTON, ONTARIO.

CONTENTS OF VOLUME 34

Adey, A. W. Scattering of electromagnetic waves by coaxial cylinders, 510.

Adey, A. W. and **Britton, J.** A microwave waveguide trombone phase shifter, 1112.

Alexander, T. K. See Chadwick, G. B., 381.

Aziz, R. A. and **Scott, G. D.** The effect of incident atomic velocity on the structure of evaporated silver films, 731.

Bainbridge, G. R. See Isenor, N. R., 993.

Bainbridge, G. R. and **Prowse, W. A.** The absorption of ultraviolet ionizing radiation in gases, 1038.

Baird, D. C. Current dependence of the superconducting transition, 725.

Baker, G. A., Sr. See Baker, G. A., Jr., 423.

Baker, G. A., Jr. and **Baker, G. A., Sr.** Structure of the mass increments of isotopes, 423.

Bardeen, J. Interaction between electrons and lattice vibrations, 1171.

Bartholomew, G. A., Litherland, A. E., Paul, E. B., and **Gove, H. E.** Note on the $T = 3/2$ state in N^{15}, 147(L).

Bauer, E. and **Wu, T.-Y.** Cross sections of dissociative recombination, 1436.

Bekefi, G. and **Farnell, G. W.** A homogeneous dielectric sphere as a microwave lens, 790.

Bell, R. E. The resolver, a circuit for reducing the counting losses of a scaler, 563.

Bell, R. E. and **Skarsgard, H. M.** Cross sections of (p, xn) reactions in the isotopes of lead and bismuth, 745.

Benedict, W. S., Herman, R., Moore, G. E., and **Silverman, S.** The strengths, widths, and shapes of infrared lines. I. General considerations, 830.

The strengths, widths, and shapes of infrared lines. II. The HCl fundamental, 850.

Benson, C. B. and **Hollis Hallett, A. C.** The oscillating sphere at large amplitudes in liquid helium, 668.

Benson, G. C. A simple formula for evaluating the Madelung constant of a NaCl-type crystal, 888.

See also van Zeggeren, F., 985.

Benson, G. C., Schreiber, H. P., and **Patterson, D.** An examination of Verwey's model for the lattice structure of the free surface of alkali halide crystals, 265.

van den Berg, G. J. See Gorter, C. J., 1281.

Bhatia, A. B. and **MacDonald, D. K. C.** On the thermoelectric power of dilute metallic alloys, 419.

Blackwell, J. H. The axial-flow error in the thermal-conductivity probe, 412.

Blakemore, J. S. Photoconductivity in indium-doped silicon, 938.

Bloembergen, N. Nuclear magnetic resonance and electronic structure of conductors, 1299.

Boivin, A., Dion, A., and **Koenig, H. P.** Étude expérimentale de la diffraction des micro-ondes par des ouvertures à symétrie de révolution, 166.

Bolling, G. F., Tiller, W. A., and **Rutter, J. W.** Growth twins in germanium, 234.

Borelius, G. Phenomenological aspects of the resistivity of pure metals, 1336.

Boucher, R. R. See Runnalls, O. J. C., 949.

Britton, J. See Adey, A. W., 1112.

Brodie, D. E. See Johns, M. W., 147(L).

Broida, H. P. See Kiess, N. H., 1471.

Buckmaster, H. A. $\Delta M = \pm 2$ transitions in dilute gadolinium ethyl sulphate, 150(L).

$\Delta M = \pm 3$ transitions in dilute gadolinium ethyl sulphate, 341(L).

Buckmaster, H. A. and **Scovil, H. E. D.** A double magnetic field modulation paramagnetic resonance spectrometer, 711.

Burgess, R. E. Line source with progressive phase shift, 149(L).

Callomon, J. H. An emission spectrum of the diacetylene ion. A study of Schüler's "T" spectrum under high resolution, 1046.

Campbell, L. L. Standard deviation of dead time correction in counters, 929.

Carroll, P. K. The spectrum of CN in the vacuum ultraviolet, 83.

Chadwick, G. B., Alexander, T. K., and **Warren, J. B.** Gamma radiation from the proton bombardment of boron ten, 381.

Chalmers, B. See Jackson, K. A., 473.

Chambers, R. G. Our knowledge of the Fermi surface, 1395.
Coish, H. R. Infeld factorization and angular momentum, 343.
Collin, R. E. Reflection and transmission at a slotted dielectric interface, 398.
Crawford, G. J. B. and **Foster, J. S.** Spin echoes in alcohols and derivatives, 653.
Dawson, W. K. Energy and angular distributions of photoprotons produced by 70 Mev. X-rays, 1480.
Dawson, W. K. and **Livesey, D. L.** The photodisintegration of oxygen nuclei into four alpha-particles, 241.
Dion, A. See Boivin, A., 166.
Dixon, W. R. See Trainor, L. E. H., 229.
Douglas, R. A., Gasten, B. R., and **Mukerji, A.** Production and properties of C^{15}, 1097.
Duckworth, H. E. See Eve, C. F., 896(L); Isenor, N. R., 993.
Eastman, P. C. See Isenor, N. R., 993.
Edwards, M. H. The index of refraction of liquid helium, 898(L).
Edwards, M. H. and **Rogers, D. H.** Comments on an experiment with persistent currents, 619.
Eichholz, G. G. and **Krzyzewski, J. V.** The half-life of mercury-203, 1167.
Embleton, T. F. W. The radiation force on a spherical obstacle in a cylindrical sound field, 276.
Ericksen, J. L. Stress deformation relations for solids, 226.
Eve, C. F. and **Duckworth, H. E.** The luminescent response of silver activated zinc sulphide to lithium ions of different energies, 896(L).
Farnell, G. W. See Bekefi, G., 790.
Feldman, T., Romanko, J., and **Welsh, H. L.** The Raman spectrum of ethylene, 737.
Feldman, T., Shepherd, G. G., and **Welsh, H. L.** The Raman spectrum of acetylene, 1425.
Fenton, K. B. See Rose, D. C., 968.
Filmer, A. J. See Hutchison, T. S., 159.
Forsyth, P. A. and **Vogan, E. L.** The duration of forward-scattered signals from meteor trails, 535.
Foster, J. S. See Crawford, G. J. B., 653.
Frederikse, H. P. R. and **Hosler, W. R.** Galvanomagnetic effects in *n*-type InSb at 4.2° K., 1377.
Friedel, J. On some electrical and magnetic properties of metallic solid solutions, 1190.
Gambling, W. A. Cathodic glow-to-arc transitions, 1466.
Garrett, C. and **Geiger, K. W.** A new Canadian primary radium standard, 1075.
Gasten, B. R. See Douglas, R. A., 1097.
Geiger, K. W. Evaporation neutrons from cosmic ray nuclear interactions in various elements, 2
See also Garrett, C., 1075.
Geoffrion, C. See Giroux, G., 153.
Geoffrion, C. and **Giroux, G.** An optimum parameter beta-ray spectrometer, 920.
Giroux, G. See Geoffrion, C., 920.
Giroux, G. and **Geoffrion, C.** Detection of electrons in the very low energy range, 153.
Godbole, E. W. The normal cathode fall in a-c. glows, 616.
Gorter, C. J. On the magnitude of the contribution of a circulation effect to the thermal conductivity of a superconductor, 1334.
Gorter, C. J., van den Berg, G. J., and **de Nobel, J.** Remarks on the anomalous behavior of alloys containing traces of manganese or similar elements, 1281.
Gove, H. E. See Bartholomew, G. A., 147(L).
Griffiths, G. M. The resonant absorption of γ-rays by N^{14}, 339(L).
Haering, R. R. and **Volkoff, G. M.** Nuclear quadrupole resonance spectrum of B^{11} in kernite, 577.
Hanna, G. C. and **Runnalls, O. J. C.** Measurement of the neutron yields from actinide–beryllium alloys, 959.
Hansen, R. C. Electromagnetic field solutions for rotational coordinate systems, 893.
Hart, J. and **Mungall, A. G.** The electrical conductivity of chlorobenzene, 491.
Hartz, T. R., Reid, G. C., and **Vogan, E. L.** V.H.F. auroral noise, 728(L).

Hedgcock, F. T. Magnetic susceptibility of low resistivity *n*-type germanium, 43. Magnetic susceptibility of rubidium and the electrical resistance anomaly, 1164.

van Heel, A. C. S. Thickness control of thin layers, 1460.

Herman, R. See Benedict, W. S., 830, 850.

Herman, R. and **Rubin, R. J.** Influence of vibration-rotation interaction on the intensities of pure rotation lines of diatomic molecules, 1119.

Herzberg, G., Lagerqvist, A., and **Miescher, E.** Fine structure analysis and mutual perturbation of the δ and β bands of the NO molecule, 622(L).

Herzberg, G. and **Shoosmith, J.** Absorption spectrum of free CH_3 and CD_3 radicals, 523(L).

Hines, C. O. and **Pugh, R. E.** The spatial distribution of signal sources in meteoric forward-scattering, 1005.

Hobson, J. P. The reflection of slow electrons from tantalum and copper, 1089.

Hollis Hallett, A. C. See Benson, C. B., 668.

Holuj, F. and **Petch, H. E.** The nuclear magnetic resonance spectrum of Na^{23} in $NaH_2PO_4{\cdot}2H_2O$, 1169(L).

Hosler, W. R. See Frederikse, H. P. R., 1377.

Hull, T. E. and **Julius, R. S.** Enclosed quantum mechanical systems, 914.

Hurd, R. A. End-fire arrays of magnetic line sources mounted on a conducting half-plane, 370. Radiation patterns of a dielectric-coated axially-slotted cylinder, 638.

Hutchison, T. S. and **Filmer, A. J.** Attenuation of 5 Mc. sound in aluminum at low temperatures, 159.

Hutchison, T. S. and **Hutton, G. J.** Mechanism of dislocation locking in attenuation of high frequency sound at low temperatures, 1498.

Hutton, G. J. See Hutchison, T. S., 1498.

International Conference on Electron Transport in Metals and Solids, 1171–1423.

Isenor, N. R., Bainbridge, G. R., Eastman, P. C., and **Duckworth, H. E.** A note on the effect of the residual gas pressure upon the spacing of mass spectroscopic doublets, 993.

Jackson, J. D. A schematic model for (p, xn) cross sections in heavy elements, 767.

Jackson, K. A. and **Chalmers, B.** Kinetics of solidification, 473.

Jacobs, I. S. See Schmitt, R. W., 1285.

Jacobs, J. A. and **Obayashi, T.** The diurnal behavior of sudden commencements of magnetic storms at Agincourt, 876.

Jakeman, D. Production of cosmic ray mesons at large zenith angles, 432.

Joffé, A. F. Heat transfer in semiconductors, 1342.

Johns, M. W., McMullen, C. C., Williams, I. R., and **Nablo, S. V.** The decay of Re^{186} and Re^{188}, 69.

Johns, M. W., Williams, I. R., and **Brodie, D. E.** The role of the 1.30 Mev. gamma-ray in the decay of In^{114}, 147(L).

Jones, G. and **Warren, J. B.** The lifetime of positrons annihilating in aluminum, 1033.

Julius, R. S. See Hull, T. E., 914.

Katzman, J. See Rose, D. C., 1, 884, 968.

Kelly, F. M. and **Sutherland, J. B.** A note on optical hyperfine structure in Cd II, 521.

Kerwin, L. Some upper limits of isotopic abundance—I: A, Mn, and Cd, 1080.

Kerwin, L. and **McElcheran, D. E.** Some upper limits of isotopic abundance—II: Ne, Cl, and Ga, 1497.

Kiess, N. H. and **Broida, H. P.** Spectrum of the C_3 molecule between 3600 Å and 4200 Å, 1471.

Klemens, P. G. Electrical resistance due to lattice imperfections in metals, 1212.

Koenig, H. P. See Boivin, A., 166.

Korringa, J. On the resistivity anomalies in some diluted alloys, 1290.

Krause, L. and **Welsh, H. L.** The Raman spectrum of dideuteroacetylene, 1431.

Krzyzewski, J. V. See Eichholz, G. G., 1167.

Kubo, R. A general expression for the conductivity tensor, 1274.

Lagerqvist, A. See Herzberg, G., 622(L).

Lancaster, J. E. and **Stoicheff, B. P.** High resolution Raman spectroscopy of gases. VII. Rotational spectra of *s*-triazine and *s*-triazine-d_3, 1016.

Langseth, A. and **Stoicheff, B. P.** High resolution Raman spectroscopy of gases. VI. Rotational spectrum of symmetric benzene-d_3, 350.

Litherland, A. E. See Bartholomew, G. A., 147(L).

Livesey, D. L. Range–energy relations for light nuclei in air and nuclear emulsion, 203.
(γ, $p + \alpha$) reactions produced in photographic emulsions, 216.
The photoprotons emitted from oxygen-16 nuclei, 1022.
See also Dawson, W. K., 241.

Lofthus, A. Emission band spectra of nitrogen. The Lyman–Birge–Hopfield system, 780.

MacDonald, A. D. and **Matthews, J. H.** Electrical breakdown in argon at ultrahigh frequencies, 395.

MacDonald, D. K. C. See Bhatia, A. B., 419.

MacDonald, D. K. C., Pearson, W. B., and **Towle, L. T.** An investigation of the sodium–potassium equilibrium diagram, 389.

MacDonald, D. K. C. and **Towle, L. T.** Integrals of interest in metallic conductivity, 418.

McElcheran, D. E. See Kerwin, L., 1497.

McKinley, D. W. R. See Millman, P. M., 50.

McKinley, D. W. R. and **McNamara, A. G.** Meteoric echoes observed simultaneously by back scatter and forward scatter, 625.

McLay, A. B. See Subbarao, M. K., 546.

McLay, A. B. and **Subbarao, M. K.** Diffraction of 3.2 cm. electromagnetic waves by dielectric rods. II. Lucite $1\frac{1}{2}$ in. diameter cylinder and semicylinder, 555.

McMullen, C. C. See Johns, M. W., 69.

McNamara, A. G. See McKinley, D. W. R., 625.

Marris, A. W. On fully developed turbulent flow in curved channels, 1134.

Mathai, P. M., Shepherd, G. G., and **Welsh, H. L.** The Raman spectrum of cyclopropane, 1448.

Matthews, J. H. See MacDonald, A. D., 395.

Mendelssohn, K. Electrical and thermal conductivity of metals, 1315.

Miescher, E. See Herzberg, G., 622(L).

Millman, P. M. and **McKinley, D. W. R.** Meteor echo durations and visual magnitudes, 50.

Moore, G. E. See Benedict, W. S., 830, 850.

Moore, R. D. See Standil, S., 1126.

Mooser, E. and **Pearson, W. B.** The chemical bond in semiconductors. The Group V B to VII B elements and compounds formed between them, 1369.

Mott, N. F. On the transition to metallic conduction in semiconductors, 1356.

Mukerji, A. See Douglas, R. A., 1097.

Mungall, A. G. See Hart, J., 491.

Myers, H. P. Paramagnetism of the γ phase in copper manganese alloys, 527.

Nablo, S. V. See Johns, M. W., 69.

Newton, T. D. Shell effects on the spacing of nuclear levels, 804.

Nielsen, H. H. See Rao, K. N., 1147.

Niven, C. D. On the effect of speed on the kinetic friction of some plastic materials on ice, 362.

de Nobel, J. See Gorter, C. J., 1281.

Obayashi, T. See Jacobs, J. A., 876.

Ogilvie, K. W. A note on the zenith angle dependence of cosmic ray protons at sea level, 1081.

Okashimo, K. See Wait, J. R., 190.

Patterson, D. See Benson, G. C., 265.

Paul, E. B. See Bartholomew, G. A., 147(L).

Pearson, W. B. See MacDonald, D. K. C., 389; Mooser, E., 1369.

Petch, H. E. See Holuj, F., 1169(L).

Pines, D. Electron interaction in solids, 1379.

Preston, M. A. See Shapiro, J., 451.

Prigogine, I. On the statistical mechanics of irreversible processes, 1236.

Proceedings of the International Conference on Electron Transport in Metals and Solids, 1171–1423.

Prowse, W. A. See Bainbridge, G. R., 1038.

Pugh, R. E. The number density of meteor trails observable by the forward-scattering of radio waves, 997.
See also Hines, C. O., 1005.

Rao, K. N. and **Nielsen, H. H.** Fermi diad $10^{0}0$ and $02^{0}0$ of nitrous oxide, 1147.

Redhead, P. A. Periodic fluctuations in oxide-cathode diodes, 1077.

Reid, G. C. See Hartz, T. R., 728(L).

Robinson, G. W. Some results of the high dispersion electronic emission spectrum of formaldehyde, 699.

Rogers, D. H. See Edwards, M. H., 619.

Romanko, J. See Feldman, T., 737.

Rose, D. C., Fenton, K. B., Katzman, J., and **Simpson, J. A.** Latitude effect of the cosmic ray nucleon and meson components at sea level from the Arctic to the Antarctic, 968.

Rose, D. C. and **Katzman, J.** The geomagnetic latitude effect on the nucleon and meson component of cosmic rays at sea level, I.
The sudden increase in cosmic ray intensity of February 23, 1956, 884.

Roulston, K. I. See Williams, R. C., 1087(L).

Rubin, R. J. See Herman, R., 1119.

Runnalls, O. J. C. See Hanna, G. C., 959.

Runnalls, O. J. C. and **Boucher, R. R.** Neutron yields from actinide–beryllium alloys, 949.

Rutter, J. W. See Bolling, G. F., 234; Tiller, W. A., 96.

Sample, J. T. Small-angle scattering of fast polarized neutrons by heavy nuclei, 36.

Scheidegger, A. E. Finite displacements in rheological bodies, 498.
Correlation tensors in statistical hydrodynamics in porous media, 692.

Schmitt, R. W. and **Jacobs, I. S.** Magnetization and magnetoresistance of some dilute alloys of Mn in Cu, 1285.

Schreiber, H. P. See Benson, G. C., 265.

Scott, G. D. See Aziz, R. A., 731.

Scovil, H. E. D. See Buckmaster, H. A., 711.

Seeger, A. On the electrical resistivity of stacking-faults in monovalent metals, 1219.
A variational principle for conduction phenomena in the presence of a magnetic field or asymmetric scattering mechanisms, 1278.

Shapiro, J. and **Preston, M. A.** A study of nucleon forces with repulsive cores. II. Low energy properties, particularly charge independence, 451.

Shepherd, G. G. See Feldman, T., 1025; Mathai, P. M., 1448.

Shoosmith, J. See Herzberg, G., 523(L).

Silverman, S. See Benedict, W. S., 830, 850.

Simpson, J. A. See Rose, D. C., 968.

Skarsgard, H. M. See Bell, R. E., 745.

Skinner, R. A quantum mechanical description of collective motions, 901.

Sondheimer, E. H. Electron–phonon equilibrium and the transport phenomena in metals at low temperatures, 1246.

Stacey, F. D. The behavior of ferromagnetics under strong compression, 304.

Standil, S. and **Moore, R. D.** Absolute pair production cross section of lead at 2.76 Mev., 1126.

Stewart, J. D. Some notes on the theory of thermal-neutron reactors, 20.

Stewart, R. W. A new look at the Reynolds' stresses, 722.

Stoicheff, B. P. See Lancaster, J. E., 1016; Langseth, A., 350.

Storey, L. R. O. A method to detect the presence of ionized hydrogen in the outer atmosphere, 1153.

Subbarao, M. K. See McLay, A. B., 555.

Subbarao, M. K. and **McLay, A. B.** Diffraction of 3.2 cm. electromagnetic waves by dielectric rods. I. Lucite and tenite 1 in. diameter cylinders, 546.

Sutherland, J. B. See Kelly, F. M., 521.

Takahashi, Y. The relationship between the statistical and field theoretical treatments of multiple meson production, 378.

Theimer, O. Selection rules and temperature dependence of the first-order Raman effect in crystals, 312.

Tiller, W. A. Alloy dendritic growth, 729(L).
See also Bolling, G. F., 234.

Tiller, W. A. and **Rutter, J. W.** The effect of growth conditions upon the solidification of a binary alloy, 96.

Towle, L. T. See MacDonald, D. K. C., 389, 418.

Trainor, L. E. H. and **Dixon, W. R.** The possibility of a phase change in nuclear matter, 229.

Vogan, E. L. See Forsyth, P. A., 535; Hartz, T. R., 728(L).

Volkoff, G. M. See Haering, R. R., 577.

Wait, J. R. Radiation resistance of dipoles in an interface between two dielectrics, 24.
Transient fields of a vertical dipole over a homogeneous curved ground, 27.
Low frequency radiation from a horizontal antenna over a spherical earth, 586.
Shielding of a transient electromagnetic dipole field by a conductive sheet, 890.

Wait, J. R. and **Okashimo, K.** Patterns of stub antennas on cylindrical structures, 190.

Wallace, P. R. A modification of the one-particle formula for nuclear gamma-radiation, 62.

Warren, J. B. See Chadwick, G. B., 381; Jones, G., 1033.

Webb, E. L. R. On the distribution of the product of diode detector waveforms, 679.

Welsh, H. L. See Feldman, T., 737, 1425; Krause, L., 1431; Mathai, P. M., 1448.

White, G. K. Conductivity of metals at low temperatures, 1328.

Wilkinson, P. G. The far ultraviolet ($C-X$) bands of N_2^+, 250.
Absorption spectra of benzene and benzene-d_6 in the vacuum ultraviolet, 596.
Absorption spectra of ethylene and ethylene-d_4 in the vacuum ultraviolet. II, 643.

Williams, I. R. See Johns, M. W., 69, 147(L).

Williams, R. C. and **Roulston, K. I.** Gamma–gamma angular correlation in W^{182}, 1087(L).

Wolfson, J. L. High-energy forbidden β-ray transitions from Cs^{134} (2.3 yr.), Co^{60} (5.3 yr.), Sc^{46} (84 d.), and Hg^{203} (47.9 d.), 256.

Wong, J. Y. On the theory of a coaxial transmission line consisting of elliptic conductors, 354.

Woods, S. B. The conductivity of sodium at low temperatures, 223.

Wu, T.-Y. Scattering of an electron by an atom and rearrangement collisions, 179.
See also Bauer, E., 1436.

Yagoda, H. Observations on stars and heavy primaries recorded in emulsions flown in Viking rocket No. 9, 122.

van Zeggeren, F. and **Benson, G. C.** The quantum mechanical calculation of the surface energy of sodium chloride—A first approximation, 985.

Ziman, J. M. The general variational principle of transport theory, 1256.

CORRECTIONS

p. 839. In equation (15a), $\pi(\gamma^0/(W^0)^2$ should read $\pi(\gamma^0/W^0)^2$.
p. 888. The right-hand side of equation (1) should read $-\alpha_M(e/a)$.
p. 889. In equation (7), $\exp[-\pi(l_1^2+l_2^2)^{\frac{1}{2}}]$ should read $\exp[-\pi\eta(l_1^2+l_2^2)^{\frac{1}{2}}]$.
In equation (8), $-(e/a)$ should read $-(e^2/a)$.

THE PHYSICAL SOCIETY

MEMBERSHIP of the Society is open to all who are interested in Physics.

FELLOWS pay an Entrance fee of £1 1*s*. ($3.00) and an Annual Subscription of £2 2*s*. ($6.00).

STUDENTS: A candidate for Studentship must be between the ages of 18 and 26, and pays an Annual Subscription of 5*s*. ($0.75).

MEETINGS: Fellows and Students may attend all Meetings of the Society including the annual Exhibition of Scientific Instruments and Apparatus.

PUBLICATIONS include the *Proceedings of the Physical Society*, published monthly in two sections, and *Reports on Progress in Physics*, published annually. Volume XVIII, 1955, is now available (price 50*s*. ($7.15)). Members are entitled to receive many of the Publications at a reduced rate.

Further information can be obtained from:

THE PHYSICAL SOCIETY

1, Lowther Gardens, Prince Consort Road

London, S.W.7, England

CANADIAN JOURNAL OF PHYSICS

Notes to Contributors

Manuscripts

(i) ***General.*** Manuscripts, in English or French, should be typewritten, double spaced, on paper $8\frac{1}{2} \times 11$ in. **The original and one copy are to be submitted.** Tables and captions for the figures should be placed at the end of the manuscript. Every sheet of the manuscript should be numbered.

Style, arrangement, spelling, and abbreviations should conform to the usage of this journal. Names of all simple compounds, rather than their formulas, should be used in the text. Greek letters or unusual signs should be written plainly or explained by marginal notes. Superscripts and subscripts must be legible and carefully placed.

Manuscripts and illustrations should be carefully checked before they are submitted. Authors will be charged for unnecessary deviations from the usual format and for changes made in the proof that are considered excessive or unnecessary.

(ii) ***Abstract.*** An abstract of not more than about 200 words, indicating the scope of the work and the principal findings, is required, except in Notes.

(iii) ***References.*** References should be listed **alphabetically by authors' names,** unnumbered, and typed after the text. The form of the citations should be that used in issues of this journal published in 1956; in references to papers in periodicals, titles should not be given and only initial page numbers are required. The names of periodicals should be abbreviated in the form given in the most recent *List of Periodicals Abstracted by Chemical Abstracts*. All citations should be checked with the original articles and each one referred to in the text by the authors' names and the year.

(iv) ***Tables.*** Tables should be numbered in roman numerals and each table referred to in the text. Titles should always be given but should be brief; column headings should be brief and descriptive matter in the tables confined to a minimum. Vertical rules should be used only when they are essential. Numerous small tables should be avoided.

Illustrations

(i) ***General.*** All figures (including each figure of the plates) should be numbered consecutively from 1 up, in arabic numerals, and each figure referred to in the text. The author's name, title of the paper, and figure number should be written in the lower left corner of the sheets on which the illustrations appear. Captions should not be written on the illustrations (see Manuscripts (i)).

(ii) ***Line Drawings.*** Drawings should be carefully made with India ink on white drawing paper, blue tracing linen, or co-ordinate paper ruled in blue only; any co-ordinate lines that are to appear in the reproduction should be ruled in black ink. Paper ruled in green, yellow, or red should not be used unless it is desired to have all the co-ordinate lines show. All lines should be of sufficient thickness to reproduce well. Decimal points, periods, and stippled dots should be solid black circles large enough to be reduced if necessary. Letters and numerals should be neatly made, preferably with a stencil (**do NOT use typewriting**) and be of such size that the smallest lettering will be not less than 1 mm. high when reproduced in a cut 3 in. wide.

Many drawings are made too large; originals should not be more than 2 or 3 times the size of the desired reproduction. In large drawings or groups of drawings the ratio of height to width should conform to that of a journal page but the height should be adjusted to make allowance for the caption.

The original drawings and one set of clear copies (e.g. small photographs) are to be submitted.

(iii) ***Photographs.*** Prints should be made on glossy paper, with strong contrasts. They should be trimmed so that essential features only are shown and mounted carefully, with rubber cement, on white cardboard with no space or only a **very** small space (less than 1 mm.) between them. In mounting, full use of the space available should be made (to reduce the number of cuts required) and the ratio of height to width should correspond to that of a journal page ($4\frac{3}{4} \times 7\frac{1}{2}$ in.); however, allowance must be made for the captions. Photographs or groups of photographs should not be more than 2 or 3 times the size of the desired reproduction.

Photographs are to be submitted in duplicate; if they are to be reproduced in groups one set should be mounted, the duplicate set unmounted.

Reprints

A total of 50 reprints of each paper, without covers, are supplied free. Additional reprints, with or without covers, may be purchased.

Charges for reprints are based on the number of printed pages, which may be calculated approximately by multiplying by 0.6 the number of manuscript pages (double-spaced typewritten sheets, $8\frac{1}{2} \times 11$ in.) and including the space occupied by illustrations. An additional charge is made for illustrations that appear as coated inserts. The cost per page is given on the reprint requisition which accompanies the galley.

Any reprints required in addition to those requested on the author's reprint requisition form must be ordered officially as soon as the paper has been accepted for publication.

Contents

	Page
The Raman Spectrum of Acetylene—*T. Feldman, G. G. Shepherd, and H. L. Welsh*	1425
The Raman Spectrum of Dideuteroacetylene—*L. Krause and H. L. Welsh*	1431
Cross Sections of Dissociative Recombination—*Ernest Bauer and Ta-You Wu*	1436
The Raman Spectrum of Cyclopropane—*P. M. Mathai, G. G. Shepherd, and H. L. Welsh*	1448
Thickness Control of Thin Layers—*A. C. S. van Heel*	1460
Cathodic Glow-to-arc Transitions—*W. A. Gambling*	1466
Spectrum of the C_3 Molecule between 3600 Å and 4200 Å—*Norman H. Kiess and Herbert P. Broida*	1471
Energy and Angular Distributions of Photoprotons Produced by 70 Mev. X-Rays—*W. K. Dawson*	1480
Notes:	
Some Upper Limits of Isotopic Abundance—II: Ne, Cl, and Ga—*Larkin Kerwin and D. E. McElcheran*	1497
Mechanism of Dislocation Locking in Attenuation of High Frequency Sound at Low Temperatures—*T. S. Hutchison and G. J. Hutton*	1498
Contents of Volume 34	1501

Printed in Canada *by* University of Toronto Press